# DESIGN OF A COMPLIANT LEVER-TYPE PASSIVE VIBRATION ISOLATOR USING QUASI-ZERO-STIFFNESS MECHANISM

by

Kamil Koçak

B.S., Mechanical Engineering, Boğaziçi University, 2008

Submitted to the Institute for Graduate Studies in
Science and Engineering in partial fulfillment of
the requirements for the degree of
Master of Science

Graduate Program in Department of Mechanical Engineering
Boğaziçi University

2011

DESIGN OF A COMPLIANT LEVER-TYPE PASSIVE

VIBRATION ISOLATOR

USING QUASI-ZERO-STIFFNESS MECHANISM

APPROVED BY:

| | |
|---|---|
| Assist. Prof. Çetin Yılmaz<br>(Thesis Supervisor) | ..... |
| Prof. Eşref Eşkinat | ..... |
| Assist. Prof. A. Deniz Yalçınkaya | ..... |

DATE OF APPROVAL: 04.09.2011

# ACKNOWLEDGEMENTS

I would like to gratefully acknowledge my thesis supervisor Assist. Prof. Çetin Yılmaz for his kindness and understanding. His guidance was invaluable to me at all stages of preparation of this thesis. I would like to thank the members of my thesis committee; Prof. Eşref Eşkinat and Assist. Prof. Arda Deniz Yalçınkaya.

I thank all of my friends, colleagues, the research assistants and the staff at the mechanical engineering department. I would like particularly to acknowledge Akın Oktav and Mustafa Ali Acar for technical support.

Finally, I would like to thank my family for their love, support and encouragement.

# ABSTRACT

## DESIGN OF A COMPLIANT LEVER-TYPE PASSIVE VIBRATION ISOLATOR USING QUASI-ZERO-STIFFNESS MECHANISM

In this thesis, design and analysis of a new passive vibration isolator using compliant lever-type and quasi-zero-stiffness (QZS) mechanisms is provided. At first, various systems are designed without QZS mechanism. It is aimed to create anti-resonance frequency by using lever-type mechanism. Anti-resonance occurs when the inertial force generated by the levered mass cancels the spring force. Since the lever-type mechanism increases the effect of the isolator mass, it is capable of isolating a relatively heavy body with little mass in itself. These designs are examined analytically, numerically and experimentally. First, the systems are modeled with lumped and distributed parameters. Then, the system is modeled by finite element method (FEM). Optimization of the design is made to get highest isolation in the widest frequency range. As a result, the optimized design with desired properties is found. At last, the optimized design is manufactured and tested. In the second part, QZS mechanism is attached to the design. This design consists of multiple parts which renders the system adjustable. The equations of negative stiffness mechanism are provided. FEM results are compared with the analytical results. The working principle of adjustable mechanisms are explained. As a result, design and analysis of a new compliant lever-type passive vibration isolator using QZS mechanisms is provided. Finally, the design is manufactured and tested. This design can also be adjusted for the designed vibration isolation frequency range and good isolation levels can be acquired especially at low frequencies.

# ÖZET

## YARI-SIFIR-DİRENGENLİK MEKANİZMASI KULLANARAK ESNEK BAĞLANTILI KALDIRAÇ-TİPİ PASİF TİTREŞİM YALITICI TASARIMI

Bu tez çalışmasında, esnek bağlantılı kaldıraç-tipi ve yarı-sıfır-direngenlik mekanizmaları kullanarak oluşturulan yeni bir pasif titreşim yalıtıcısının tasarımı ve analizi yapılmıştır. Başlangıçta, yarı-sıfır-direngenlik mekanizması olmadan çeşitli sistem tasarımları yapılmıştır. Tasarımda kaldıraç-tipi mekanizma kullanılarak atalet bağlaşımıyla antirezonans frekansı elde edilmesi amaçlanmıştır. Bu antirezonans frekansı, kaldıracın oluşturduğu atalet kuvveti ile sistemin direngenliğinden ötürü oluşan kuvvetin birbirini dengelediği frekansta oluşmaktadır. Kaldıraç-tipi mekanizma, yalıtıcının kütlesinin yalıtımdaki etkisini yükselttiği için daha az kütle ile daha etkili yalıtım yapılabilmesini sağlamaktadır. Yapılan tasarımlar analitik, sayısal ve deneysel olarak incelenmiştir. Öncelikle, sistem toplu ve sürekli parametreli olarak modellenmiştir. Sonrasında sistem sonlu elemanlar yöntemiyle modellenmiştir. En geniş frekans aralığında en yüksek yalıtıma ulaşılabilmek için tasarımın eniyilemesi yapılmıştır. Sonuç olarak amaçlanan özelliklere sahip eniyilenmiş tasarım elde edilmiştir. En sonunda da eniyilenmiş tasarım üretilmiş ve test edilmiştir. İkinci bölümde sisteme yarı-sıfır-direngenlik mekanizması eklenmiştir. Bu tasarım, sistemi ayarlanabilir hale getiren bir çok parçadan oluşmaktadır. Negatif direngenlik mekanizmasının denklemleri sunulmuştur. Sonlu elemanlar yönteminin sonuçları analitik sonuçlarla karşılaştırılmıştır. Sonuç olarak yarı-sıfır-direngenlik mekanizması kullanılarak yeni bir esnek bağlantılı kaldıraç-tipi pasif titreşim yalıtıcısının tasarımı ve analizi sunulmuştur. Son adımda ise tasarım üretilmiş ve test edilmiştir. Bu tasarım ayrıca istenen titreşim yalıtımı frekans aralığına göre ayarlanabilir ve özellikle düşük frekanslarda yüksek yalıtım seviyeleri elde edilebilir.

# TABLE OF CONTENTS

ACKNOWLEDGEMENTS . . . . . iii
ABSTRACT . . . . . iv
ÖZET . . . . . v
LIST OF FIGURES . . . . . viii
LIST OF TABLES . . . . . xv
LIST OF SYMBOLS . . . . . xvi
LIST OF ACRONYMS/ABBREVIATIONS . . . . . xviii
1. INTRODUCTION . . . . . 1
1.1. Research Objective and Motivation . . . . . 1
1.2. Literature Review . . . . . 2
1.3. Thesis Overview . . . . . 10
2. COMPLIANT LEVER-TYPE MECHANISM . . . . . 12
2.1. The Lumped Parameter Model . . . . . 12
2.2. The Distributed Parameter Model . . . . . 14
2.2.1. Lever with Distributed Mass . . . . . 14
2.2.2. Flexure Hinges . . . . . 17
2.2.3. Optimization of the Design . . . . . 19
2.3. The Finite Element Model . . . . . 22
2.3.1. Static Structural Analysis . . . . . 22
2.3.2. Modal Analysis . . . . . 24
2.3.3. Harmonic Analysis . . . . . 24
2.4. Experimental Modal Analysis . . . . . 29
2.4.1. Analyzing Test Results . . . . . 30
3. QUASI-ZERO-STIFFNESS MECHANISM . . . . . 39
3.1. Analysis of the System with Quasi-Zero-Stiffness Mechanism . . . . . 41
3.1.1. Stress Constraints in the Design . . . . . 53
3.2. Adjustment Systems . . . . . 55
3.2.1. Compressive Force Adjustment System for the Bistable Mechanism 55
3.2.2. Adjustable Isolator Mass . . . . . 55

3.2.3. Leveling System for the Isolator . . . . . 56
3.3. Experiments for the System with Quasi-Zero-Stiffness Mechanism . . . 57
4. RESULTS AND DISCUSSION . . . . . 66
5. CONCLUSIONS . . . . . 71
APPENDIX A: TECHNICAL DRAWINGS . . . . . 73
REFERENCES . . . . . 91

# LIST OF FIGURES

Figure 1.1. (a) Swinging of a pendulum, (b) The motion of a plucked string. . 1

Figure 1.2. A schematic diagram of DVA's where $M$: main mass, $m_a$: auxiliary mass, $k_a$: stiffness of the spring between the auxiliary mass and the main mass, $k$: stiffness between the main mass and the ground. . . 4

Figure 1.3. A schematic diagram of lever-type DAVI's. . . . . 5

Figure 1.4. A schematic diagram of quasi-zero-stiffness mechanism. . . . . 7

Figure 1.5. Force-displacement graph of the isolator shown in Figure 1.4. $F_0$=$m.g$ on the graph. . . . . 8

Figure 2.1. Isolation system with lumped parameters. . . . . 12

Figure 2.2. Isolation system with distributed mass lever. . . . . 15

Figure 2.3. Lever with flexure hinges. . . . . 17

Figure 2.4. Lever arm representation for stiffness analysis after deformation. . 18

Figure 2.5. The result of the topology optimization of the lever [44]. . . . . 20

Figure 2.6. Front view of the compliant isolator. . . . . 20

Figure 2.7. Isometric view of the compliant isolator. . . . . 22

Figure 2.8. Static structural analysis of the compliant isolator. . . . . 23

Figure 2.9. The transmissibility plot of the single degree of freedom model of the compliant isolator. . . . . 24

Figure 2.10. Mode shape of the system at 140.48 Hz. . . . . 25

Figure 2.11. Mode shape of the system at 3375.4 Hz. . . . . 26

Figure 2.12. Frequency response plot of the system via finite element analysis. . 27

Figure 2.13. Frequency response plot of the SDOF analytic and FEM model for $M$=1.145 kg. . . . . 28

Figure 2.14. Frequency response plot of the SDOF analytic and FEM model for $M$=0.145 kg. . . . . 29

Figure 2.15. The manufactured vibration isolator design and extra mass. . . . . 30

Figure 2.16. Impact hammer test of the isolator design. . . . . 31

Figure 2.17. Experimental frequency response plot for isolator mass of 1.145 kg by hard tip hammer (Sample frequency = 8192 Hz). . . . . 34

Figure 2.18. Coherence plot for isolator mass of 1.145 kg by hard tip hammer (Sample frequency = 8192 Hz). . . . . 35

Figure 2.19. Experimental frequency response plot for isolator mass of 1.145 kg by soft tip hammer (Sample frequency = 4096 Hz). . . . . 35

Figure 2.20. Coherence plot for isolator mass of 1.145 kg by soft tip hammer (Sample frequency = 4096 Hz). . . . . 36

Figure 2.21. Experimental frequency response plot for isolator mass of 0.145 kg by hard tip hammer (Sample frequency = 4096 Hz). . . . . 36

Figure 2.22. Coherence plot for isolator mass of 0.145 kg by hard tip hammer (Sample frequency = 4096 Hz). . . . . 37

Figure 2.23. Experimental frequency response plot for isolator mass of 0.145 kg by soft tip hammer (Sample frequency = 2048 Hz). . . . . 37

Figure 2.24. Coherence plot for isolator mass of 0.145 kg by soft tip hammer (Sample frequency = 2048 Hz). . . . . 38

Figure 3.1. First two buckling modes for a clamped-clamped beam. . . . . 40

Figure 3.2. Front view of the isolator design with QZS mechanism. . . . . 41

Figure 3.3. Isometric view of the isolator design with quasi-zero-stiffness mechanism. . . . . 42

Figure 3.4. Flexure hinges that produce positive stiffness. . . . . 43

Figure 3.5. Isometric view of positive stiffness elements. . . . . 43

Figure 3.6. A schematic diagram for the calculation of the stiffness in vertical direction. Here, $P_{cr}$ is the compression force within the beam. . . . 44

Figure 3.7. A schematic diagram of buckled beams used in this study. . . . . 45

Figure 3.8. Force - displacement graph for a bistable mechanism [18]. . . . . 45

Figure 3.9. Apex height of the beam. . . . . 45

Figure 3.10. Bistable mechanism that produce negative stiffness. . . . . 46

Figure 3.11. Isometric view of bistable mechanism. . . . . 47

Figure 3.12. Force - displacement graph for the designed bistable mechanism. . 48

Figure 3.13. Force - displacement graph for the designed bistable mechanism in finite element analysis. . . . . 49

Figure 3.14. Static structural analysis of the positive stiffness elements. . . . . 50

Figure 3.15. Mode shape of the system at 7.1719 Hz. . . . . 51

Figure 3.16. Mode shape of the system at 249.28 Hz. . . . . 52

Figure 3.17. Frequency response plot via harmonic analysis. . . . . 53

Figure 3.18. Compressive force adjustment system for the bistable mechanism. 55

Figure 3.19. Adjustable isolator mass. . . . . 56

Figure 3.20. Leveling system for the isolator. . . . . 57

Figure 3.21. The manufactured vibration isolator design with quasi-zero-stiffness mechanism. . . . . 58

Figure 3.22. Test setup of the system with quasi-zero-stiffness mechanism. . . . 58

Figure 3.23. Coherence plot for movable isolator mass at the near end and parallel beams are not pre-stressed. . . . . 59

Figure 3.24. Experimental frequency response plot for movable isolator mass at the near end and parallel beams are not pre-stressed. . . . . 60

Figure 3.25. Coherence plot for movable isolator mass at the near end and parallel beams are pre-stressed. . . . . 60

Figure 3.26. Experimental frequency response plot for movable isolator mass at the near end and parallel beams are pre-stressed. . . . . 61

Figure 3.27. Comparison of the experimental frequency responses for movable isolator mass at the near end. . . . . 62

Figure 3.28. Coherence plot for movable isolator mass in the middle of the lever and parallel beams are not pre-stressed. . . . . 62

Figure 3.29. Experimental frequency response plot for movable isolator mass in the middle of the lever and parallel beams are not pre-stressed. . . 63

Figure 3.30. Coherence plot for movable isolator mass in the middle of the lever and parallel beams are pre-stressed. . . . . 64

Figure 3.31. Experimental frequency response plot for movable isolator mass in the middle of the lever and parallel beams are pre-stressed. . . . . 64

Figure 3.32. Comparison of the experimental frequency responses for movable isolator mass in the middle of the lever. . . . . 65

Figure 4.1. Frequency response plot of the SDOF analytic and FEM model for $M = 1.145$ kg (Figure 2.13 is restated). . . . . 66

Figure 4.2. Frequency response plot of the SDOF analytic and FEM model for $M = 0.145$ kg (Figure 2.14 is restated). . . . . 67

Figure 4.3. Experimental frequency response plot for isolator mass of 1.145 kg with sample frequency 4096 Hz (Figure 2.19 is restated). . . . . 68

Figure 4.4. Experimental frequency response plot for isolator mass of 0.145 kg with sample frequency 2048 Hz (Figure 2.23 is restated). . . . . 68

Figure A.1. Part of the leveling system for the isolator. . . . . 73

Figure A.2. Bottom part of the main structure. . . . . 74

Figure A.3. Part between the positive stiffness mechanism and isolator mass. . 75

Figure A.4. M6 threaded rod at the bottom of the system. . . . . 76

Figure A.5. Flexure hinges. . . . . 77

Figure A.6. Isolator mass. . . . . 78

Figure A.7. M8 threaded rod that enables to change the position of the isolator mass. . . . . 79

Figure A.8. Cover to satisfy clamped-clamped boundary conditions. . . . . 80

Figure A.9. M4 bolt. . . . . 80

Figure A.10. Metric 4 nut. . . . . 81

Figure A.11. Metric 6 nut. . . . . 81

Figure A.12. Metric 8 nut. . . . . 82

Figure A.13. Left part of the negative stiffness mechanism. . . . . 82

Figure A.14. Part in the middle of the negative stiffness mechanism. . . . . 83

Figure A.15. Right part of the negative stiffness mechanism. . . . . 84

Figure A.16. M6 threaded rod at the right of the system. . . . . 85

Figure A.17. Side parts of the main structure. . . . . 86

Figure A.18. Spring steels that produce negative stiffness. . . . . 87

Figure A.19. Part between two flexure hinges. . . . . 88

Figure A.20. Final Design. . . . . 89

Figure A.21. Design without QZS mechanism. . . . . 90

# LIST OF TABLES

Table 2.1. The first 10 resonance frequencies of the compliant isolator. . . . . 25

Table 3.1. The first 5 resonance frequencies of the system in which the movable isolator mass is in the middle of the lever and the parallel beams are not pre-stressed. . . . . 50

# LIST OF SYMBOLS

| | |
|---|---|
| $E_1$ | Elastic modulus of the flexure hinges |
| $E_2$ | Elastic modulus of the beam material in quasi-zero-stiffness mechanism |
| $F$ | Force |
| $f(t)$ | Driving force |
| $H(\omega)$ | Frequency response function of the system |
| $I$ | Mass moment of inertia of the lever arm about the mass center in the case of lever with distributed mass |
| $I_1$ | Mass moment of inertia of flexure hinges |
| $I_2$ | Mass moment of inertia of the beam in quasi-zero-stiffness mechanism |
| $k$ | Stiffness of the isolation system from the base to the load |
| $k_b$ | Extra positive stiffness due to negative stiffness beam elements when they are not pre-compressed |
| $k_n$ | Negative stiffness |
| $k_p$ | Positive stiffness |
| $L$ | Lagrangian |
| $l_a$ | Length of the flexure hinges |
| $l_1$ | Length of the lever |
| $l_2$ | Distance between two hinges |
| $l_3$ | Distance between the left hinge and center of isolator mass |
| $l_4$ | Distance between the left hinge and the movable isolator mass |
| $M$ | Mass of the main body |
| $M_o$ | Moment on the leftmost of the lever |
| $m_{is}$ | Isolator mass |
| $m_m$ | Movable isolator mass |
| $R_{xf}$ | Cross-correlation function for the two signals $x(t)$ and $f(t)$ |
| $R_{xx}$ | Autocorrelation function of the random signal $x(t)$ |
| $S_{ff}$ | Power spectral density of the response |
| $S_{xf}$ | Cross-spectral density for the two signals $x(t)$ and $f(t)$ |

| | |
|---|---|
| $S_{xx}$ | Power spectral density of the random signal $x(t)$ |
| $t$ | Thickness of the flexure hinges |
| $T$ | Kinetic energy of the system |
| $T(\omega)$ | Transmissibility |
| $V$ | Potent energy of the system |
| $w$ | Depth of the whole planar mechanism |
| $x$ | Displacement of the main body |
| $x(t)$ | Random signal |
| $y$ | Displacement of the base |
| $z$ | Displacement of the isolator mass |
| | |
| $\alpha$ | Lever ratio |
| $\beta$ | Ratio of distance between the left hinge and center of isolator mass $l_3$ to distance between two hinges $l_2$ |
| $\gamma^2$ | Coherence function |
| $\delta$ | Displacement of the main body in static structural analysis |
| $\eta$ | Ratio of distance between the left hinge and movable isolator mass $l_4$ to distance between two hinges $l_2$ |
| $\theta_1$ | Angle between the lever and horizontal axis in the case of lever with distributed mass |
| $\theta$ | Angle between the flexure hinges and vertical axes |
| $\mu$ | Ratio of isolator mass to mass of the main body |
| $\omega_p$ | Resonance frequency (pole) of a system having a single pole |
| $\omega_z$ | Anti-resonance frequency (zero) of a system having a single zero |
| $\omega_0$ | Natural frequency of a single degree of freedom mass-spring system with mass $M$ and stiffness $k$ |

# LIST OF ACRONYMS/ABBREVIATIONS

| | |
|---|---|
| AMD | Auxiliary Mass Damper |
| DOF | Degree of Freedom |
| DVA | Dynamic Vibration Absorber |
| FEM | Finite Element Method |
| Hz | Hertz |
| PSD | Power Spectral Density |
| SDOF | Single Degree of Freedom |
| QZS | Quasi-Zero-Stiffness |
| WEDM | Wire Electrical Discharge Machining |

# 1. INTRODUCTION

Any motion that repeats itself after an interval of time is called vibration or oscillation. People became interested in vibration when the first musical instruments, probably drums or whistles, were discovered [1]. Since then, people have applied critical investigation to study the phenomenon of vibration. The swinging of a pendulum (Figure 1.1a) and the motion of a plucked string (Figure 1.1b) are typical examples of vibration. The theory of vibration deals with the study of oscillatory motion of bodies and the forces associated with them.

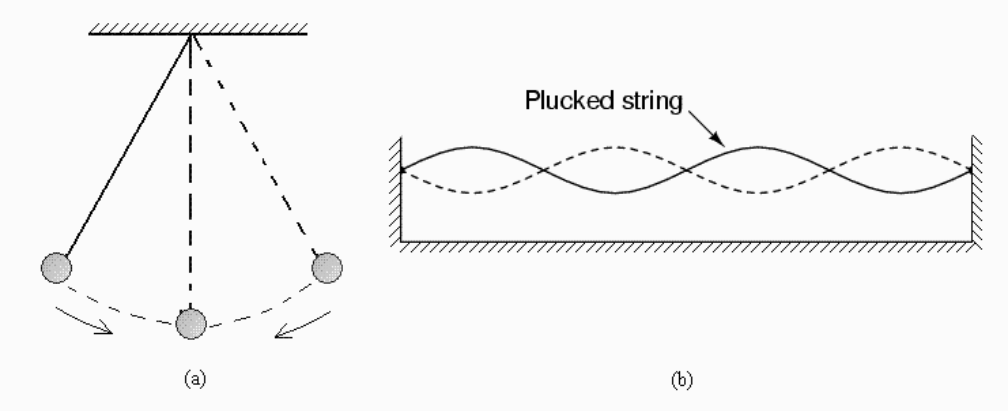



Figure 1.1. (a) Swinging of a pendulum, (b) The motion of a plucked string.

## 1.1. Research Objective and Motivation

The aim of this thesis is to analyze and design of a new passive vibration isolator. This study consists of two main parts. In the first part, design and analysis of a new passive vibration isolator using compliant lever-type mechanism is provided. The system consists of a single piece because of the usage of flexure hinges. By this means, both manufacturing of the system will be easy and undesired results such as friction, wear and backlash between the parts will be eliminated. It is aimed to create anti-resonance frequency by using lever-type mechanism. Anti-resonance occurs when the inertial force generated by the levered mass cancels the spring force. Since the lever-type mechanism increases the effect of the isolator mass, it is capable of isolating a

relatively heavy body with little mass in itself. The design is examined both analytically and numerically. Then, test results of the manufactured design are compared with the analytical and numerical models. In the second part, quasi-zero-stiffness mechanism is added to the system. The new design consists of several parts because it is aimed to be adjusted for several different conditions. The test results for the second design are also provided.

The main motivation of this study is to contribute to the solution of a general problem in vibration isolation. Achieving vibration isolation at low frequencies by just passive means is a challenging problem. If just masses and linear springs are used in isolators to achieve good isolation levels at low frequencies, the spring stiffness should be low which result in large deflections and/or the masses in the system should be large which is generally undesirable due to the space and weight limitations. The large mass problem can be circumvented by the use of inertial coupling in the system. Moreover, low stiffness problem can be solved by the use of nonlinear quasi-zero-stiffness springs. There are several vibration isolators using inertial coupling method, but there is more to be done about lever-type systems, the combinations of these systems with compliant mechanisms and quasi-zero-stiffness mechanisms.

## 1.2. Literature Review

The movement of a vibrating body from its undisturbed position to its extreme position in one direction, then to its extreme position in the other direction passing through its equilibrium position, and back to equilibrium position is called a cycle of vibration. The number of cycles per unit time is called the frequency of the oscillation. If a system, after an initial disturbance, is left to vibrate on its own, the frequency with which it oscillates without external forces is known as its natural frequency. A machine or system may experience excessive vibration if it is acted upon by a force whose excitation frequency nearly coincides with a natural frequency of the machine or system. This phenomenon is known as resonance, and it leads to excessive deflections and failure [1].

Vibration isolation is a procedure by which the undesirable effects of vibration are reduced. Basically, it involves the insertion of a resilient member (or isolator) between the vibrating mass (or equipment) and the source of vibration so that a reduction in the dynamic response of the system is achieved under specific conditions of vibration excitation. An isolation system is said to be active or passive depending on whether or not external power is required for the isolator to perform its function.

A vibration isolation system is called *passive* if external power is not required for the isolator to perform its function. This is called *passive isolation*. A passive isolator consists of a resilient member (stiffness) and an energy dissipater (damping). Examples of passive isolators include metal springs, pneumatic springs, cork, etc. A vibration isolation system is called *active* if it uses external power to perform its function. This is called *active isolation*. Active vibration isolation systems contain, along with the spring, a feedback circuit which consists of an accelerometer, a controller, amplifier and an actuator. The acceleration (vibration) signal is processed by a control circuit and amplifier. Then it feeds the actuator, which generates motion. As a result of such a feedback system, a considerably stronger suppression of vibrations is achieved compared to passive systems [2].

In this study, a passive isolator will be designed and analyzed. However, its effectiveness will be increased with the use of inertial coupling and quasi-zero-stiffness mechanisms.

The effectiveness of an isolator is stated in terms of its transmissibility ($Tr$). Force transmissibility can be defined as the ratio of the amplitude of the force transmitted to that of the excitation force. If $Tr$ is greater than 1, amplification of the excitation force is observed, and if $Tr$ is less than 1, isolation is observed on the mass (or load). When the amplitude of the force transmitted is much more than that of the excitation force at one frequency, which means $Tr$ is much more than 1, resonance occurs and this is the most undesired case for isolation because of its destructive effects to the system. This frequency is known as the resonance frequency (pole). Some vibration isolators try to minimize these resonance frequencies and achieve isolation only after some frequency

known as stop-band frequency. This can be done by decreasing the stiffness and/or increasing the mass of the system. However, for most applications there is a minimum stiffness requirement and a maximum load requirement [3]. On the other hand, when the amplitude of the excitation force is much more than that of the force transmitted which means $Tr$ nearly equals to 0 at some frequency, 100% isolation is achieved theoretically at that frequency, and this frequency is known as the anti-resonance frequency (zero). In a linear lumped parameter system, anti-resonance frequencies can be generated by two different methods. The first method is to add dynamic vibration absorbers (DVA's). The second method is to generate inertial coupling [3].

In 1911, Frahm invented the dynamic vibration absorber. A schematic diagram of a DVA can be seen in Figure 1.2. In a DVA the disturbing vibrations are avoided by means of an auxiliary body which is arranged within or on the main body whose vibrations are to be attenuated. This auxiliary body is caused to vibrate by the vibrations of the main body and the natural vibrations of the auxiliary body have as nearly as possible the same period as those of the main body. The action of this device depends upon the fact that the resonance vibrations of the main body are canceled by the secondary resonance vibrations of the smaller auxiliary body [4].

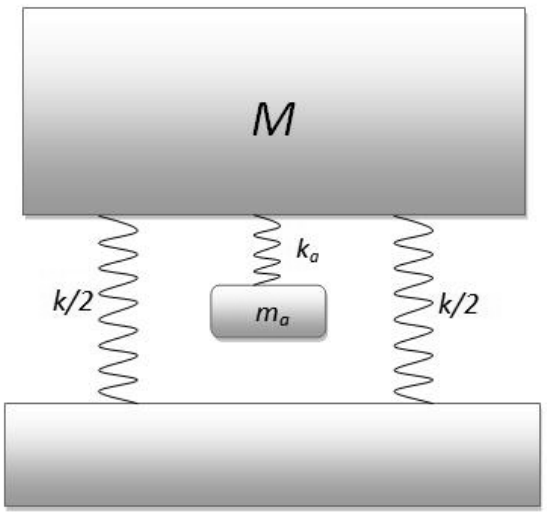



Figure 1.2. A schematic diagram of DVA's where $M$: main mass, $m_a$: auxiliary mass, $k_a$: stiffness of the spring between the auxiliary mass and the main mass, $k$: stiffness between the main mass and the ground.

DVA's with damping are called as auxiliary mass dampers (AMD's). In general, the undamped dynamic vibration absorber is effective only for a system that is subjected to a constant frequency excitation or in some cases by an excitation force that is a constant multiple of a rotational speed. In this case, it is possible to modify the vibration pattern and to reduce its amplitude significantly by the use of an auxiliary mass on a spring tuned to the frequency of the excitation. In the case of AMD's, if it is impossible to incorporate damping into a structure that vibrates excessively, it may be possible to provide the damping in an auxiliary system attached to the structure. When used in this manner, the auxiliary system is one form of a damper. It is important to note that these systems are used for reducing the amplification but not for isolation [5].

Vibration isolators that use inertial coupling to create anti-resonance frequencies were first developed in the 1960's by researchers in the aerospace industry. Because of the strict requirements on stiffness and mass of the isolators used in this industry, new kind of vibration isolators developed [3]. Dynamic Antiresonant Vibration Isolator's (DAVI's), which are invented by Flannelly [6], generates anti-resonance frequencies by inertial coupling. DAVI uses a levered mass-spring combination to generate an anti-resonance frequency in the system (see Figure 1.3).

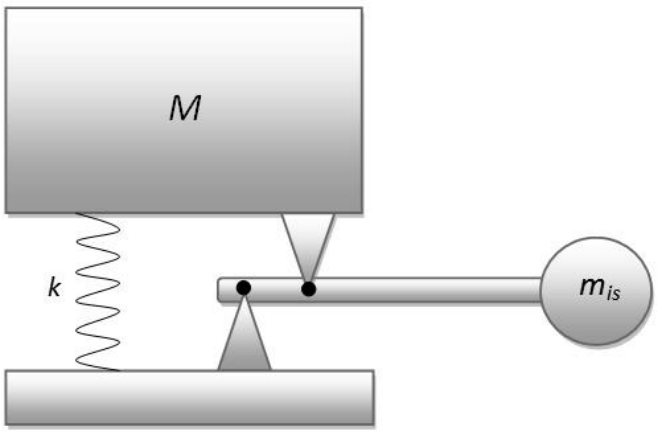



Figure 1.3. A schematic diagram of lever-type DAVI's.

Anti-resonance occurs when the inertial force generated by the levered mass can-

cels the spring force. This anti-resonance frequency depends on the mass of the isolator, the spring stiffness and the lever ratio. One of the most important features of DAVI's is, unlike DVA's; they are implemented on the load path; so the degree of freedom of the system is not increased [3]. Flannelly's invention provides simple vibration isolator which at certain predetermined excitation frequencies gives greater isolation with considerably lower static deflections than conventional isolators. This vibration isolator has such an antiresonant frequency which is independent of the mass of the isolated body. Also it is capable of isolating a relatively heavy body with little mass in itself. This feature is useful in applications where weight reduction is important such as aircraft or spacecraft. DAVI's also may be combined with damping to reduce the amplification of the excitation vibration in the vicinity of the resonant frequency without seriously impairing the isolation properties at frequencies above resonance [6].

Flannelly generated large inertial forces by amplifying the motion of the small mass on the lever. This result can also be achieved by using hydraulic leverage instead of mechanic leverage. In 1965, Goodwin [7] designed an anti-resonant vibration isolator by using hydraulic leverage. He showed that fluid-type systems can provide higher leverage than mechanical ones. A small mass of a fluid could generate the desired inertial forces, enabling weight savings on the system [8]. Braun [9] also used the same method as Goodwin and designed a vibration isolator with a spring mechanism and a fluid transmission mechanism interposed between a vibrating member and a support member. In this design, fluid pressure change compensates as a dynamic force the dynamic portion of the spring force transmitted from the spring mechanism to the support member [9].

As mentioned earlier, to minimize resonance frequencies, stiffness of the isolator has to be decreased. However, a smaller stiffness results in a larger static displacement of the mass. This trade-off between isolation and static displacement can be overcome by using quasi-zero-stiffness (QZS) mechanism which is characterized by an appreciable static stiffness but very small (theoretically zero) dynamic stiffness [10]. (see Figure 1.4).

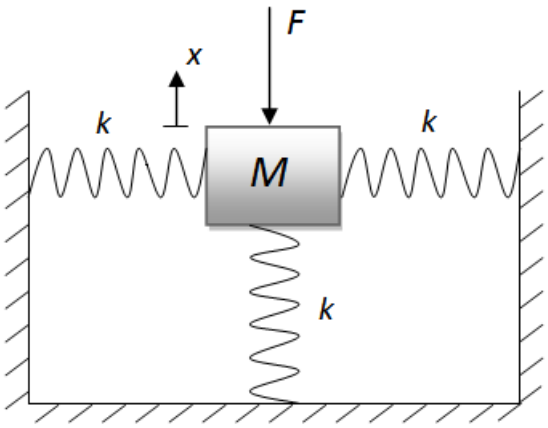



Figure 1.4. A schematic diagram of quasi-zero-stiffness mechanism.

It is possible to achieve an isolator with close to zero stiffness which results in a low natural frequency by careful choice of system parameters. In Figure 1.5, the slope of the curve gives stiffness. Observe that for the given force $F_0$, the resultant displacement is $x_0$ and the slope of the curve at that point nearly equals to zero. Due to its nonlinear force-displacement behavior, we observe a small static displacement [11]. QZS mechanisms are generally achieved by combining a negative stiffness element with a positive stiffness element. In Figure 1.4, if the static equilibrium position is as seen, the horizontal springs act as a negative stiffness in the vertical direction counteracting the positive stiffness of the vertical spring. The penalty for using this mechanism is that the system becomes stiffer than the vertical spring alone for large excursions from the equilibrium position [11].

Mechanism is a mechanical device used to transfer or transform motion, force, or energy. Traditional rigid-body mechanisms consist of rigid links connected by movable joints. Compliant mechanisms also transfer or transform motion, force, or energy. Unlike rigid-link mechanisms, compliant mechanisms gain at least some of their mobility from the deflection of flexible members rather than from movable joints only. There are several advantages of compliant mechanisms. Part-count reduction, reduced assembly time and simplified manufacturing processes cause cost reduction [12]. With the aid of

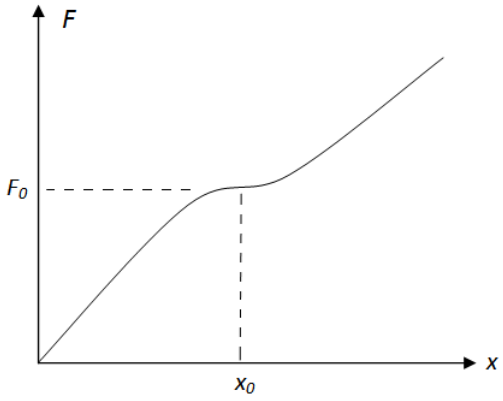



Figure 1.5. Force-displacement graph of the isolator shown in Figure 1.4. $F_0$=$m.g$ on the graph.

CNC (computer numerical control) and WEDM (wire electrical discharge machining) technologies, flexure hinges can be monolithically manufactured with other components of the entire mechanisms [13]. These mechanisms have high precision and reliability. In addition, fewer movable joints results in reduced wear, friction, backlash, weight, maintenance and need for lubrication. On the other hand, compliant mechanisms have their own problems. Analysis and design of compliant mechanisms are typically more difficult than for rigid body mechanisms [12]. Unlike ideal revolute joints, flexure hinges have finite stiffness in the output direction. Therefore, the rotational center will change when flexure hinges generate displacement output [13]. In some applications, having energy stored in flexible members is a disadvantage. For example, if a mechanism's function is to transfer energy from the input to an output, not all of the energy is transferred, but some is stored in the mechanism. Compliant links that remain under stress for long periods of time or at high temperatures may experience stress relaxation or creep. Also, a compliant link cannot produce a continuous rotational motion such as is possible with a pin joint. The motion from the deflection of compliant links is limited by the strength of the deflecting members [12].

One of the important parts of the compliant mechanisms is their flexure hinges. Elliptical, circular and corner filleted hinges are commonly used hinge type examples

for compliant mechanisms. Comparison and analysis of these hinge types are performed in [13–16]. In this study, corner filleted flexure hinges are used. These type of hinges provides relatively high compliance [15].

One of the studies that combines compliant mechanism with vibration isolation is the work in [17]. In [17], an active vibration isolator in low frequencies using compliant mechanism is developed.

To have quasi-zero-stiffness, our design has a bistable mechanism that produce negative stiffness very similar in [18–22]. The typical implementation of the mechanisms in these studies are curved centrally-clamped parallel beams, which will be used in this study as well. Negative stiffness elements in our design are fixed-fixed, buckled beams. A study for single-mode responses of a fixed-fixed buckled beam under the case of a uniform, transverse, harmonic excitation is provided in [23].

In [24, 25], compliant and bistable mechanisms are combined. In [26, 27], optimization methods for fully compliant bistable mechanisms are provided. In [28], a new method is presented for fabricating compliant mechanisms that allow thin flexures to be easily made in metal. In [29, 30], compliant mechanism for displacement amplification purpose is used. In [31], mechanical amplifier design with compliant mechanism is provided. Compliant cellular trusses are used for morphing aircraft structures in [32]. In [33], the development of reliable and scalable compliant components to replace bearings and helical springs. As the size of mechanisms decrease, assembly and maintenance become difficult and the minimum size of traditional elements such as bearings and springs are limited. A limiting factor of usefulness of bearings is the backlash in them. This is a disadvantage for high precision applications. Compliant mechanisms are also being used in surgical tools. In [34], there is an example work for this. In [35], design and development of a multiple DOF compliant robot is provided. In [35], definition of possible applications of flexure joints is presented. In [36], the basic principles of compliant mechanisms design methodology are presented. Flexible bearings count on the elastic properties of matter and combining flexible bearings with adequate actuators and sensors allows nanometric positioning resolutions to be obtained.

In [37], a system which uses negative-stiffness mechanisms to cancel the stiffness of a spring suspension is presented. In [37], the key features of negative stiffness mechanism vibration isolation systems are summarized. Passiveness, compactness, no air, 6-DOF isolation, providing system resonant frequencies below 0.2 Hz are some of them. In [38], a negative stiffness mechanism vibration isolator system is also presented and this system performs ten times better than air springs. These negative stiffness mechanism isolators offer unsurpassed vibration control in the 2 to 100 Hz range. The design in [39] has very similar vertical negative stiffness flexures to the negative stiffness element of the design provided in this research.

In [40, 41], an investigation of wire electrical discharge machining of thin cross-sections and compliant mechanisms is provided. Effects of electrical discharge machining process parameters on thin cross-section cutting of some specific metals are investigated in these studies. [42] is another study which manufactures compliant mechanisms by wire electrical discharge machining. In [43], a parallel linear compliant mechanism is proposed for two DOF ultra precision linear motions. The joints of the compliant mechanism were implemented by different kinds of flexure hinges. This parallel linear compliant mechanism is also machined by wire electric discharge machining.

So far, literature about vibration isolators, quasi-zero-stiffness, compliant mechanism and wire electrical discharge machining is reviewed and summarized. This study combines all these topics and provides analysis and design of a new passive vibration isolator.

## 1.3. Thesis Overview

The thesis outline is as follows: in Chapter 1, the research objective and motivation is stated. Then, brief discussion of literature is provided. In Chapter 2, firstly the lumped parameter model is presented. Then the distributed parameter model; lever with distributed mass, flexure hinges are examined. Optimization of the design is performed using a topology optimization application. Next, finite element model is provided with static structural analysis, modal analysis, and harmonic analysis.

Then, experimental modal analysis is provided. Finally, the analytic and finite element model's results are compared with the test results. In Chapter 3, equations and finite element analysis of negative stiffness mechanism is provided. Drawings of the designs are presented. Test results of the system with QZS mechanism are provided. The adjustable mechanisms are explained. In Chapter 4, the results of the study is examined and discussed. Finally in Chapter 5, summary of the overall study is given and conclusions are presented.

# 2. COMPLIANT LEVER-TYPE MECHANISM

In this section, passive vibration isolators are designed using a compliant lever-type mechanism.

## 2.1. The Lumped Parameter Model

Before investigating the compliant system with distributed parameters, a lumped parameter model is analyzed. The lumped parameter model can be seen in Figure 2.1.

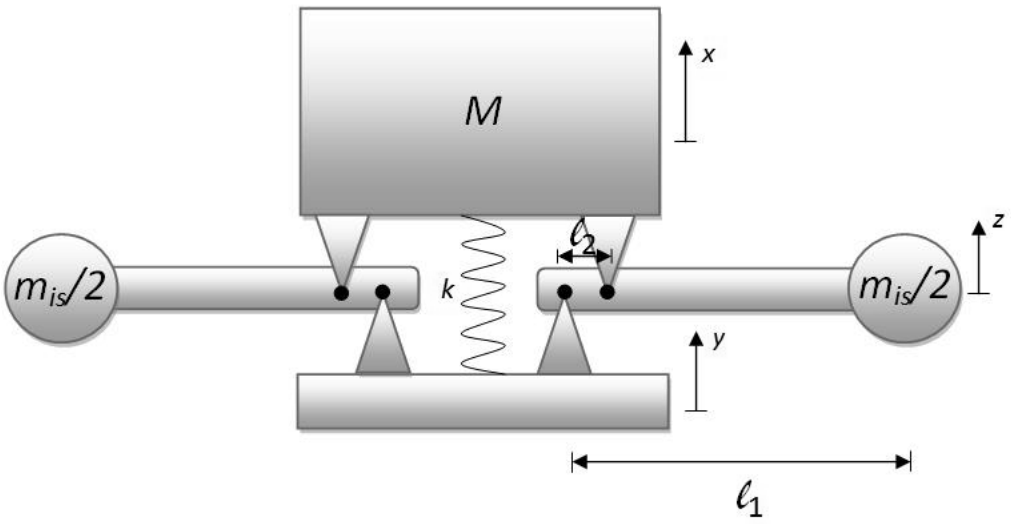



Figure 2.1. Isolation system with lumped parameters.

If we assume the levers are rigid and the system oscillates with small amplitude, the system can be solved in terms of $z$, $x$ and $y$ (See Equation 2.1).

$$z = \alpha x - (\alpha - 1)y, \tag{2.1}$$

where

$$\alpha = l_1/l_2. \tag{2.2}$$

Equation 2.3, is the equation of motion for this system.

$$(1 + \mu\alpha^2)\ddot{x} + \omega_0^2 x = \mu\alpha(\alpha - 1)\ddot{y} + \omega_0^2 y, \tag{2.3}$$

where

$$\mu = m_{is}/M, \tag{2.4}$$

and

$$\omega_0 = \sqrt{k/M}. \tag{2.5}$$

This lumped parameter system has single degree of freedom. Therefore, it has one resonance and one anti-resonance frequency. When Equation 2.3 is solved, the resonance frequency of the system is found as

$$\omega_p = \frac{\omega_0}{\sqrt{1 + \mu\alpha^2}} = \sqrt{\frac{k}{M + m_{is}\alpha^2}}, \tag{2.6}$$

and the anti-resonance frequency of the system is found as

$$\omega_z = \frac{\omega_0}{\sqrt{\mu\alpha(\alpha - 1)}} = \sqrt{\frac{k}{m_{is}\alpha(\alpha - 1)}}. \tag{2.7}$$

When these equations are examined, one can see that the effective mass of the system can be increased by increasing $\alpha$. From Equation 2.3, one can deduce that increasing $\alpha$ will increase inertia forces. For this reason, with small isolator mass ($m_{is}$) relatively large inertia force can be generated.

Finally, displacement transmissibility for this system can be obtained as

$$T(\omega) = \frac{1 - \omega^2/\omega_z^2}{1 - \omega^2/\omega_p^2}. \tag{2.8}$$

## 2.2. The Distributed Parameter Model

Several vibration isolators are designed using lever-type mechanism and analysis of these systems are made in [3]. In these designs, systems are modeled with lumped parameters as above. However, in reality there are other modes and resonance frequencies arising from the elements of the system such as levers or hinges. Thus, examining the system with distributed parameters will give more accurate results.

### 2.2.1. Lever with Distributed Mass

The distributed parameter model will be introduced step by step. Firstly, we account for the distributed mass of the lever. The system with single lever arm and its variables can be seen in Figure 2.2. Mass and inertia of the lever arm are taken into account in this model.

If the lever in the system is assumed as rigid, and the system oscillates with small amplitude, the displacement of the center of mass ($z$) can be solved in terms of $x$ and $y$.

$$z = \beta x + (1 - \beta)y, \tag{2.9}$$

where

$$\beta = l_3/l_2. \tag{2.10}$$

In addition, the angle between the lever and horizontal axis can be stated in terms of

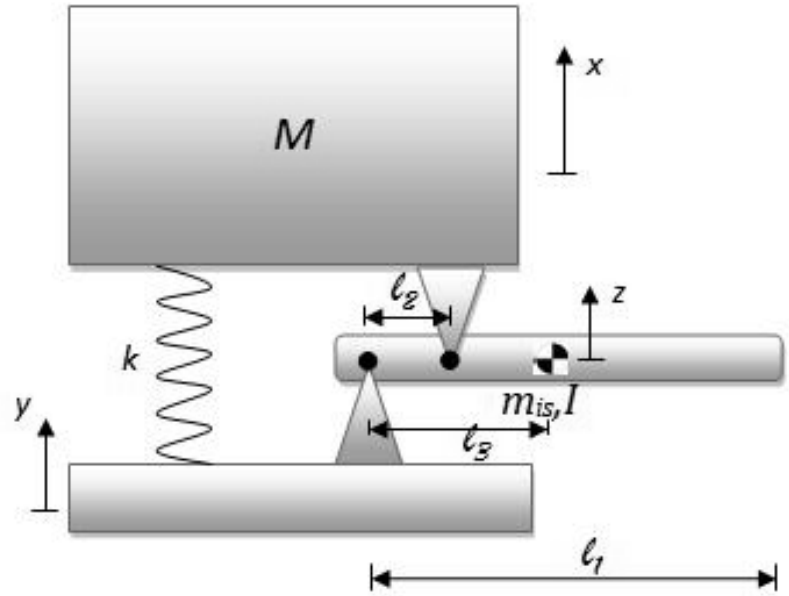



Figure 2.2. Isolation system with distributed mass lever.

$x$ and $y$. Denoting this angle by $\theta$ and assuming that $\theta$ is small we get

$$\theta = \frac{(x-y)}{l_2} = \left(\frac{\alpha}{l_1}\right)(x-y) \tag{2.11}$$

Using only $x$ and $y$ variables, the Lagrange equations of the system can be found as below.

$$L = T - V, \tag{2.12}$$

where $L$ is the Lagrangian, $T$ is the kinetic energy of the system and $V$ is the potential energy of the system. Therefore, $T$ and $V$ are found as

$$T = \frac{1}{2}M\dot{x}^2 + \frac{1}{2}I\frac{\alpha^2}{l_1^2}(\dot{x}-\dot{y})^2 + \frac{1}{2}m_{is}(\beta\dot{x} - (\beta-1)\dot{y})^2, \tag{2.13}$$

$$V = \frac{1}{2}k(x-y)^2, \tag{2.14}$$

$$\frac{d}{dt}\left(\frac{\partial L}{\partial \dot{x}}\right) - \frac{\partial L}{\partial x} = 0, \tag{2.15}$$

$$\frac{\partial L}{\partial \dot{x}} = M\dot{x} + I\frac{\alpha^2}{l_1^2}\dot{x} + m_{is}\beta^2\dot{x} - m_{is}\beta(\beta-1)\dot{y} - I\frac{\alpha^2}{l_1^2}\dot{y}, \tag{2.16}$$

$$\frac{d}{dt}(\frac{\partial L}{\partial \dot{x}}) = M\ddot{x} + I\frac{\alpha^2}{l_1^2}\ddot{x} + m_{is}\beta^2\ddot{x} - m_{is}\beta(\beta-1)\ddot{y} - I\frac{\alpha^2}{l_1^2}\ddot{y}, \tag{2.17}$$

$$\frac{\partial L}{\partial x} = -kx + ky, \tag{2.18}$$

where $I$ is defined as the mass moment of inertia of the lever arm about the mass center and $m_{is}$ is defined as the mass of the lever arm.

Equation of motion of the system is given in Equation 2.19,

$$\left(M + I\frac{\alpha^2}{l_1^2} + m_{is}\beta^2\right)\ddot{x} + kx = \left(m_{is}\beta(\beta-1) + I\frac{\alpha^2}{l_1^2}\right)\ddot{y} + ky. \tag{2.19}$$

Thus, resonance and anti-resonance frequencies of the system are,

$$\omega_p = \sqrt{\frac{k}{M + I\frac{\alpha^2}{l_1^2} + m_{is}\beta^2}}, \tag{2.20}$$

and

$$\omega_z = \sqrt{\frac{k}{m_{is}\beta(\beta-1) + I\frac{\alpha^2}{l_1^2}}}, \tag{2.21}$$

respectively.

While comparing the results from analytical and numerical models, the ratio of the anti-resonance frequency over resonance frequency will be helpful. This ratio does

not depend on the stiffness of the system and it is given in Equation 2.22.

$$\frac{\omega_z}{\omega_p} = \sqrt{\frac{M + I\frac{\alpha^2}{l_1^2} + m_{is}\beta^2}{m_{is}\beta(\beta-1) + I\frac{\alpha^2}{l_1^2}}}. \tag{2.22}$$

### 2.2.2. Flexure Hinges

In Figure 2.2, there are two hinges and a helical spring in the system. One can replace these components by two flexure hinges. Consider the system in Figure 2.3. The thin vertical lines are beam springs. When a force is applied to the system as shown in Figure 2.3, these beam springs deform such that their middle points act like hinges. Hence, they are called as flexure hinges. In Figure 2.3, $l_a$ is the length of the flexure hinges, $l_2$ is the length of the lever arm between two hinges, and $F$ is the vertical force on the right hinge.

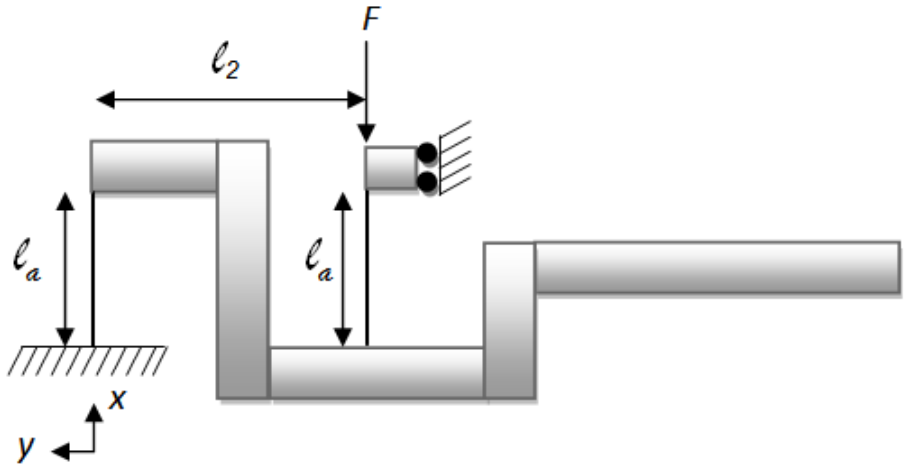



Figure 2.3. Lever with flexure hinges.

After deformation, the part of the lever arm between two hinges will become as in Figure 2.4. Force $F$ on the right hinge will generate a moment $M_o$ on the leftmost of the lever arm. If $E_1$ is the elastic modulus and $I_1$ is the inertia of the flexure hinges,

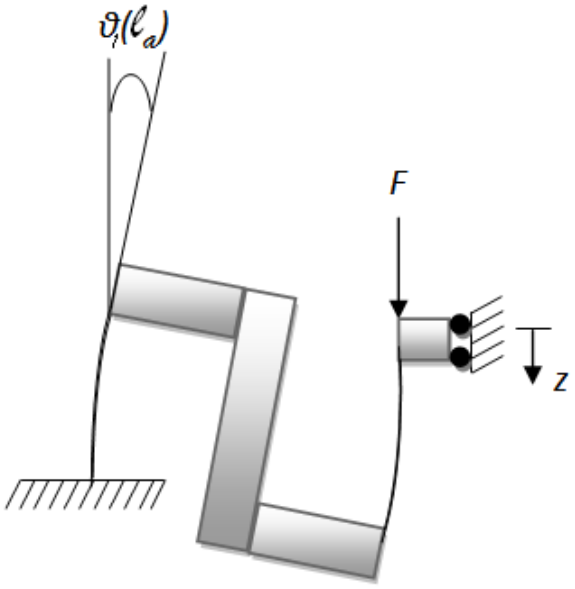



Figure 2.4. Lever arm representation for stiffness analysis after deformation.

$$\frac{\partial^2 y}{\partial x^2} = \frac{M_o}{E_1 I_1}, \tag{2.23}$$

$$\theta_1(l_a) = \frac{\partial y}{\partial x}|_{x=l_a} = \frac{M_o l_a}{E_1 I_1}, \tag{2.24}$$

are found where $\theta_1(x)$ is the angle between the flexure hinges and vertical axes. Assuming small $\theta_1$, we can get the displacement $z$ as,

$$z = \theta_1(l_a) l_2 = \frac{M_o l_a l_2}{E_1 I_1}, \tag{2.25}$$

Assuming identical flexure hinges, the two flexure hinges would bend by the same amount in opposite directions. Then, moment in the middle of the section with length

$l_2$ will be zero. Consequently, we can get $M_o$ as

$$M_o = \frac{Fl_2}{2}. \tag{2.26}$$

Using Equation 3.29 in Equation 2.25, we get

$$z = \theta_1 l_2 = \frac{Fl_2^2 l_a}{2E_1 I_1}, \tag{2.27}$$

Then the stiffness of the system is,

$$k = \frac{F}{z} = \frac{2E_1 I_1}{l_2^2 l_a}. \tag{2.28}$$

### 2.2.3. Optimization of the Design

In this study, it is aimed to optimize the design to get maximum isolation in the widest frequency range. To optimize the model in the Section 2.2.1, the topology optimization application in [44] is used. Topology optimization is introduced by Bendsoe and Kikuchi in 1988 [45]. Since then, various studies are conducted in the area. The topology optimization method solves the problem of distributing a given amount of material in a design domain subject to load and boundary conditions, such that the stiffness of the structure is maximized. The design domain is gray in the beginning. This means all the material is distributed to the domain. When the iterations starts, some parts of the domain become white which refers there is no material there and some parts become black which refers that material is present there for the given problem. In the end the application maximizes the stiffness of the system for the given mass. This objective function will also maximize the natural frequencies, thus it is convenient for our objective and it can be used in this study. The result of the application is in Figure 2.5. The model which is the result of the topology optimization (see Figure 2.5) is simplified in order to obtain robustness of the lever arm and ease of production.

In Figure 2.6, there is no auxiliary mass on tip of the lever arm. Lever arm is

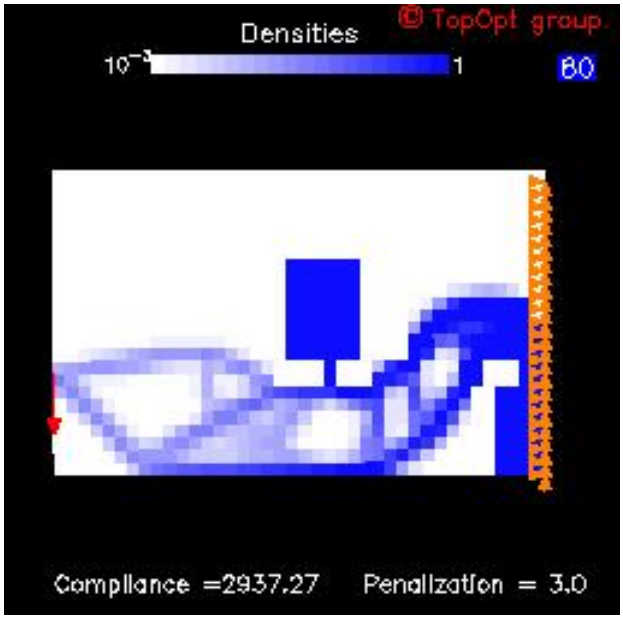



Figure 2.5. The result of the topology optimization of the lever [44].

not assumed massless in the analysis anymore, so the auxiliary mass can be thought as distributed to the lever arm.

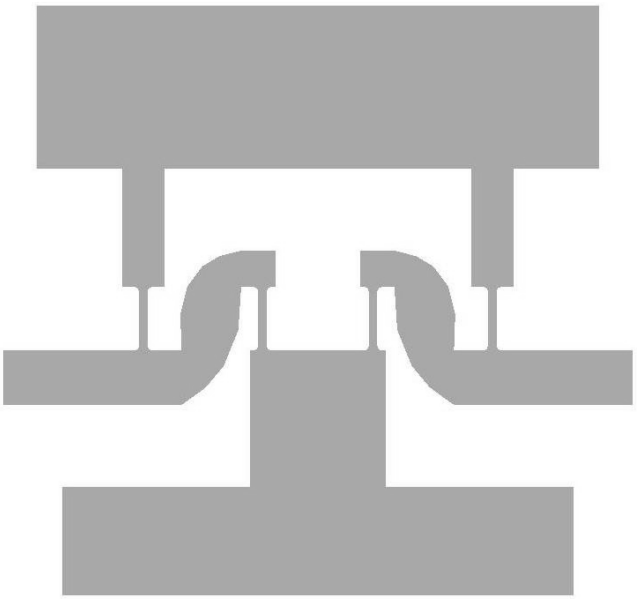


Figure 2.6. Front view of the compliant isolator.

The parameters of the passive vibration isolator design is selected as below:

$$M = 1.145\,kg,\ m_{is} = 7.2 \times 10^{-2}\,kg,\ I = 7.1 \times 10^{-6}\,kgm^2,$$
$$l_1 = 30.5\,mm,\ l_2 = 14\,mm,\ l_3 = 14\,mm. \tag{2.29}$$

Using Equation 2.22 and the given parameters in Equation 2.29, the frequency ratio,

$$\frac{\omega_z}{\omega_p} = 5.9, \tag{2.30}$$

is found.

In the above calculation the lever is assumed rigid, therefore the system has single degree of freedom.

In Figure 2.6 the thickness of the flexure hinges ($t$) is 1 mm, length of the flexure hinges ($l_a$) is 7 mm, length of the lever between two flexure hinges ($l_2$) is 14 mm, and depth of the whole planar mechanism ($w$) is 20 mm. Using the given parameter values in Equation 2.29 and assuming steel as the flexure hinge material ($E_1$ = 200 GPa),

$$I_1 = \frac{1}{12} w t^3, \tag{2.31}$$

stiffness is obtained as

$$k = \frac{2E_1 I_1}{l_2^2 l_a} = \frac{E_1 w t^3}{6 l_2^2 l_a} = 0.972 \times 10^6\ N/m. \tag{2.32}$$

To observe the natural frequency value originated from flexibility of the lever arm and the effect of this to the ratio found in Equation 2.30, finite element model of the system will be constructed in the following section.

## 2.3. The Finite Element Model

The model used in finite element analysis is shown in Figure 2.7. The model has 65 mm height, 74 mm width and 20 mm depth. There is a 1 kg point mass which brings the mass of the main body ($M$) to 1.145 kg on top of the model. The reason for adding extra mass is to isolate the vibration of the load aside from the mass of the isolator system.

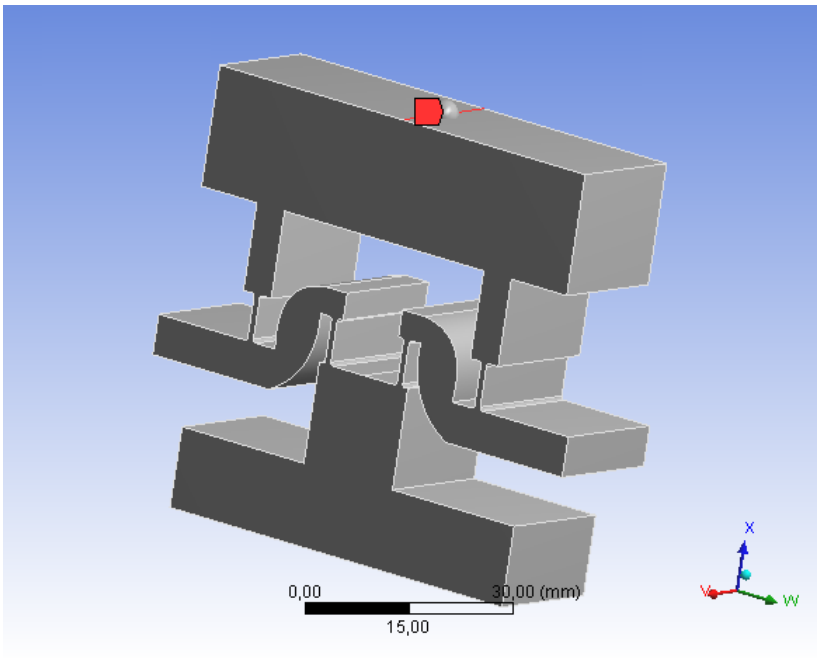



Figure 2.7. Isometric view of the compliant isolator.

### 2.3.1. Static Structural Analysis

To find the stiffness of the system, its bottom surface is fixed and a force with 100 N magnitude is applied from top surface as shown in Figure 2.8.

The stiffness of the system is found as below for the resultant displacement.

$$k = \frac{F}{\delta} = \frac{100}{9.754 \times 10^{-5}} = 1.025 \times 10^{6}\ N/m. \tag{2.33}$$

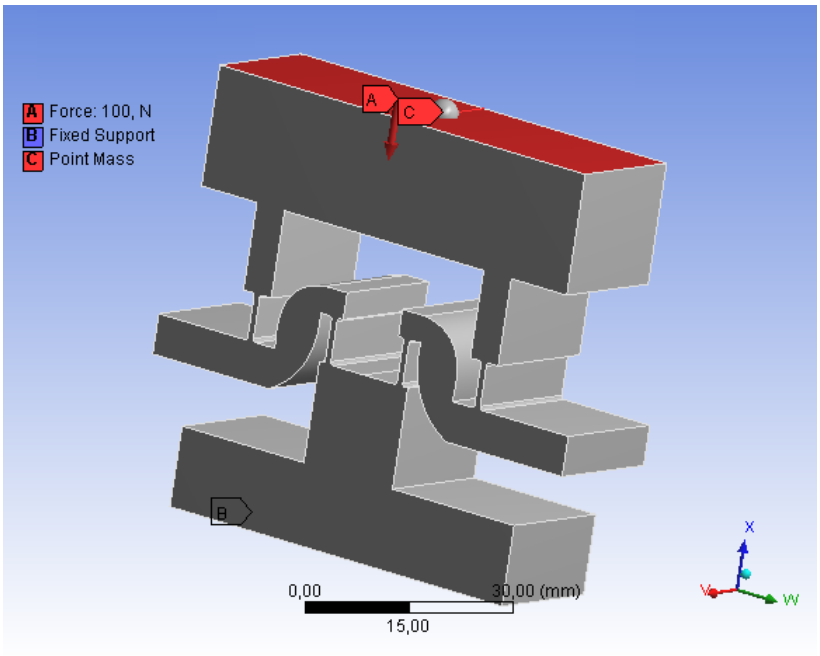



Figure 2.8. Static structural analysis of the compliant isolator.

We see that stiffness value is close to the one in Equation 2.32.

The parameters given in Equation 2.29 is used for a lever with single arm. There are two separate lever arms in the existing system and total mass and inertia of these arms are equal to the values in Equation 2.29. If the parameters and the stiffness in Equation 2.33 are put into Equation 2.20 and 2.21, the first resonance and anti-resonance frequencies of the system are found as below, respectively.

$$\omega_p = \sqrt{\frac{k}{M + I\frac{\alpha^2}{l_1^2} + m_{is}\beta^2}} = 143.9\ Hz, \tag{2.34}$$

$$\omega_z = \sqrt{\frac{k}{m_{is}\beta(\beta - 1) + I\frac{\alpha^2}{l_1^2}}} = 846.6\ Hz. \tag{2.35}$$

If the system is modeled as single degree of freedom, the transmissibility plot in

Figure 2.9 is obtained.

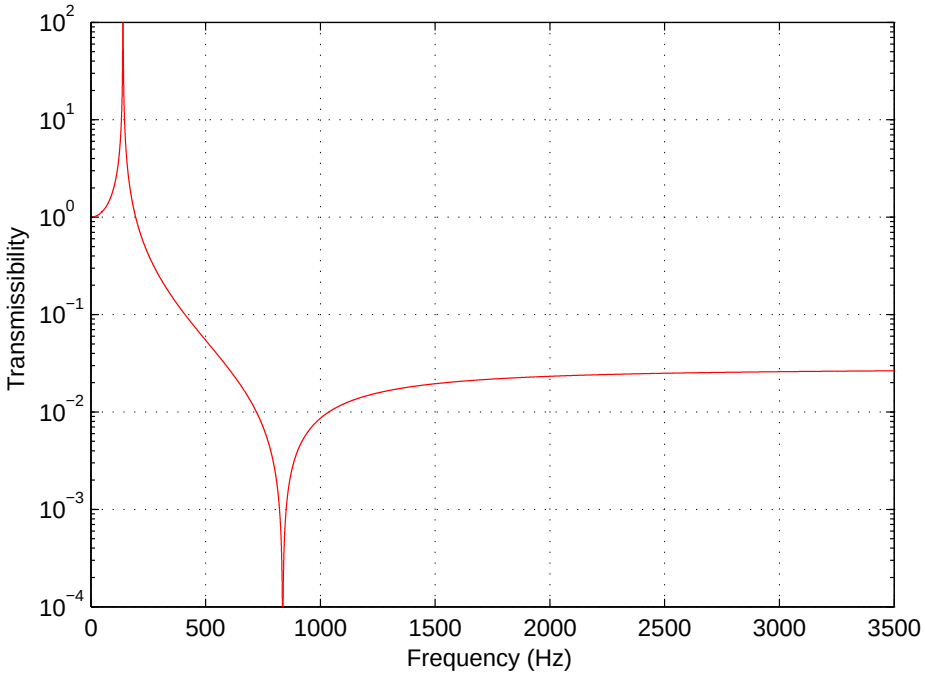



Figure 2.9. The transmissibility plot of the single degree of freedom model of the compliant isolator.

### 2.3.2. Modal Analysis

In modal analysis, the first 10 resonance frequencies of the compliant isolator are found. These frequencies can be seen in Table 2.1. From these frequencies, first two modes which cause motion in vertical direction (X direction in Figure 2.10) are the second (140.48 Hz) and seventh (3375.4 Hz) modes. Mode shapes at these two frequencies are provided in Figure 2.10 and 2.11, respectively. As it can be seen, the frequency value at the second mode (140.48 Hz) is similar to previous calculation in Equation 2.34.

### 2.3.3. Harmonic Analysis

Since the first two modes which cause motion in vertical direction are at 140.48 Hz and 3375.4 Hz, vibration isolation operation will be carried out between these two

Table 2.1. The first 10 resonance frequencies of the compliant isolator.

| **Mode** | **Frequency [Hz]** |
|---|---|
| 1 | 63.777 |
| 2 | 140.48 |
| 3 | 263.76 |
| 4 | 598.81 |
| 5 | 1193.2 |
| 6 | 1477.6 |
| 7 | 3375.4 |
| 8 | 3765 |
| 9 | 5373 |
| 10 | 7542.3 |

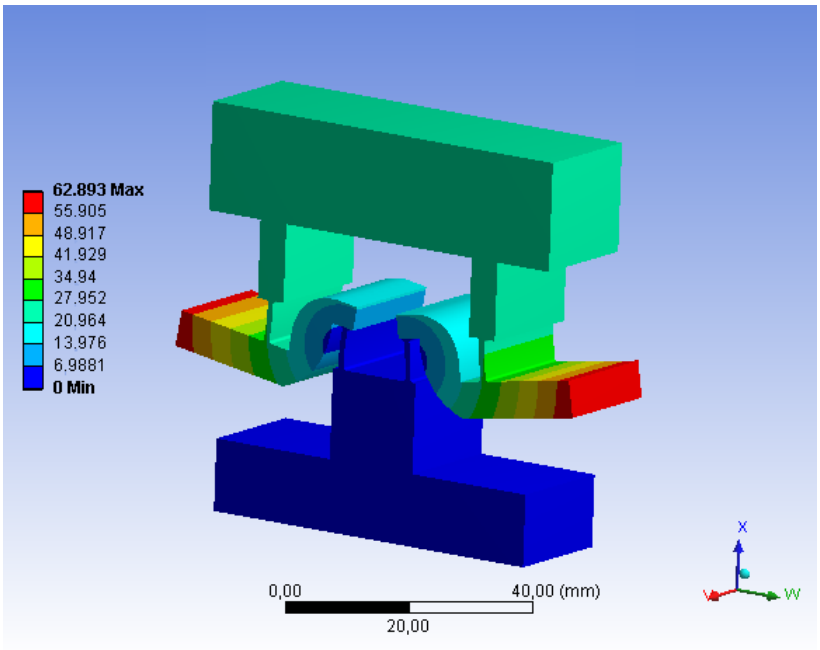



Figure 2.10. Mode shape of the system at 140.48 Hz.

frequency values. In this manner, the frequency range of the harmonic analysis is selected as 0-3750 Hz. In harmonic analysis, an upwards displacement with 1 mm amplitude is applied to the model from the bottom surface and whole frequency range is scanned with 10 Hz steps. The frequency response (frequency-displacement) plot of

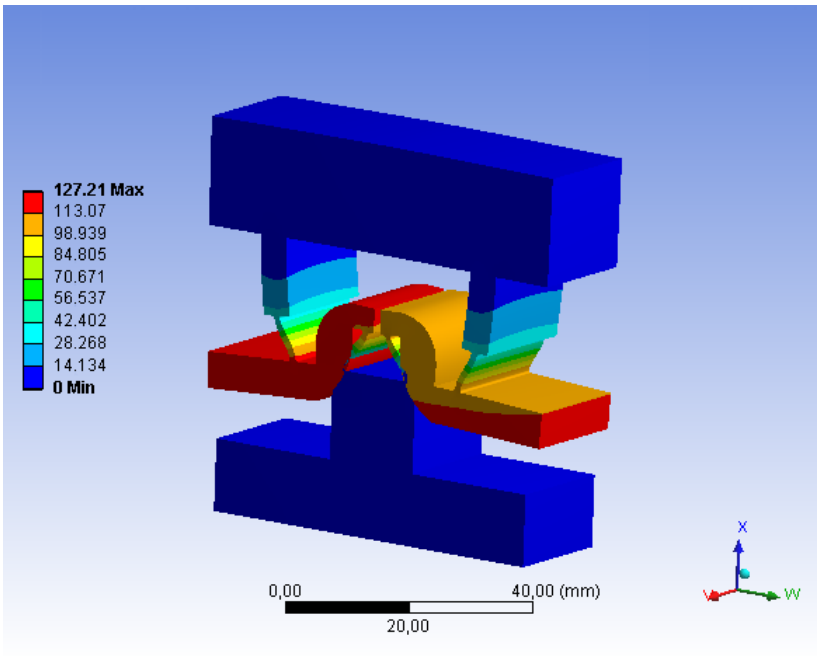



Figure 2.11. Mode shape of the system at 3375.4 Hz.

the system in the desired range is in Figure 2.12. In this plot, the resonance frequencies at 140.48 Hz and 3375.4 Hz, and the first anti-resonance frequency at 830 Hz can be seen. This result is compatible with Equation 2.35 that gives $\omega_z = 846.6$ Hz. If we want to compare the results without using stiffness of the system, we can use the anti-resonance to resonance frequency ratio given in Equation 2.22. After harmonic analysis, the result of this ratio is,

$$\frac{\omega_z}{\omega_p} = \frac{830}{140} = 5.9. \tag{2.36}$$

The previous analytical study also gave the same result. Thus, finite element analysis confirms the correctness of the model used in analytic study.

The finite element analysis is performed excluding the effect of damping, therefore the amplitudes in Figure 2.12 seems very high. However, in reality these amplitudes will be less due to the effect of damping in the material. Here, the positions of the

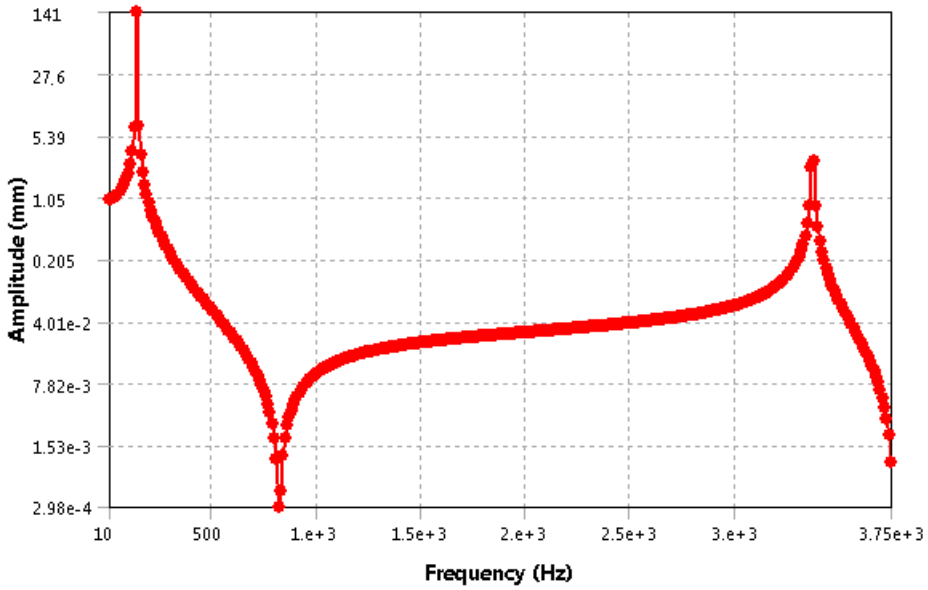



Figure 2.12. Frequency response plot of the system via finite element analysis.

resonance and anti-resonance frequencies are important.

When the harmonic analysis results are examined, it can be seen that there will be very good isolation around the anti-resonance frequency. For example, if the desired transmissibility level is 1/100, it can be attained between 720-1020 Hz. Besides, relatively small isolation levels can be attained in wider frequency range. For example, if the desired transmissibility level is 1/10, the model will achieve this rate between 410-3210 Hz, which is much wider than the previous case. In addition, if the thickness and/or length of the hinges in the design is changed, the stiffness of the system can also be changed and the resonance and anti-resonance frequencies can be adjusted to the desired isolation frequency. If higher isolation level is required at some frequency, then the desired isolation level can be achieved by adjusting the anti-resonance frequency to that frequency.

In Figure 2.13, the graphs of the two models in Figure 2.9 and 2.12 are plotted in the same graph. Figure 2.13 tells us that the model with single degree of freedom

and finite element model is very similar along the first resonance and anti-resonance frequencies. However at high frequencies, other resonance frequencies in the finite element model step in and cause differentiation from single degree of freedom model.

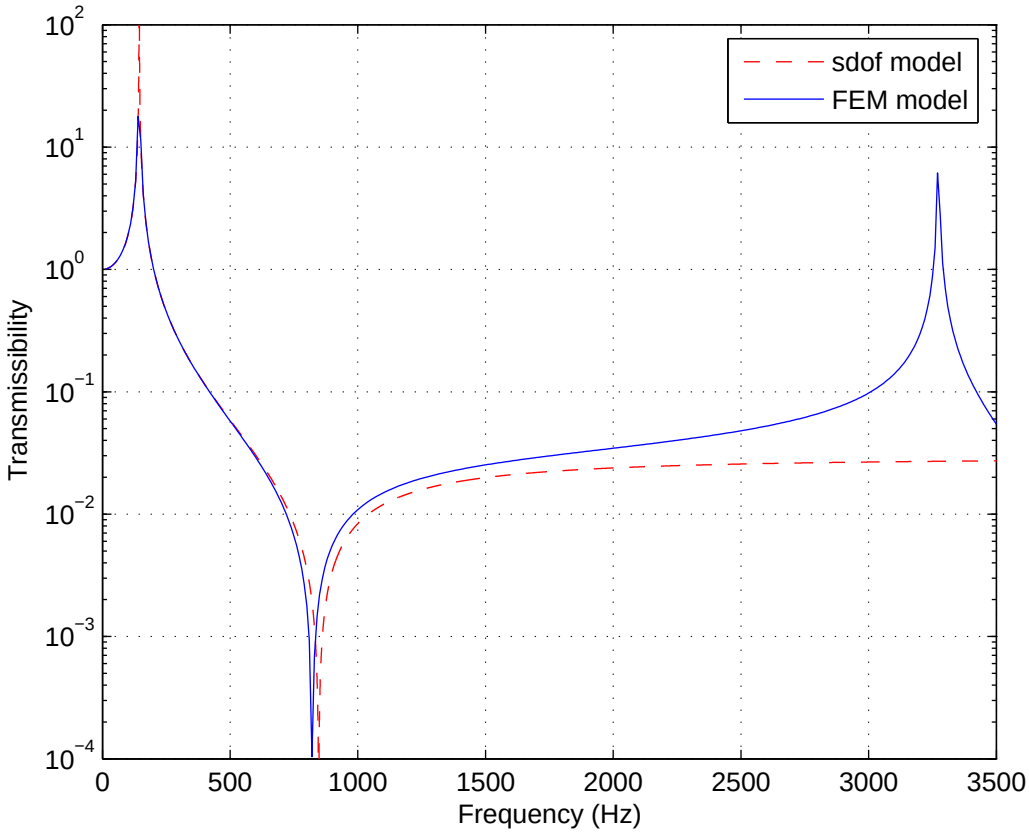



Figure 2.13. Frequency response plot of the SDOF analytic and FEM model for $M$=1.145 kg.

As a comparison, we determine the frequency response plot of the system without the extra point mass (1 kg). In that case $M = 0.145$ kg. Figure 2.14 shows the frequency response plot for the FEM and the single degree of freedom analytical model. It can be seen that resonance in this case is around 320 Hz. However, the anti-resonance frequency didn't change (830 Hz) since the anti-resonance frequency is independent of $M$. Moreover, the second resonance frequency in the FEM model became 3396 Hz which is very close to the case with the extra point mass.

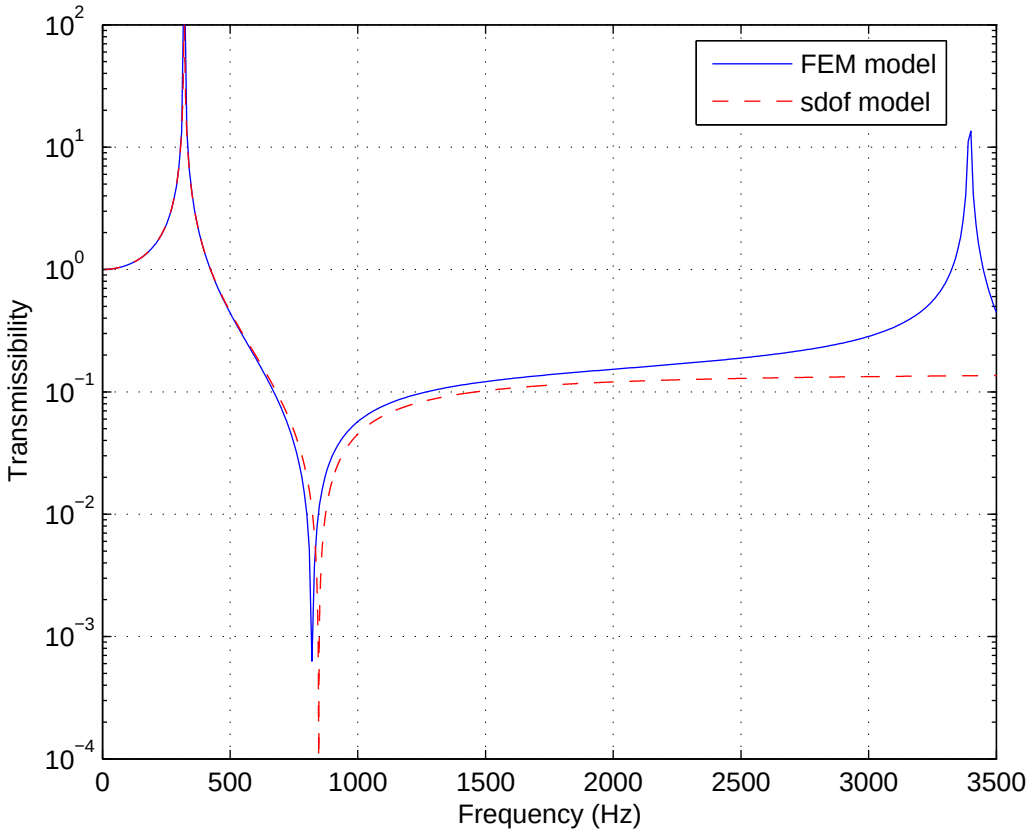



Figure 2.14. Frequency response plot of the SDOF analytic and FEM model for $M$=0.145 kg.

## 2.4. Experimental Modal Analysis

The first design which is lever-type vibration isolator using compliant mechanism is manufactured with wire electrical discharge machining (WEDM). The designed isolator and 1 kg extra mass which brings the mass of the main body ($M$) to 1.145 kg can be seen in Figure 2.15. This extra mass was simplified as a point mass in finite element analysis. To attach the extra mass to the vibration isolator, a bolt passing through its center of gravity is used (see Figure 2.15).

Experimental modal analysis is performed by impact hammer test. The test setup can be seen in Figure 2.16. The vibration isolator is hanged horizontally with strings. By doing this, it is aimed that the system should oscillate freely in the horizontal direction and there wouldn't be any other stiffness element that can ruin the experiment



Figure 2.15. The manufactured vibration isolator design and extra mass.

in that direction. The hammer is hit from the bottom surface of the system. With the impulse coming from the tip of the hammer, it would result in all modes of vibration being excited up to the cutoff frequency of the impact hammer. An appropriate hammer tip is chosen such that the cutoff frequency is above our target frequency range. A load cell is attached to the end of the hammer to record the force and an accelerometer is attached to the top surface of the system to record the acceleration.

### 2.4.1. Analyzing Test Results

Random signal analysis in testing is an important issue. The transducer used to measure both the input and output during a vibration test usually contains noise [46]. Also, performing a number of identical tests and averaging the results increase confidence level in a measured quantity. The autocorrelation function of the random signal $x(t)$ is,

$$R_{xx}(\tau) = \lim_{T\to\infty} \frac{1}{T} \int_0^T x(t)x(t+\tau)dt. \tag{2.37}$$

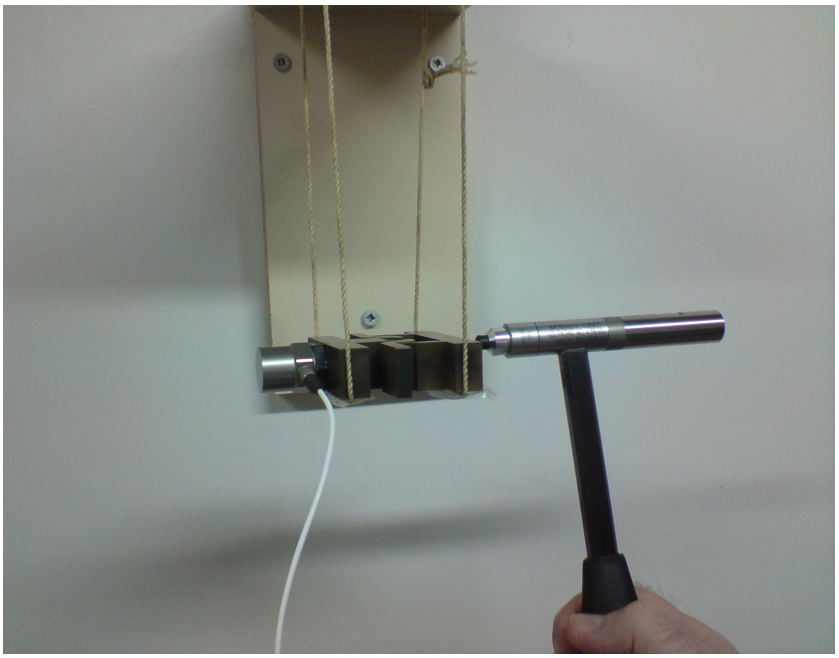


Figure 2.16. Impact hammer test of the isolator design.

The power spectral density (PSD) of a signal is the Fourier transform of the signal's autocorrelation function:

$$S_{xx}(\omega) = \frac{1}{2\pi}\int_{-\infty}^{\infty} R_{xx}(\tau)e^{-j\omega\tau}d\tau. \tag{2.38}$$

PSD of the input or driving force can be related to the PSD of the response ($S_{ff}(\omega)$) and frequency response function ($H(\omega)$) of the system by

$$S_{xx}(\omega) = |H(\omega)|S_{ff}(\omega). \tag{2.39}$$

The frequency response function can also be related to the cross-correlation between two signals $x(t)$ and $f(t)$. The cross-correlation function ($R_{xf}(\tau)$), for the two signals $x(t)$ and $f(t)$, is defined in Equation 2.40. If $x(t)$ is the response of the structure to the driving force $f(t)$, then

$$R_{xf}(\tau) = \lim_{T\to\infty}\frac{1}{T}\int_{0}^{T} x(t)f(t+\tau)dt. \tag{2.40}$$

Similarly, the cross-spectral density is the Fourier transform of the cross-correlation function:

$$S_{xf}(\omega) = \frac{1}{2\pi}\int_{-\infty}^{\infty} R_{xf}(\tau)e^{-j\omega\tau}d\tau. \tag{2.41}$$

The frequency response function, $(H(j\omega))$, is related to the spectral density functions by the two equations

$$S_{fx}(\omega) = H(j\omega)S_{ff}(\omega). \tag{2.42}$$

$$S_{xx}(\omega) = H(j\omega)S_{xf}(\omega). \tag{2.43}$$

Equation 2.42 and 2.43 hold if the structure is excited by a random input $f(t)$ resulting in the response $x(t)$. Note that Equation 2.42 and 2.43 use different power spectral densities to calculate the same quantity. This fact can be used to check the consistency of $H(j\omega)$. The coherence function, $\gamma^2$, is defined to be the ratio of the two values of $H(j\omega)$ calculated from Equation 2.42 and 2.43 [46]. Coherence function is,

$$\gamma^2 = \frac{|S_{xf}(\omega)|^2}{S_{xx}(\omega)S_{ff}(\omega)} \tag{2.44}$$

which always lies between 0 and 1. Actually, the coherence should be 1 if the measurements are consistent. It should be independent of how it is calculated. However, in reality it is not always 1. Coherence is a measure of the noise in the signal or nonlinearities in the system. As it goes from 1 to 0, noise in the signal or nonlinearities increase. In practice, data with a coherence of less than 0.75 are not used and indicate that the test should be done over, or the data should be examined over a smaller frequency range [46].

Our experiment is carried out in two steps: one with the extra mass, and one without the extra mass. Each experiment is performed 10 times. The results are aver-

aged and coherence values are calculated by the computer program that is connected to the experiment setup. In fact, we had to repeat each experiment so many times to get 10 acceptable results. The reason for this is we got a double impact error in most of the trials.

Figure 2.17 shows the results of the experiment with the extra mass and hard tip hammer. The frequency range of interest for this hammer tip is 0-4096 Hz. The sample frequency is 8192 Hz to prevent aliasing. The cutoff frequency is above this value. The frequency resolution in all of the experiments is 0.5 Hz. In Figure 2.17, results for 0-3500 Hz range is given. There is a peak at about 250 Hz. This peak originates from the uneven swing of the system. Neglecting this, the first resonance frequency is about at 350 Hz. This value is higher than the analytical and finite element analysis results. There is a decrease in amplitude between 700-1200 Hz. However, we cannot detect the exact location of anti-resonance frequency from this graph. And there is a peak about 1700 Hz which is unexpected. Coherence is also low at 1700 Hz. Coherence plot for Figure 2.17 is given in Figure 2.18. From Figure 2.18, we can deduce that after 1550 Hz, coherence is below 0.75 and the results are unreliable. After repeating the experiment, we decided to examine the data over a smaller frequency range. One level smaller frequency range is 0-2048 Hz. In addition, this range is the only one which contains 0-1550 Hz. Thus, softer hammer tip with 0-2048 Hz frequency range of interest is used. Figure 2.19 shows the results for this experiment. Figure 2.20 is the coherence plot for Figure 2.19. In Figure 2.20, we see that coherence values are relatively good up to 1680 Hz. In Figure 2.19, first resonance frequency is at 352 Hz and there is a minimum point at 566 Hz. Since transmissibility is also minimum at 566 Hz, this frequency can be noted as anti-resonance frequency. We expect the anti-resonance frequency to be around 820 Hz. However, 1033 Hz is a local minimum and also a candidate for anti-resonance frequency. Nevertheless, we cannot determine the exact location of anti-resonance frequency.

In Figure 2.21, the results of the experiment without the extra mass by hammer tip with sample frequency 4096 Hz is presented. Here, the frequency range of interest is 0-2048 Hz. Coherence plot of this experiment is in Figure 2.22. In Figure 2.21,

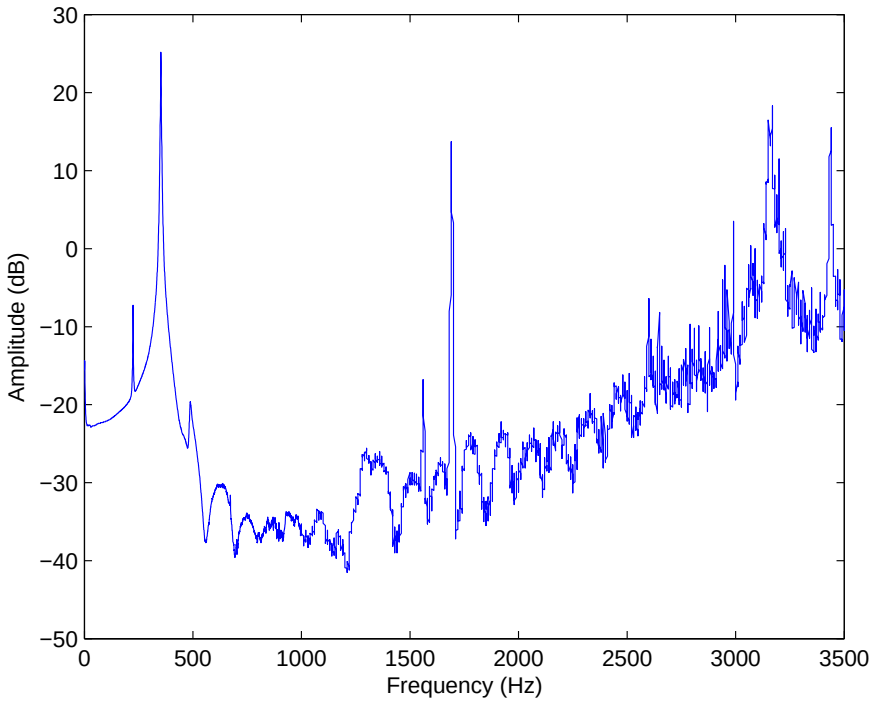



Figure 2.17. Experimental frequency response plot for isolator mass of 1.145 kg by hard tip hammer (Sample frequency = 8192 Hz).

resonance frequencies are shown at 453 Hz and 1199 Hz. However, coherence value at 1199 Hz is below 0.75, thus this second resonance frequency is unreliable. We have found the first resonance frequency at 320 Hz from analytical model and FEM model. The experimental result, 453 Hz, does not agree with this result. Possible anti-resonance frequencies are also shown in Figure 2.21 at 859 Hz and 932.5 Hz. The analytical model has given the anti-resonance frequency at 846 Hz and FEM model at 830 Hz. The experimental results are compatible with these results. However, there are many local minimum points between 700-1000 Hz. Therefore, we decided to focus on a smaller frequency range. Figure 2.23 shows the results for the experiment without extra mass and frequency range of interest 0-1024 Hz. Figure 2.24 is the coherence plot for Figure 2.23. Coherence values in this experiment is in acceptable range which is 1-0.95. Thus, observing Figure 2.23, the first resonance frequency is at 454.5 Hz and the first anti-resonance frequency can be at either 803 Hz or 924 Hz. Again, the resonance frequency doesn't agree with the analytic and FEM results and the location of anti-resonance frequency cannot be detected exactly.

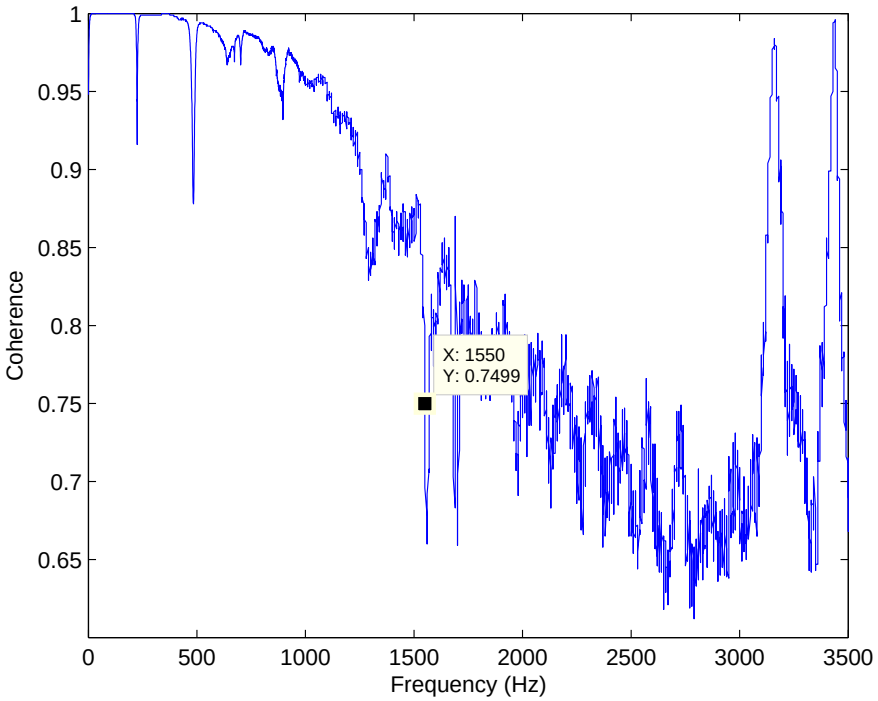



Figure 2.18. Coherence plot for isolator mass of 1.145 kg by hard tip hammer (Sample frequency = 8192 Hz).

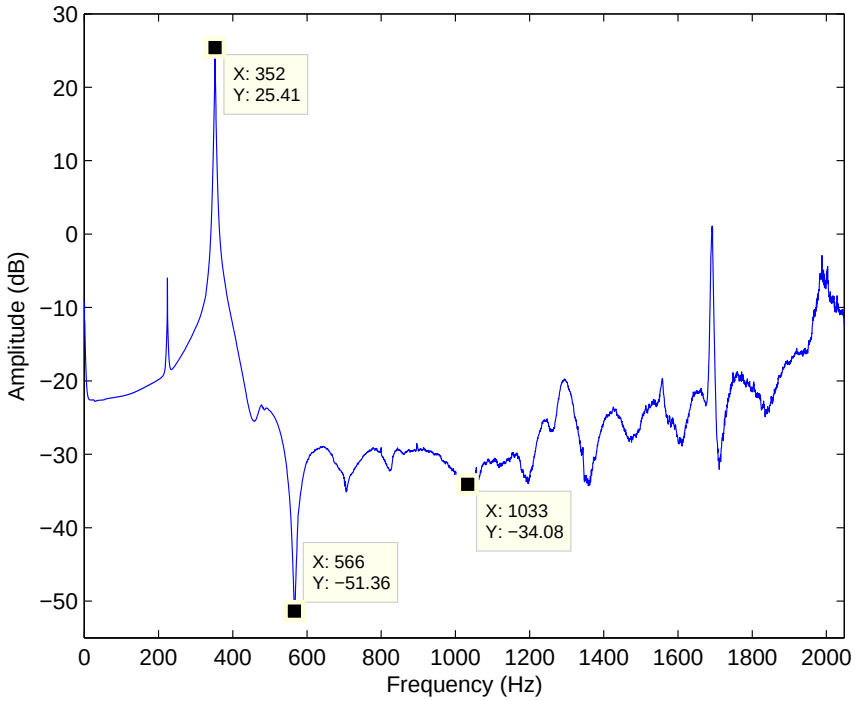



Figure 2.19. Experimental frequency response plot for isolator mass of 1.145 kg by soft tip hammer (Sample frequency = 4096 Hz).

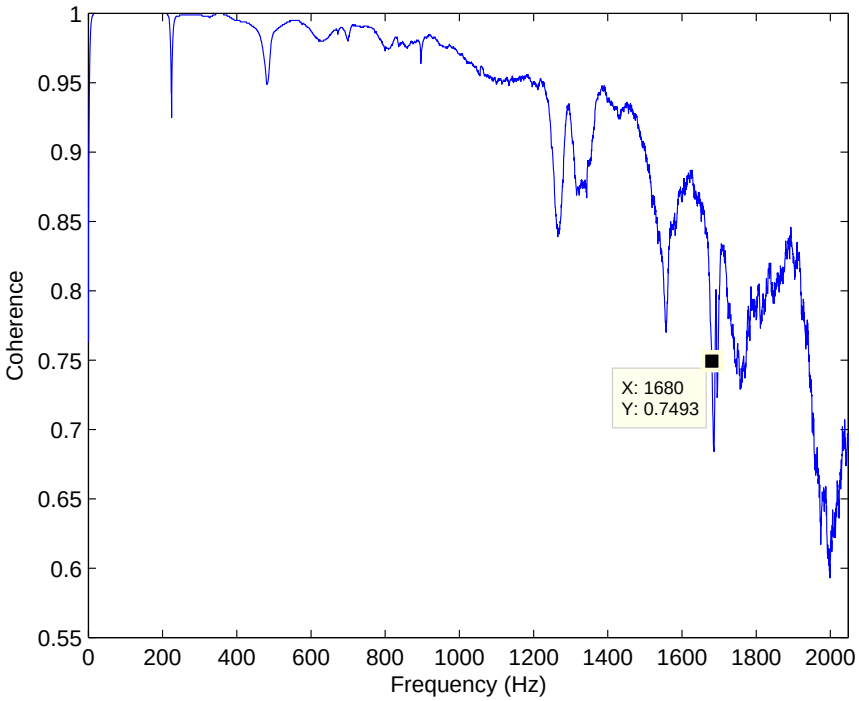



Figure 2.20. Coherence plot for isolator mass of 1.145 kg by soft tip hammer (Sample frequency = 4096 Hz).

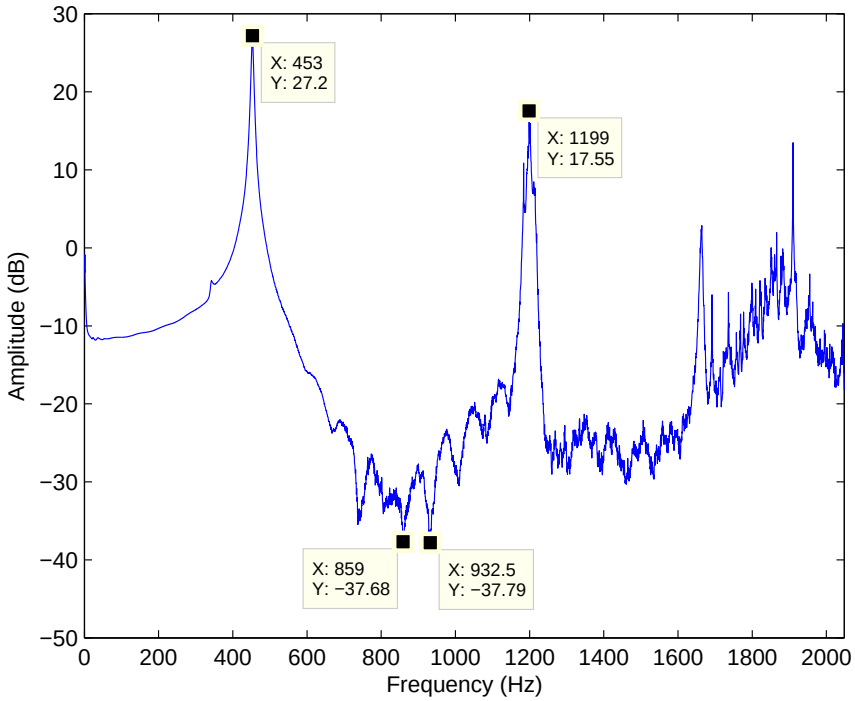



Figure 2.21. Experimental frequency response plot for isolator mass of 0.145 kg by hard tip hammer (Sample frequency = 4096 Hz).

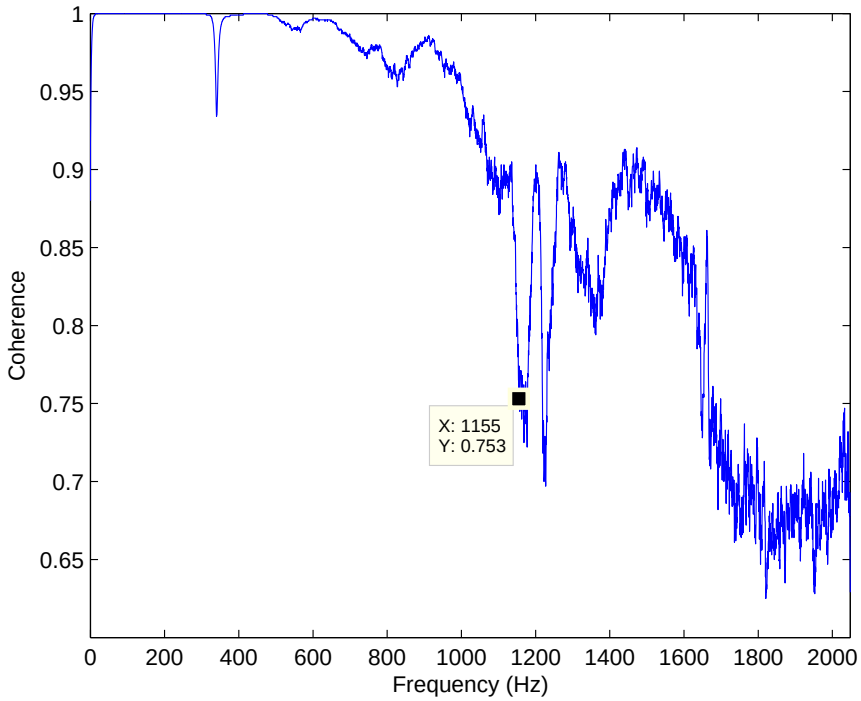



Figure 2.22. Coherence plot for isolator mass of 0.145 kg by hard tip hammer (Sample frequency = 4096 Hz).

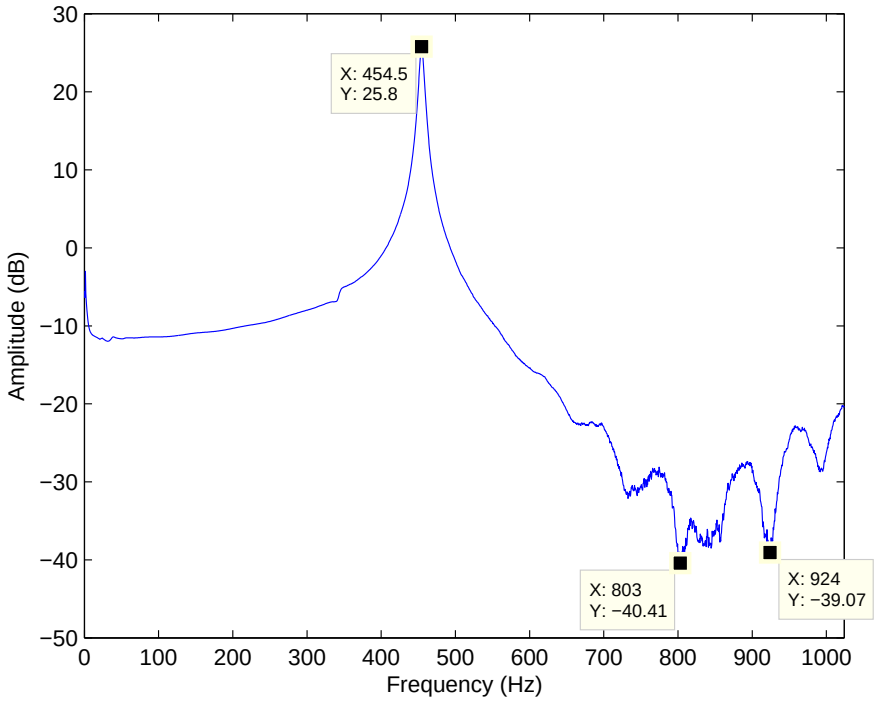



Figure 2.23. Experimental frequency response plot for isolator mass of 0.145 kg by soft tip hammer (Sample frequency = 2048 Hz).

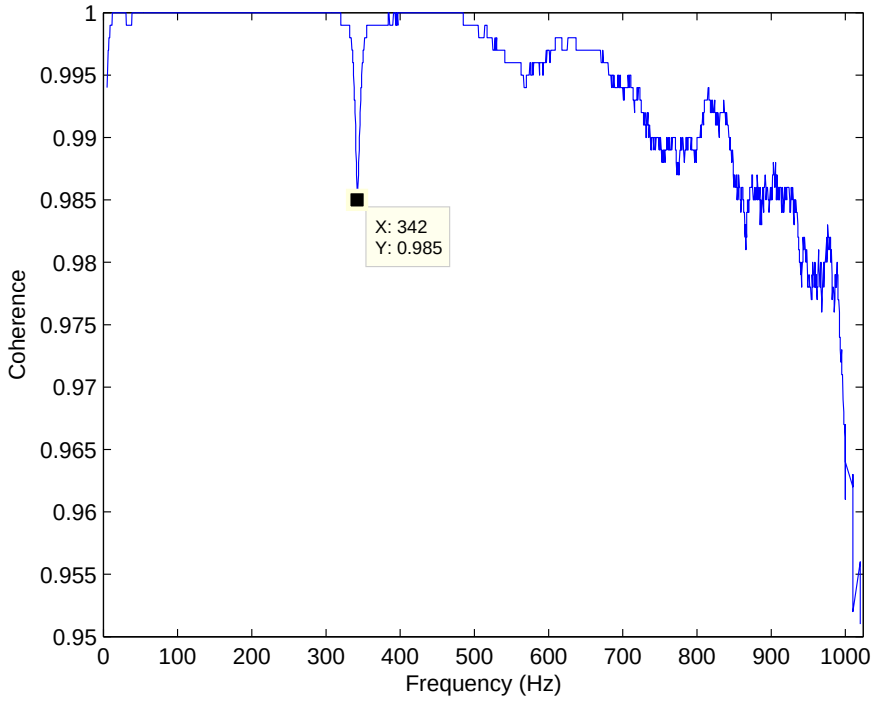



Figure 2.24. Coherence plot for isolator mass of 0.145 kg by soft tip hammer (Sample frequency = 2048 Hz).

# 3. QUASI-ZERO-STIFFNESS MECHANISM

In the design of the bistable buckled straight-beam mechanisms, straight beam is axially compressed to buckle to stable positions at either side. Since bistable mechanism is obtained when beams are in compression, negative stiffness is attained. Modeling buckling modes of this mechanism is provided below [18]. The beam equation describing a straight beam subjected to an axial load $p$ is

$$E_2 I_2 \frac{d^4 w}{dx^4} + p \frac{d^2 w}{dx^2} = 0 \tag{3.1}$$

where $w$ is the lateral beam displacement, $E_2$ is the elastic modulus of the beam material and $I_2$ is the moment of inertia of the beam. With clamped-clamped conditions, the boundary conditions of Equation 3.1 are

$$w(0) = w(l) = 0, \quad \left(\frac{dw}{dx}\right)_{x=0} = \left(\frac{dw}{dx}\right)_{x=l} = 0. \tag{3.2}$$

where $l$ is the length of the beam. Normalize the axial force by

$$N^2 = \frac{pl^2}{E_2 I_2}. \tag{3.3}$$

This is a homogeneous Sturm-Liouville problem, for which the eigenvalues $N_j$ must satisfy

$$\sin\left(\frac{N_j}{2}\right)\left[\tan\left(\frac{N_j}{2}\right) - \frac{N_j}{2}\right] = 0 \tag{3.4}$$

which allows two kinds of solution, namely

$$\left.\begin{array}{l} w_j(x) = C\left[1 - \cos\left(N_j \frac{x}{l}\right)\right] \\ N_j = (j+1)\pi \end{array}\right\} j = 1, 3, 5... \tag{3.5}$$

and

$$\left.\begin{array}{l} w_j(x) = C\left[1 - 2\frac{x}{l} - \cos\left(N_j \frac{x}{l}\right) + \frac{2\sin(N_j \frac{x}{l})}{N_j}\right] \\ N_j = 2.86\pi, 4.92\pi... \end{array}\right\} j = 2, 4, 6... \tag{3.6}$$

A common bistable mechanism involves a prestressed straight beam buckled into its first mode [47]. Since buckling can take either an up or down direction, this creates two stable positions for the mechanism. First two buckling modes can be seen in Figure 3.1.

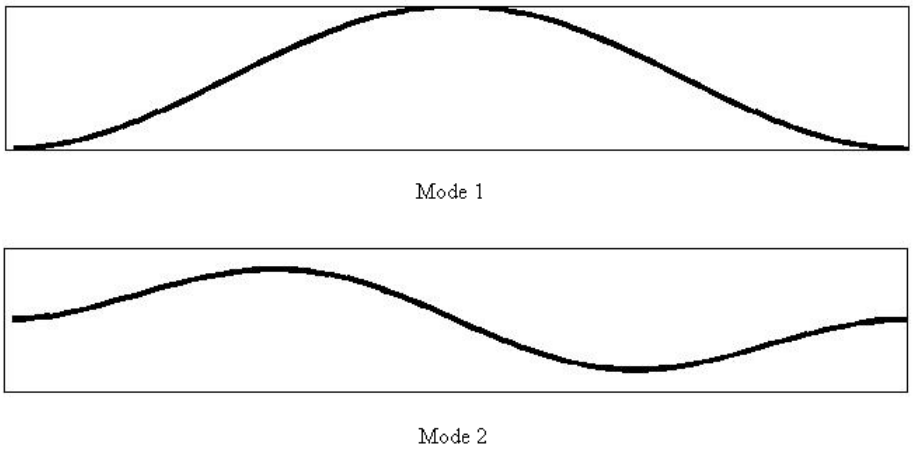



Figure 3.1. First two buckling modes for a clamped-clamped beam.

In this section, quasi-zero-stiffness mechanism is included in the isolator design. The isolator system is modified such that it became adjustable. Although flexure hinges are still being used, the isolator system (see Figure 3.2 and Figure 3.3) does not consist of a single piece anymore. In the current design, the length or even the thickness of the flexure hinges can be altered, so that the stiffness of the system can be changed. Notice that there is only one lever in this system, since the quasi-zero-stiffness mechanism enables parallel motion.

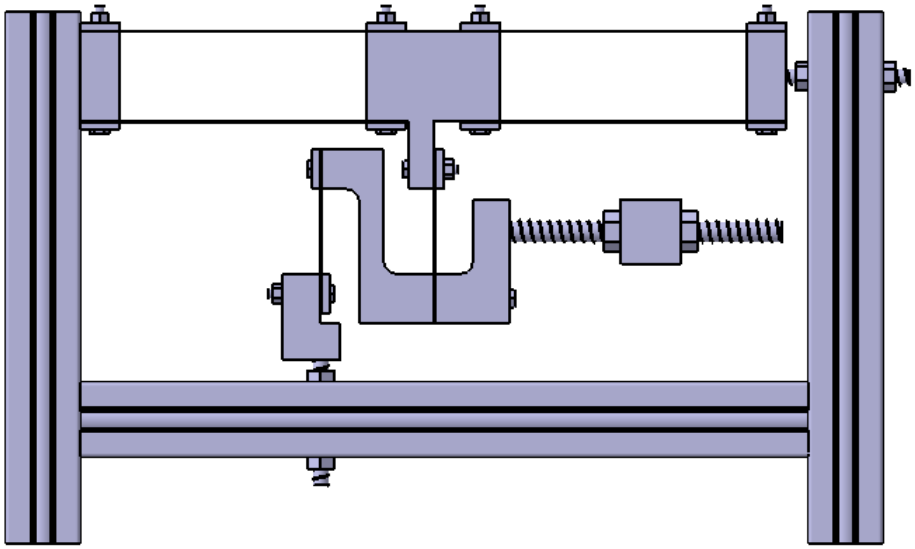


Figure 3.2. Front view of the isolator design with QZS mechanism.

### 3.1. Analysis of the System with Quasi-Zero-Stiffness Mechanism

In Section 2.2.2, positive stiffness of the system was found as

$$k_p = \frac{2E_1 I_1}{l_2^2 l_a}. \tag{3.7}$$

where $E_1$ is the elastic modulus and $I_1$ is the inertia of the flexure hinges, $l_a$ is the length of the flexure hinges, and $l_2$ is the length of the lever arm between two hinges (see Figure 3.4 and 3.5).

To have quasi-zero-stiffness, our design has a bistable mechanism that produce negative stiffness very similar in [18–22]. This mechanism consists of two parallel beams. These beams are axially compressed to buckle to produce negative stiffness in the vertical direction. Critical force for the beam with pinned-pinned conditions is

$$P_{cr} = \frac{\pi^2 E_2 I_2}{l^2}. \tag{3.8}$$

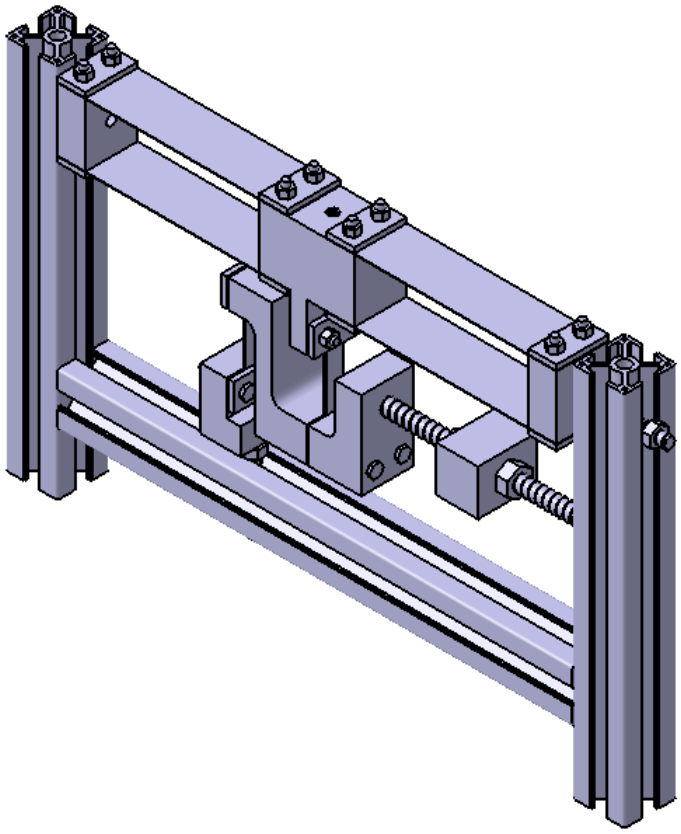


Figure 3.3. Isometric view of the isolator design with quasi-zero-stiffness mechanism.

where $E_2$ is the elastic modulus and $I_2$ is the inertia of the negative stiffness elements, $l$ is the length of the negative stiffness elements. Likewise, critical force for the beam with clamped-clamped conditions is 4 times of the pinned-pinned case which is

$$P_{cr} = \frac{4\pi^2 E_2 I_2}{l^2}. \tag{3.9}$$

In Figure 3.6, under small vertical displacement vertical force exerted by an initially horizontal buckled beam which has initial length $l$ can be seen. Inserting $P_{cr}$ in Equation 3.9 to the equation found in Figure 3.6,

$$F = \frac{-4\pi^2 E_2 I_2 y}{l^3} \tag{3.10}$$

is found. In Figure 3.7, a schematic diagram of buckled beams used in this study can

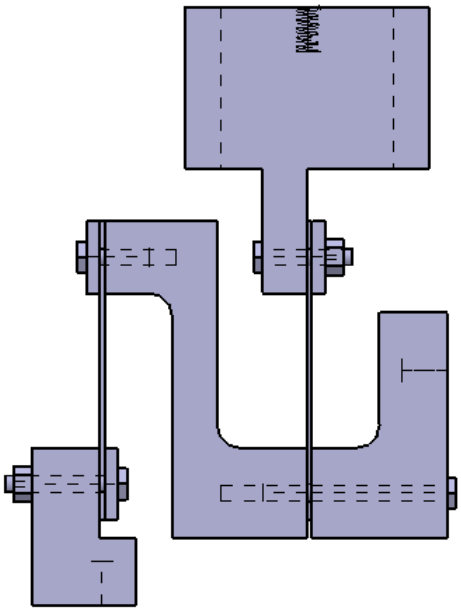


Figure 3.4. Flexure hinges that produce positive stiffness.

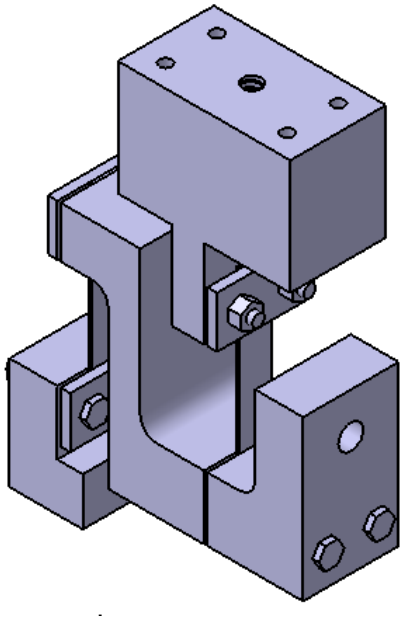


Figure 3.5. Isometric view of positive stiffness elements.

be seen. Notice that there are 4 beams that has $l/2$ length with clamped-clamped

conditions, so the force in the vertical direction is

$$F = 4 \times \frac{-4\pi^2 E_2 I_2 y}{(l/2)^3} = \frac{-128\pi^2 E_2 I_2 y}{l^3}. \tag{3.11}$$

Thus, negative stiffness is found as

$$k_n = \frac{F}{y} = \frac{-128\pi^2 E_2 I_2}{l^3} = \frac{-1263.3 E_2 I_2}{l^3}. \tag{3.12}$$

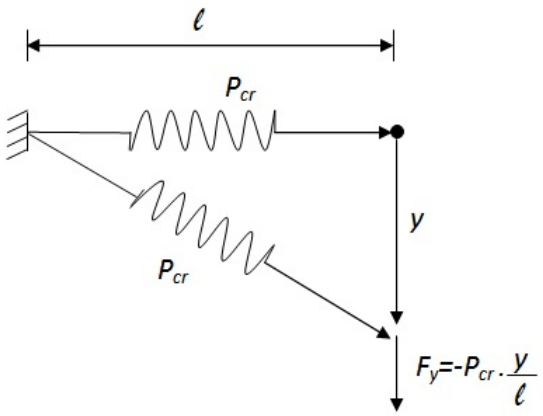



Figure 3.6. A schematic diagram for the calculation of the stiffness in vertical direction. Here, $P_{cr}$ is the compression force within the beam.

As a case study, this result can be compared with the one in [18]. In Figure 3.8, the lateral force applied to the center of the beam versus deflection of the center of the beam is presented [18]. Slope of the force-displacement curve gives the stiffness and the slope is negative between $0.16h$ - $1.92h$. Here, $h$ (see Figure 3.9) is the apex height of the center of the beam in its first buckling mode. The values given in Figure 3.8 are valid for $h$ that is larger than 6 times the thickness of the beam. The negative slope in Figure 3.8 gives the equation for negative stiffness as

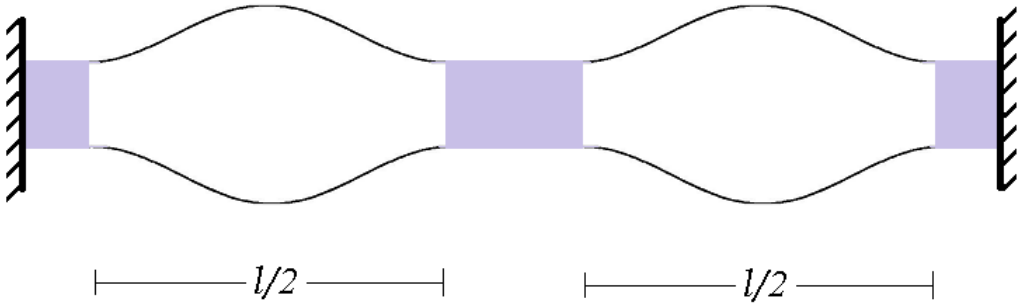



Figure 3.7. A schematic diagram of buckled beams used in this study.

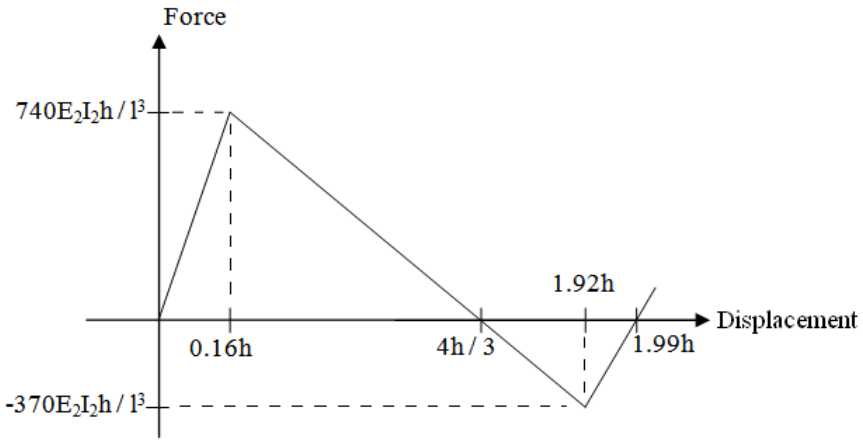



Figure 3.8. Force - displacement graph for a bistable mechanism [18].

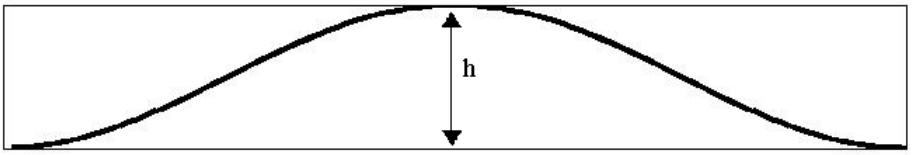



Figure 3.9. Apex height of the beam.

$$k_n^* = -\frac{1110 E_2 I_2}{1.76 l^3}. \tag{3.13}$$

In the current design, there are two beams (see Figure 3.10 and 3.11), thus $I_2$ becomes $2I_2$ and negative stiffness equation becomes

$$k_n = -\frac{2220 E_2 I_2}{1.76 l^3} = -\frac{1261.4 E_2 I_2}{l^3}. \tag{3.14}$$

Notice that negative stiffness values found in Equation 3.12 and Equation 3.14 are very similar.

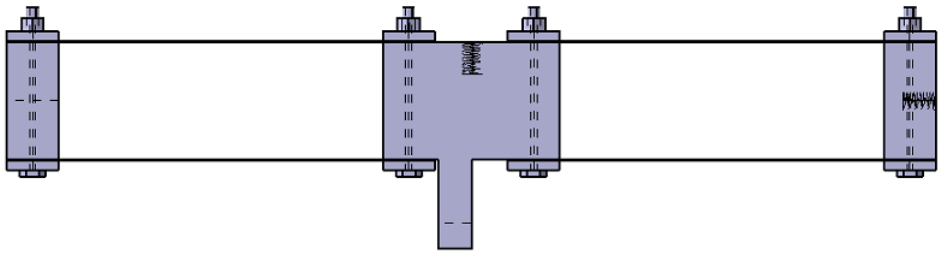


Figure 3.10. Bistable mechanism that produce negative stiffness.

In Figure 3.11, parallel beams are made from spring steel which have high yield strength ($\sim$ 1100 MPa). Clamped-clamped boundary conditions are obtained for these beams with the help of small cover plates which are fixed with bolts and nuts.

For zero stiffness

$$k_p + k_n = 0 \tag{3.15}$$

has to be satisfied. Inserting Equation 3.7 and 3.14 into Equation 3.15, we get

$$k_p + k_n = \frac{2 E_1 I_1}{l_2^2 l_a} - \frac{2220 E_2 I_2}{1.76 l^3} = 0 \tag{3.16}$$

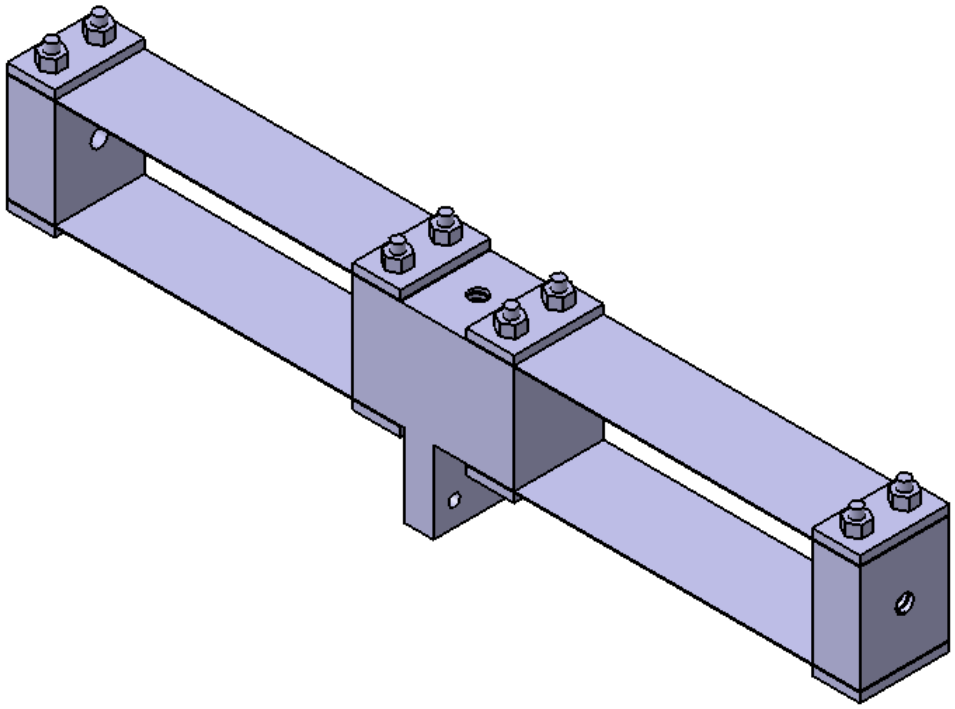


Figure 3.11. Isometric view of bistable mechanism.

From which, we can deduce

$$\frac{E_1 I_1}{l_2^2 l_a} = \frac{630.7 E_2 I_2}{l^3} \tag{3.17}$$

Inserting the parameters of our system ($t$ = 0.4 mm, $l_2$ = 46 mm, $l$ = 200 mm, $l_a$= 34.3 mm, $w$ = 30 mm, $E_2$ = 200 GPa) to the graph given in Figure 3.8, we obtain the graph in Figure 3.12. Here, the negative slope of the curve gives half of the negative stiffness value as we have two beams. Thus,

$$k_n^* = -\frac{11.84 + 5.92}{(7.68 - 0.64)10^{-3}} = -\frac{17.76}{(7.04)} \times 10^3 = -2523\ N/m \tag{3.18}$$

$$k_n = 2k_n^* = -5046 N/m. \tag{3.19}$$

In Figure 3.13, force-displacement graph for bistable mechanism in FEM analysis can be seen. Again slope gives the stiffness which is

$$k_n = -\frac{12.46 + 6.205}{7.624 - 0.64} \times 10^3 = -\frac{18.665}{6.984} \times 10^3 = -2672.5\ N/m. \tag{3.20}$$

$$k_n = 2k_n^* = -5345\ N/m. \tag{3.21}$$

Notice that Figure 3.12 and Figure 3.13 are very similar as well as the results in Equation 3.19 and Equation 3.21.

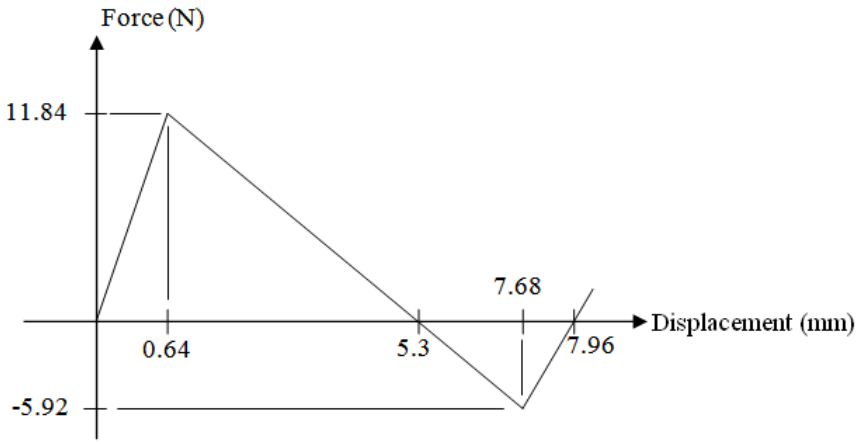



Figure 3.12. Force - displacement graph for the designed bistable mechanism.

Notice that the negative stiffness of the system was found $-5046$ N/m from the analytical study (see Equation 3.19). While designing the system, this stiffness value is equated to the positive stiffness which originates from flexure hinges, and the length of the flexure hinges ($l_a$) is found as 34.3 mm. With this length and other parameters ($M = 1.174$ kg, $m_{is} = 0.24$ kg, $I = 5.28 \times 10^{-4}\ m^4$, $l_1 = 185$ mm, $\alpha = 4.02$, $\beta = 1.26$) when movable isolator mass ($m_m = 0.165$ kg) is in the middle of the lever ($l_4 = 135$ mm), the system is modeled and analyzed using FEM. In Figure 3.14, static structural analysis of the positive stiffness elements is shown. The system is fixed from the bottom

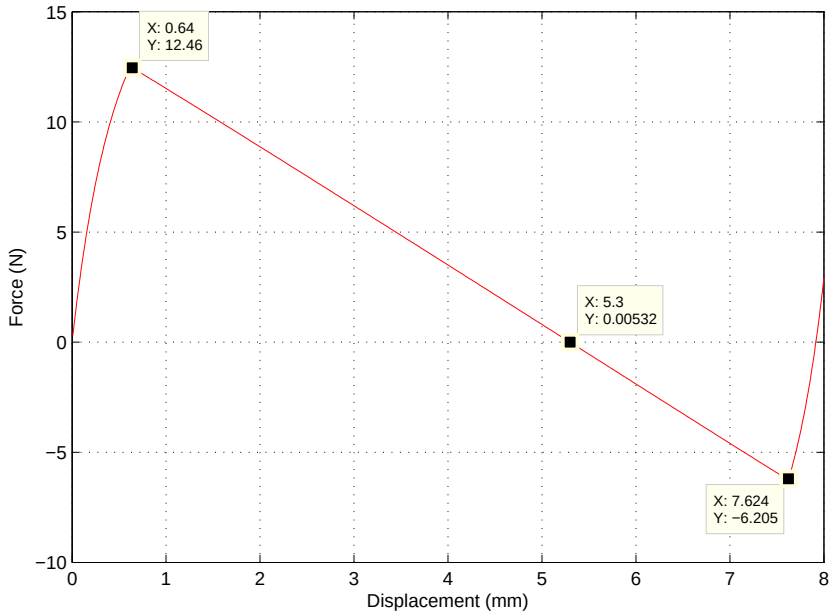



Figure 3.13. Force - displacement graph for the designed bistable mechanism in finite element analysis.

surface and a frictionless support is added as shown in Figure 3.14 in the absence of the negative stiffness elements. A 1 N force is applied from the top surface in vertical direction (-$X$ in Figure 3.14). The displacement of the load is measured as 0.1991 mm. Therefore, the stiffness values is found as

$$k = \frac{F}{\delta} = \frac{1}{0.1991 \times 10^{-3}} = 5023\ N/m. \tag{3.22}$$

Notice that this values is very close to the one found in Equation 3.19. Thus, the analytical solution agrees with the FEM solution.

After confirming that stiffness values agrees with each other, modal analysis of the whole system (with negative stiffness elements) is performed. Notice that the negative stiffness beam elements can generate negative stiffness only when they are pre-compressed. When they are not pre-compressed, they generate positive stiffness. The extra positive stiffness due to these beams can be found as

$$k_b = \frac{48 E_2 I_2}{l^3} \tag{3.23}$$

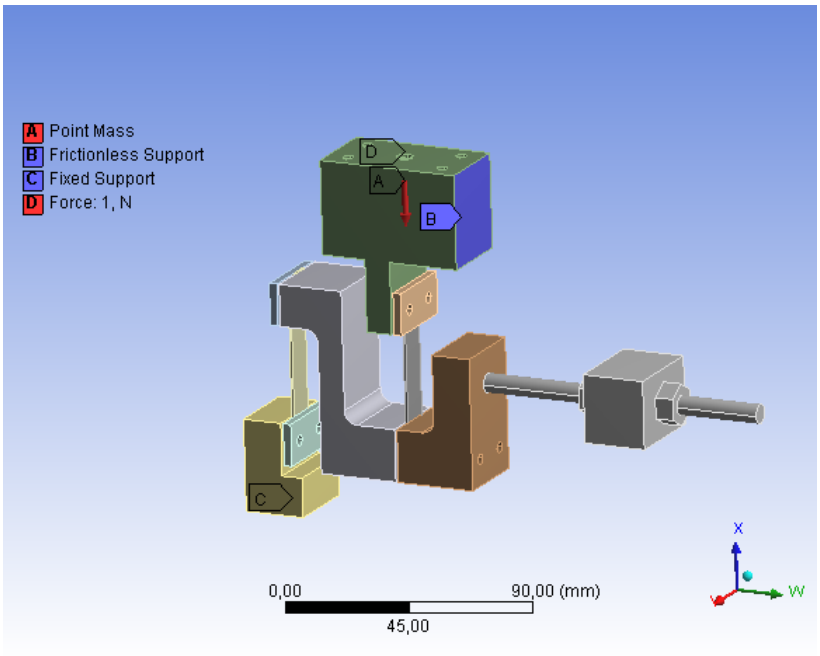



Figure 3.14. Static structural analysis of the positive stiffness elements.

For $E_2 = 200$ GPa and $I_2 = 1.6 \times 10^{-13}\ m^4$ we get $k_b = 1536$ N/m. So, the overall stiffness is 6581 N/m. The first 5 resonance frequencies of the system are shown in Table 3.1.

Table 3.1. The first 5 resonance frequencies of the system in which the movable isolator mass is in the middle of the lever and the parallel beams are not pre-stressed.

| **Mode** | **Frequency [Hz]** |
|---|---|
| 1 | 7.1719 |
| 2 | 87.992 |
| 3 | 249.28 |
| 4 | 1230.6 |
| 5 | 2202.3 |

The shape of the first mode in Table 3.1 can be seen in Figure 3.15. System has a vertical movement in this frequency. Thus, we can compare it with the analytical

calculations and the experimental results. Using Equation 2.20 and 2.21, and adding the movable isolator mass to the system, the equation for the resonance and anti-resonance frequencies are found as

$$\omega_p = \sqrt{\frac{k}{M + I\frac{\alpha^2}{l_1^2} + m_{is}\beta^2 + m_m\eta^2}}, \tag{3.24}$$

and

$$\omega_z = \sqrt{\frac{k}{m_{is}\beta(\beta-1) + m_m\eta(\eta-1) + I\frac{\alpha^2}{l_1^2}}}, \tag{3.25}$$

respectively, where $m_m$ is the movable isolator mass and $\eta$ is the ratio of $l_4$ (distance between the left hinge and movable isolator mass) to $l_2$ (distance between two hinges). Using these two equations and the parameters of the system ($k = 6581$ N/m, $M = 1.174$ kg, $m_{is} = 0.24$ kg, $m_m = 0.165$ kg, $I = 5.28 \times 10^{-4}$ $m^4$, $l_1 = 185$ mm, $\alpha = 4.02$, $\beta = 1.26$, $\eta = 2.93$) where $l_4 = 135$ mm, the resonance and anti-resonance frequencies are found as 7.2 Hz and 11.5 Hz, respectively.

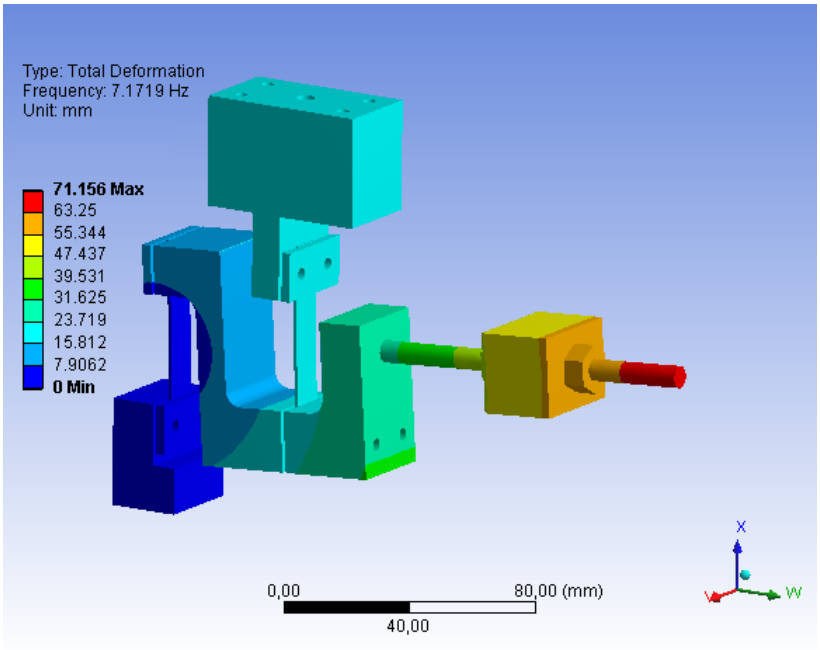



Figure 3.15. Mode shape of the system at 7.1719 Hz.

In Table 3.1, we see that the first resonance frequency (7.2 Hz) agrees with the analytical solution (7.2 Hz). Moreover, the third mode in Table 3.1 is a dominant mode in the vertical direction and its shape is shown in Figure 3.16. This mode is at 249 Hz and it limits the isolation frequency range.

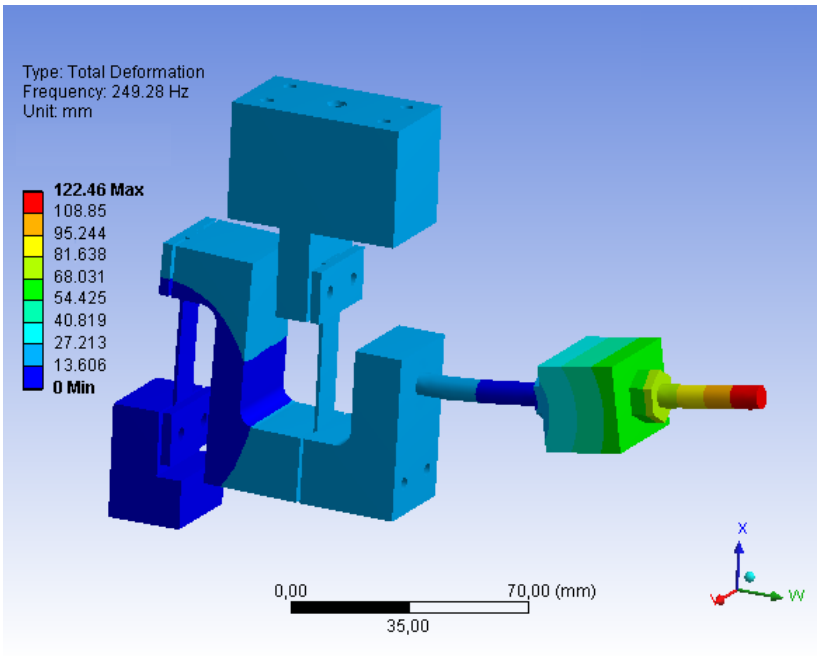



Figure 3.16. Mode shape of the system at 249.28 Hz.

Figure 3.17 shows the frequency response plot of the system in Figure 3.14 with the positive stiffness effects of parallel beams via harmonic analysis. Since the FEM analysis is performed excluding the effect of damping, the amplitudes in Figure 3.17 are higher than the real case. Here, the positions of the resonance and anti-resonance frequencies are important. The harmonic analysis is conducted with 0.25 Hz resolution. From Figure 3.17, one can see that the first resonance frequency is at 7.25 Hz and the second resonance frequency is at 249 Hz while the anti-resonance frequency is at 11.5 Hz. Notice that the first resonance frequency (7.25 Hz) agrees with the results found in the analytical calculation (7.2 Hz) and the modal analysis (7.2 Hz). Moreover, the anti-resonance frequency (11.5 Hz) is the same with the value found in the analytical calculation. Thus, the FEM results agree very well with the analytical results.

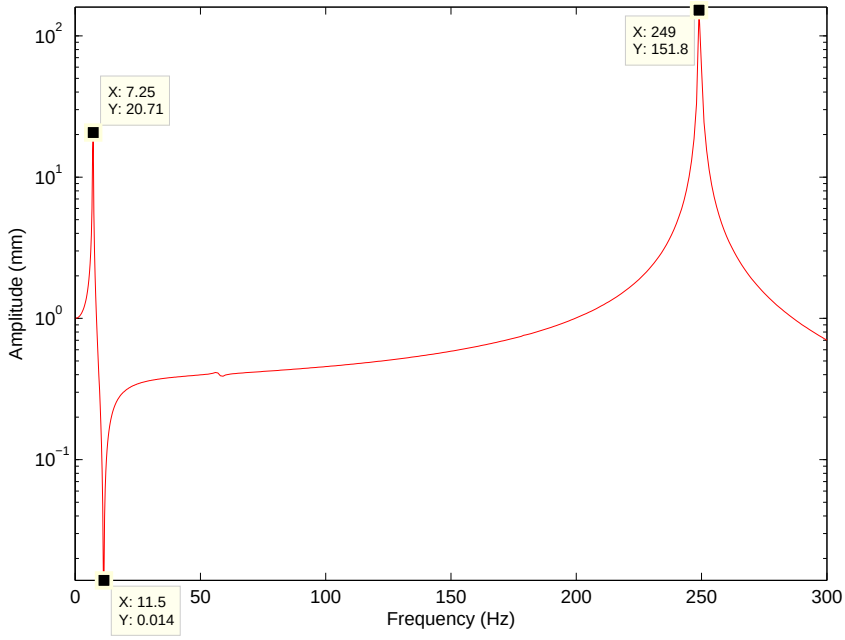



Figure 3.17. Frequency response plot via harmonic analysis.

### 3.1.1. Stress Constraints in the Design

While designing the system, we have to be careful not to exceed yield strengths of the materials. In our design, there are two critical maximum stresses: one for the flexure hinges at positive stiffness elements and the other for the bistable mechanism that produce negative stiffness. These parts are made from spring steel which have very high yield strength values around 1100 MPa. There is also cyclic loading hence the design load should be such that we have infinite life. Ultimate tensile strength of the spring steels is around 1500 MPa. Surface factor, $C_S$, of the cold-drawn spring steels for the given tensile strength can be taken as 0.6. Load factor, $C_L$, equals 1 because there is bending loading in the system. For a 99% reliability, reliability factor, $C_R$, is taken as 0.814. Therefore the stress on the spring steel for infinite life is

$$S_n = \frac{S_u}{2} C_L C_S C_R = \frac{1500}{2}(1)(0.6)(0.814) = 366.3\ MPa \tag{3.26}$$

With a safety factor 2, maximum allowable stress is found as

$$\sigma_{all} = \frac{366.3}{2} = 183.15\, MPa \tag{3.27}$$

The stress in the positive stiffness beam element is

$$\sigma_p = \frac{Mc}{I_1} \tag{3.28}$$

where $M$ is the moment on the midpoint of $l_2$, the length between two flexure hinges. $M$ is

$$M = \frac{Fl_2}{2} \tag{3.29}$$

where $F$ equals 10 N and $l_2 = 46\, mm$ for our system. Inserting Equation 3.29 to Equation 3.28, the stress is found as

$$\sigma_p = \frac{Fl_2c}{2I_1} \tag{3.30}$$

where $c = 0.5\, mm$ is half of the thickness of the flexure hinges and $I_1 = 9.1667 \times 10^{-13}\, m^4$. Maximum stress in the negative stiffness beam elements should not exceed the second buckling mode, which results

$$\sigma_n = \frac{2E_2\pi^2 th}{l^2} \tag{3.31}$$

where $t = 0.4\, mm$ is the thickness of the beams in bistable mechanism, $h = 4\, mm$ is the apex height of the beam, and $E_2 = 200\, GPa$.

With the given parameters, $\sigma_p$ and $\sigma_n$ found as 125.5 and 157.9 MPa, respectively. Both of these stress values are smaller than the allowable stress given in Equation 3.27. Therefore, stress requirements are satisfied.

## 3.2. Adjustment Systems

### 3.2.1. Compressive Force Adjustment System for the Bistable Mechanism

In Figure 3.18, compressive force adjustment system for the bistable mechanism can be seen. Here, the bistable mechanism in Figure 3.10 and 3.11 is attached to the right part of the case by means of a threaded rod. There are two nuts on this rod which are placed on two sides of the case. These nuts are there to adjust the horizontal position of the bistable mechanism and to fasten it. The mechanism works as follows: firstly, threaded rod is attached to the right of the bistable mechanism passing through the hole in the case. Observe that the left nut has to be between bistable mechanism and the case. Then the horizontal position of the bistable mechanism is adjusted. Finally, the two nuts on the threaded rod are tightened. The compressive force or stress in bistable mechanism can be adjusted with this adjustment system.

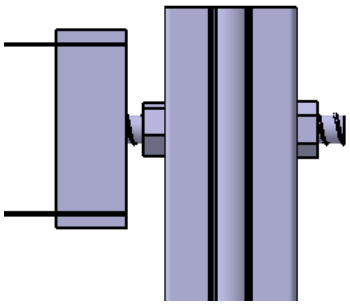


Figure 3.18. Compressive force adjustment system for the bistable mechanism.

### 3.2.2. Adjustable Isolator Mass

In Figure 3.19, the adjustable isolator mass is shown. The left of Figure 3.19 is the positive stiffness mechanism where the thin vertical elements are flexure hinges made from spring steel. The thickness of these hinges can be changed by replacing them with elements that have different thicknesses. In the right of the Figure 3.19, there is a threaded rod with an isolator mass and two nuts on the two sides of this mass.

After the threaded rod is attached to the right of the positive stiffness mechanism, this isolator mass is placed on the rod with two nuts on the two sides. These nuts fasten the isolator mass to the rod. Observe that the isolator mass can be replaced with relatively heavier or lighter ones. Also the horizontal position of the isolator mass can be adjusted. This refers to the $l_1$ parameter in Figure 2.1. Since lever ratio ($\alpha$) given in Equation 2.2 is dependent of $l_1$, $\alpha$ can also be changed. Thus, with this mechanism both isolator mass and lever ratio become adjustable.

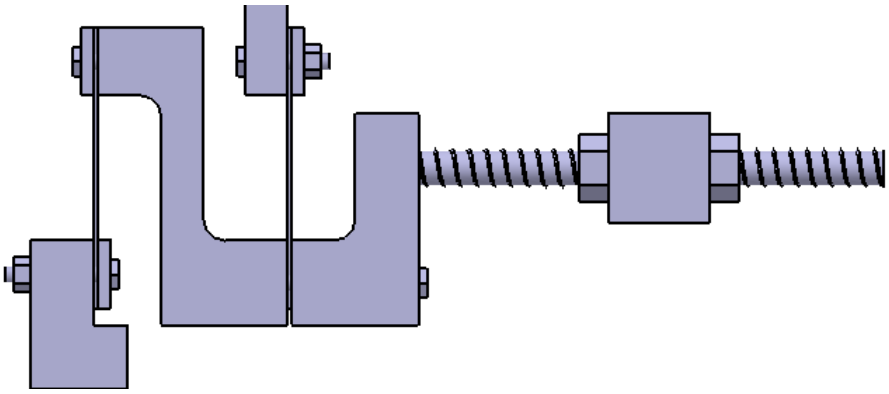


Figure 3.19. Adjustable isolator mass.

### 3.2.3. Leveling System for the Isolator

In Figure 3.20, the leveling system for the isolator can be seen. With this mechanism, the length of the flexure hinges can be altered without changing the hinge elements. Also, if the vertical position of the bistable mechanism changes due to the change in the isolator mass or the mass of the other elements, this leveling mechanism can be used to adjust the vertical position. In Figure 3.20, the positive stiffness mechanism is attached to the bottom of the case by means of a threaded rod. This rod passes through the bottom of the case and there are two nuts above and below of this case element. Just like in the compressive force adjustment mechanism, these nuts are fastened to the case after the position is adjusted.

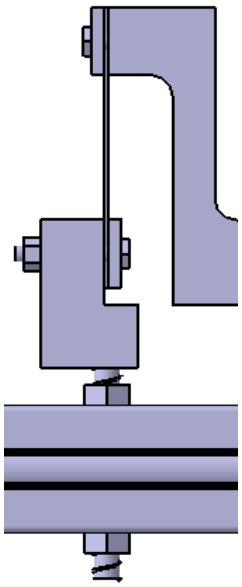


Figure 3.20. Leveling system for the isolator.

### 3.3. Experiments for the System with Quasi-Zero-Stiffness Mechanism

In this section, testing of the isolator system with quasi-zero-stiffness mechanism is covered. In Figure 3.21, the manufactured isolator system is shown. There is a 1 kg load on top of it. To attach the extra mass to the vibration isolator, a bolt passing through its center of gravity is used.

The system is excited by an impact hammer and the acceleration at the output end is measured by an accelerometer. The test setup can be seen in Figure 3.22. The vibration isolator is hanged vertically with rubber cords. Rubber cords are chosen because they have very low stiffness in vertical direction and the system can oscillate freely. The hammer is hit from the bottom of the system. An accelerometer is attached to the top of the system to measure the accelerations.

In the first experiment, movable isolator mass is placed to the near end of the lever. To eliminate the effect of negative stiffness mechanism, first experiment is conducted while parallel beams are not pre-stressed. Coherence plot for this experiment is

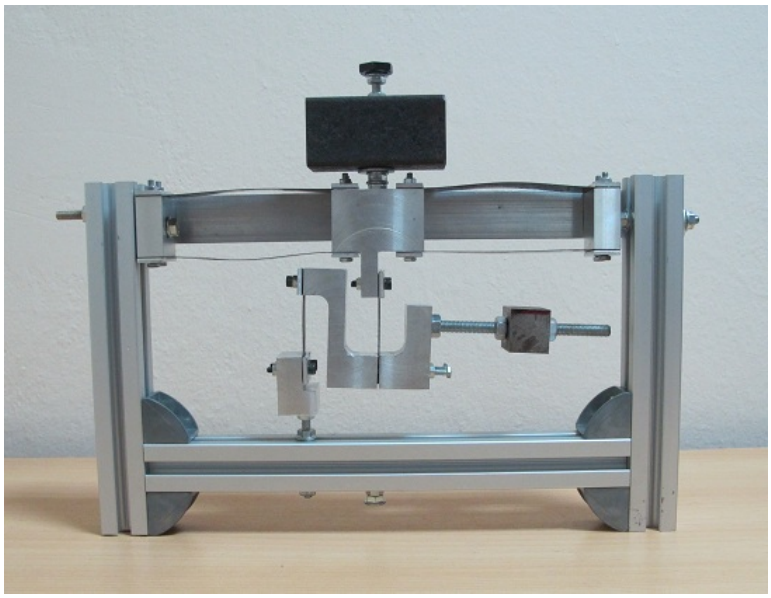


Figure 3.21. The manufactured vibration isolator design with quasi-zero-stiffness mechanism.

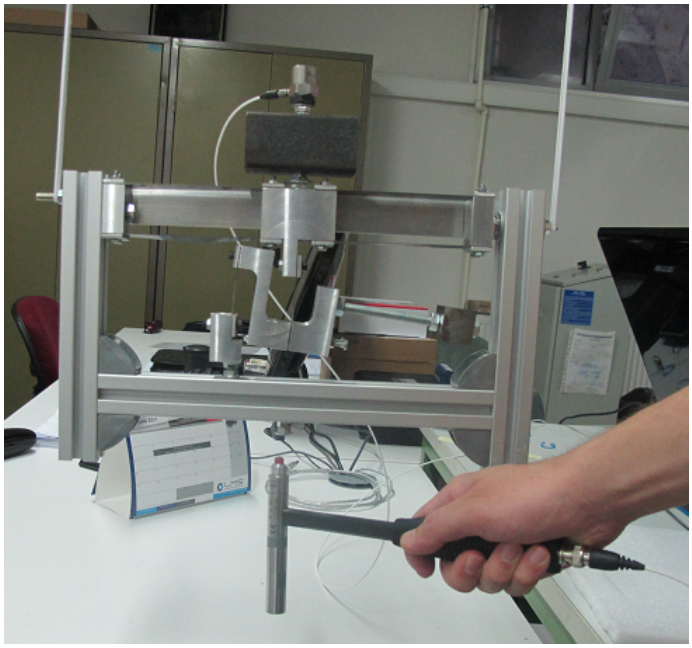


Figure 3.22. Test setup of the system with quasi-zero-stiffness mechanism.

shown in Figure 3.23. Notice that minimum coherence value is around 0.86 and at 0.5 Hz. Therefore, the coherence values are acceptable in the frequency range of interest.

In Figure 3.24, frequency response plot for the first experiment can be seen. The first peak at 1 Hz is because of the oscillation of the rubber cords. This resonance frequency is due to boundary conditions and can be neglected. The resonance frequency of the system is at 11 Hz while anti-resonance frequency is at 16.5 Hz.

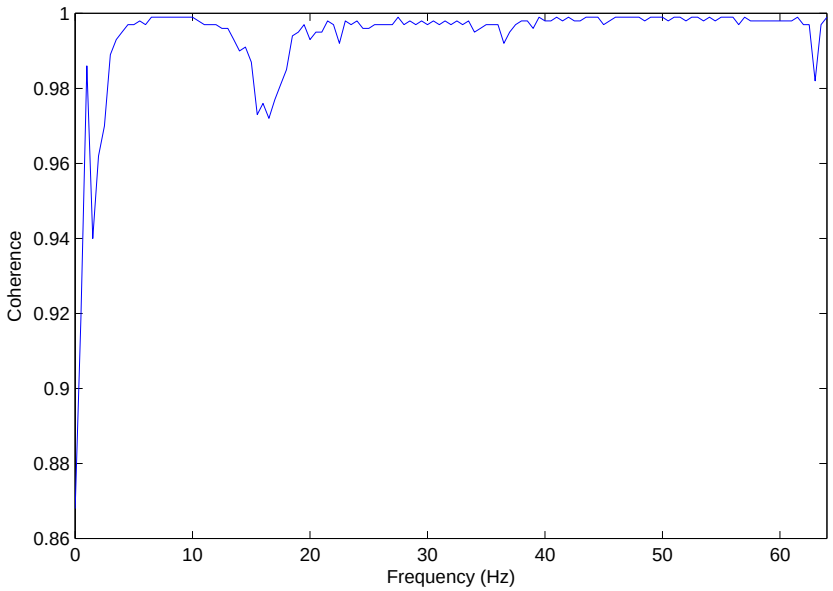



Figure 3.23. Coherence plot for movable isolator mass at the near end and parallel beams are not pre-stressed.

In the second experiment, parallel beams are pre-stressed to produce negative stiffness. Isolator mass stayed at the same location. Coherence plot for this experiment can be seen in Figure 3.25. Notice that minimum coherence value is 0.85. Thus, data in the given range are acceptable. In Figure 3.26, frequency response plot of the second experiment can be seen. Again there is a resonance at around 1 Hz originated from boundary conditions. Neglecting this, the resonance frequency of the system is at 3.5 Hz while anti-resonance frequency is at 4.5 Hz.

The effect of negative stiffness can be seen in Figure 3.27. Blue curve is obtained in the first experiment. After adding the pre-stress to the negative stiffness elements, total stiffness of the system decreases so does the resonance and anti-resonance frequencies. In Figure 3.27, red curve shows the results of the second experiment and notice that

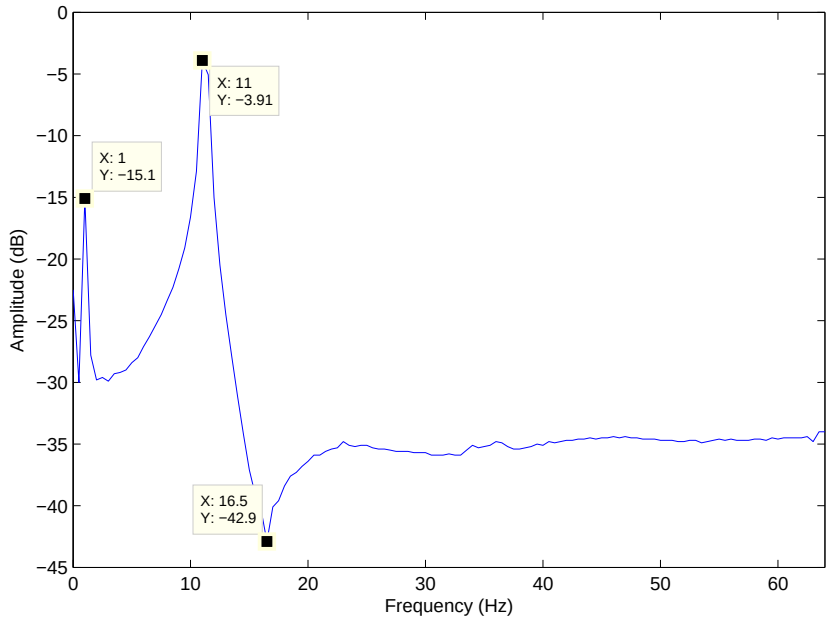



Figure 3.24. Experimental frequency response plot for movable isolator mass at the near end and parallel beams are not pre-stressed.

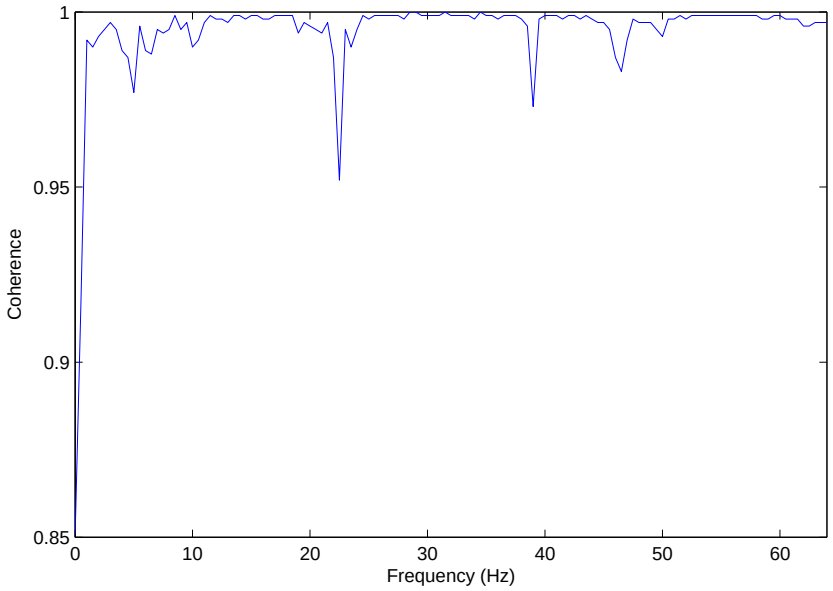



Figure 3.25. Coherence plot for movable isolator mass at the near end and parallel beams are pre-stressed.

while the resonance frequency at 1 Hz which originates from the boundary conditions stay at the same location, other resonance and anti-resonance frequencies shifted to the left. Ideally, the resonance and the antiresonance frequencies can go down to zero with

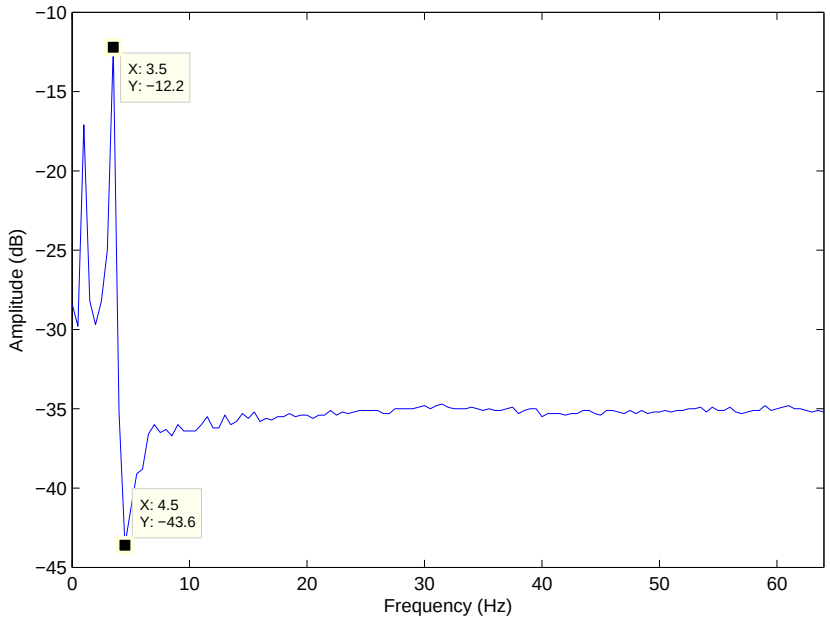



Figure 3.26. Experimental frequency response plot for movable isolator mass at the near end and parallel beams are pre-stressed.

proper tuning. When the actual system is tuned, the resonance at 11 Hz is decreased to 3.5 Hz and the anti-resonance at 16.5 Hz is decreased to 4.5 Hz. So, the negative stiffness elements work not perfectly but quite effectively in reducing stiffness of the overall system.

In the third experiment, movable isolator mass is placed in the middle of the lever. Again the experiment is conducted while parallel beams are not pre-stressed. Coherence plot for this experiment is shown in Figure 3.28. Notice that minimum coherence value is 0.825 and at 112.5 Hz. Hence, the coherence values are acceptable. In Figure 3.29, frequency response plot for the third experiment can be seen. The resonance frequencies of the system are at 9 Hz and 205.5 Hz while anti-resonance frequency is at 12.5 Hz.

In the fourth experiment, parallel beams are pre-stressed to produce negative stiffness. Isolator mass stayed at the same location. Coherence plot for this experiment can be seen in Figure 3.30. Notice that minimum coherence value is 0.88. Thus, data in the given range are acceptable. In Figure 3.31, frequency response plot of the fourth

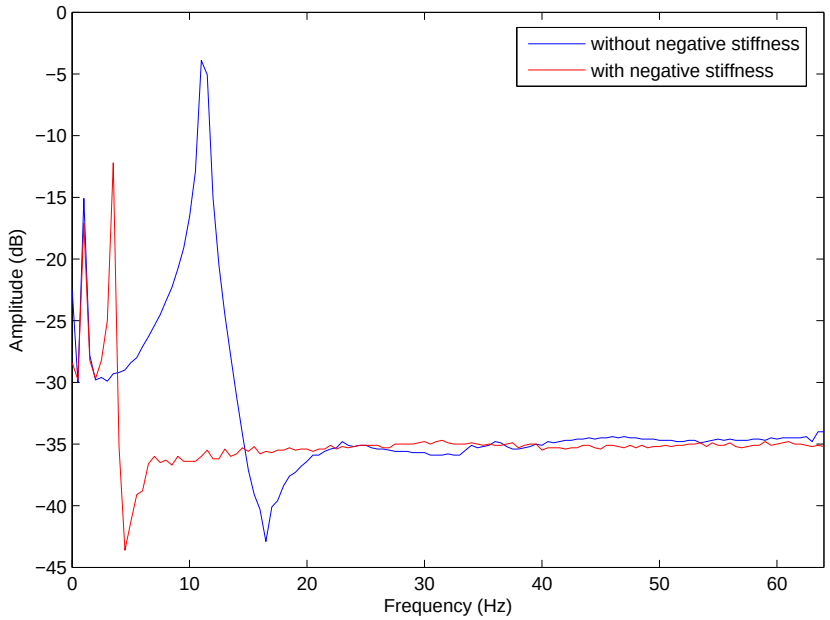



Figure 3.27. Comparison of the experimental frequency responses for movable isolator mass at the near end.

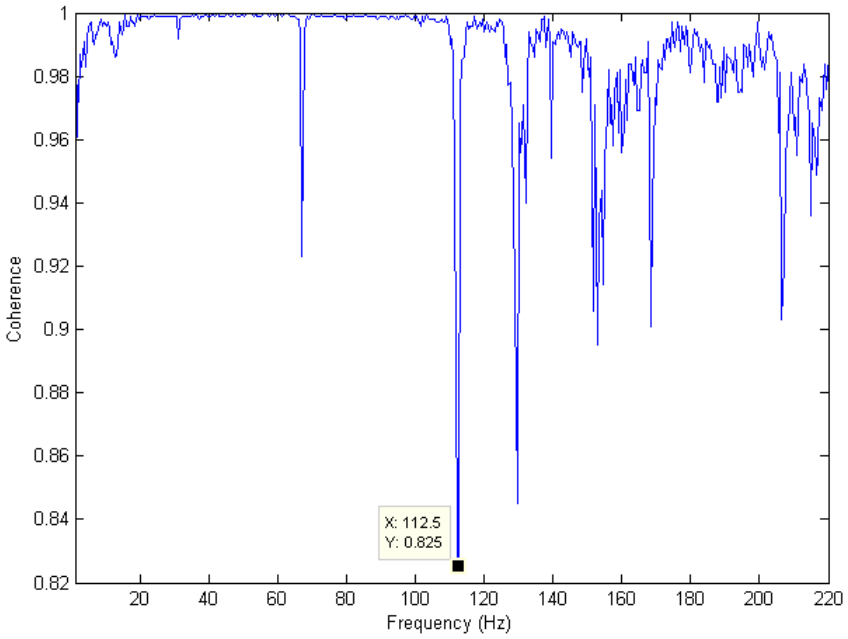



Figure 3.28. Coherence plot for movable isolator mass in the middle of the lever and parallel beams are not pre-stressed.

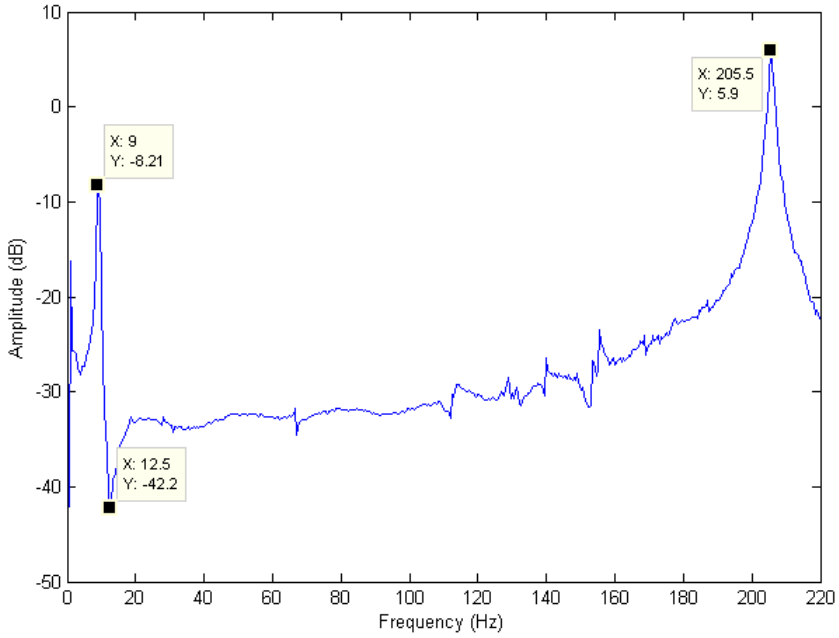



Figure 3.29. Experimental frequency response plot for movable isolator mass in the middle of the lever and parallel beams are not pre-stressed.

experiment can be seen. The resonance frequencies of the system are at 3.5 Hz and 205 Hz while anti-resonance frequency is at 4.5 Hz. Notice that the resonance frequency at 205 Hz stayed in the same location while the resonance frequency at 9 Hz shifted to 3.5 Hz and anti-resonance frequency at 12.5 Hz shifted to 4.5 Hz as expected. In Figure 3.32, comparison of the third and fourth experiments can be seen.

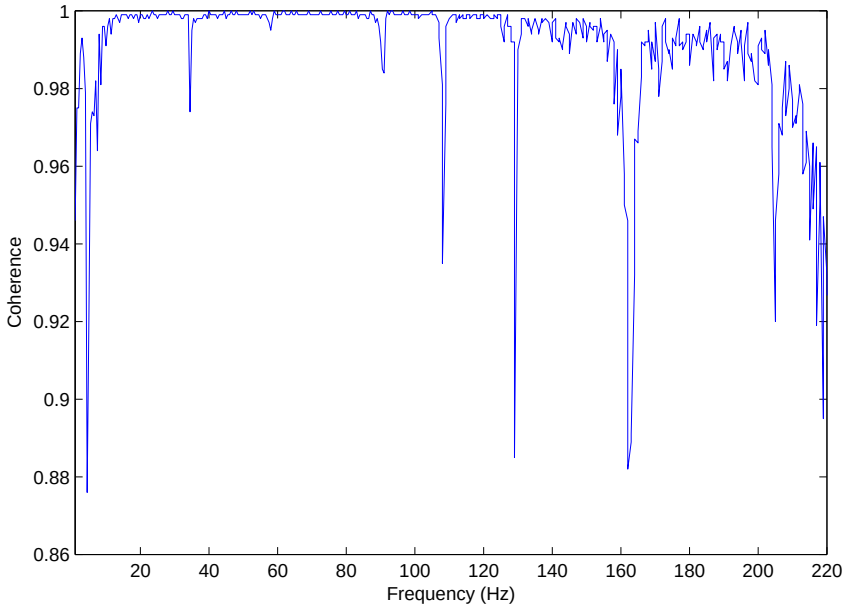



Figure 3.30. Coherence plot for movable isolator mass in the middle of the lever and parallel beams are pre-stressed.

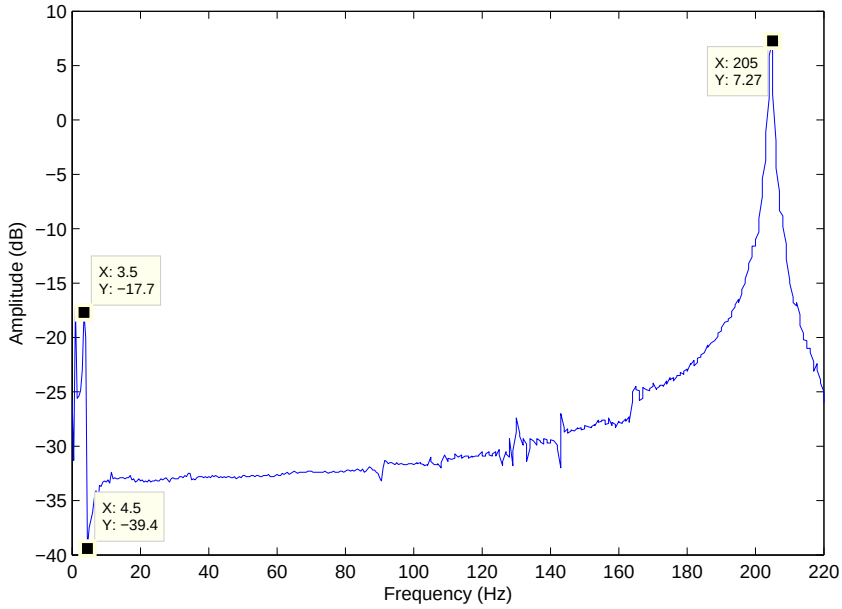



Figure 3.31. Experimental frequency response plot for movable isolator mass in the middle of the lever and parallel beams are pre-stressed.

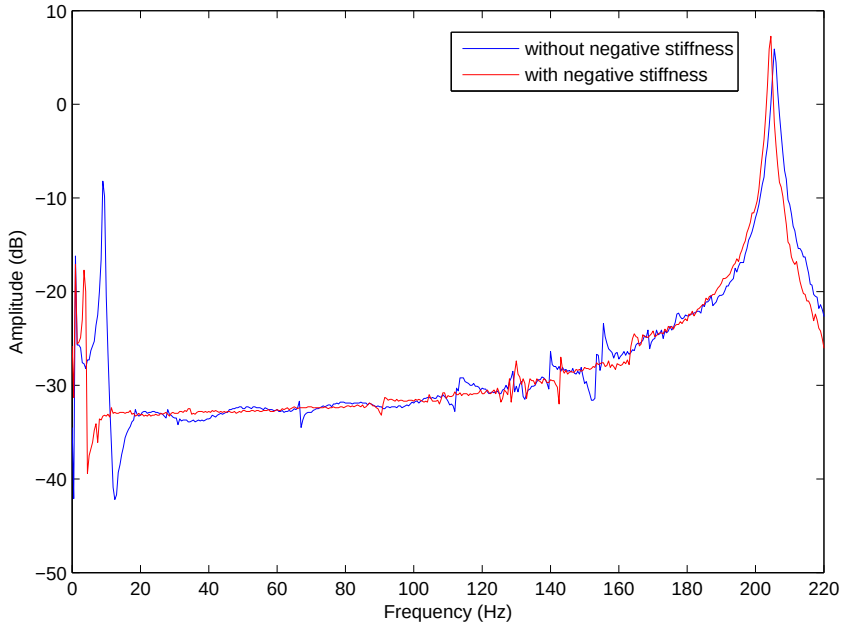



Figure 3.32. Comparison of the experimental frequency responses for movable isolator mass in the middle of the lever.

# 4. RESULTS AND DISCUSSION

This study consists of two main parts. In the first part, passive vibration isolators are designed using a compliant lever-type mechanism. Firstly, the analytical and FEM models are constructed. Then the results of these models are compared with the experimental results. These results are reshown below:

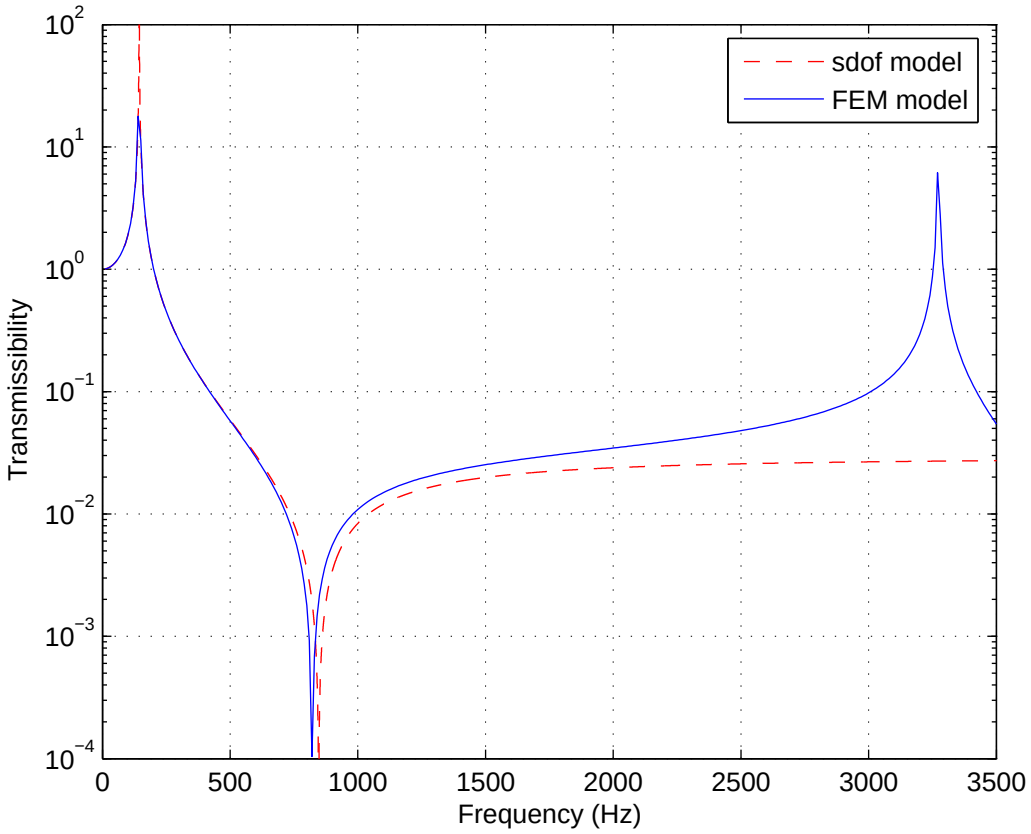



Figure 4.1. Frequency response plot of the SDOF analytic and FEM model for $M =$ 1.145 kg (Figure 2.13 is restated).

In Figure 4.1 and 4.2, we see that the results of the model with single degree of freedom and the results of the finite element model agree with each other along the first resonance and anti-resonance frequencies. However at high frequencies, other resonance frequencies in the finite element model step in and cause differentiation from the single degree of freedom model. Comparing the results of SDOF model

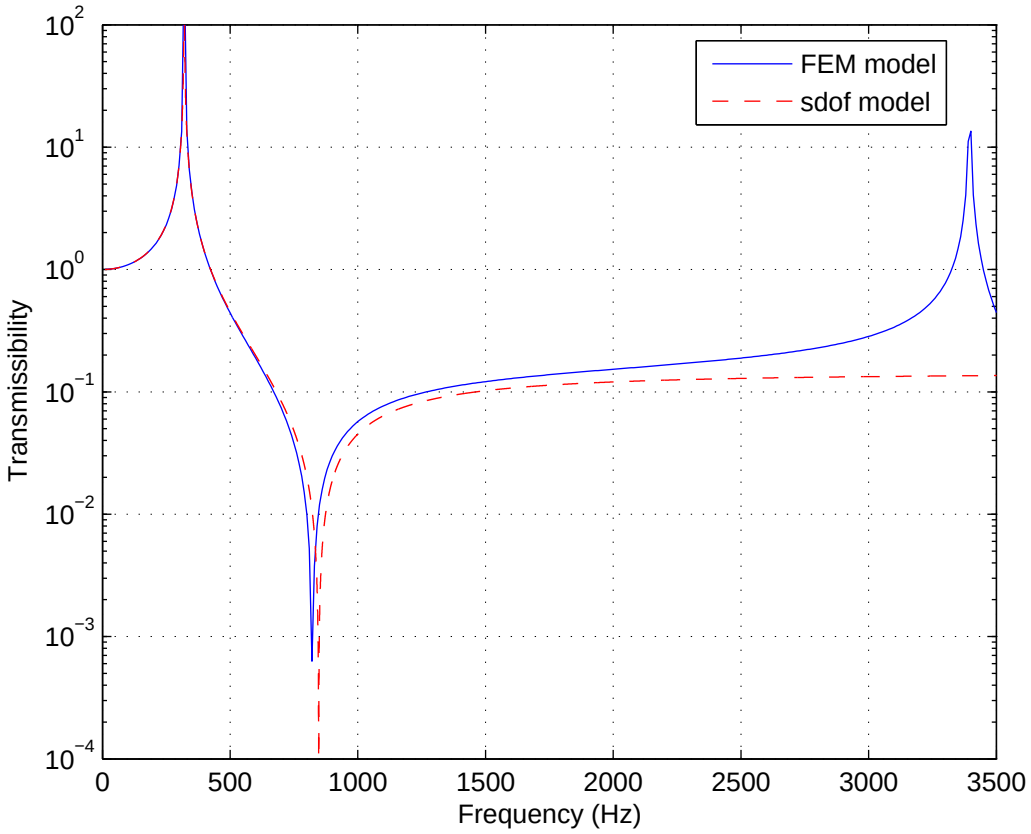



Figure 4.2. Frequency response plot of the SDOF analytic and FEM model for $M =$ 0.145 kg (Figure 2.14 is restated).

and FEM model with the experimental results (Figure 4.1 vs. 4.3 and Figure 4.2 vs. 4.4), we see that resonance frequencies of experimental results are higher than the results of SDOF and FEM model. In addition, we cannot detect the exact location of anti-resonance frequencies in the experiments. We think that there are two main reasons for the differences in resonance frequencies and ambiguity in the location of anti-resonance frequencies. The first reason is the disadvantage of impact hammer test at high frequencies. The resonance range of the results in SDOF model and FEM model is 0-3500 Hz and the coherence we acquired in impact hammer test after approximately 1500 Hz is below 0.75, therefore the results of the experiments at high frequencies are unreliable. The second reason, proposes the cause of errors at low frequencies. The designed isolator is manufactured with wire electrical discharge machining process and the producer firm of the design couldn't provide us precise dimension values. The equipment they have also wasn't capable of producing dimensions less than 0.5 mm.

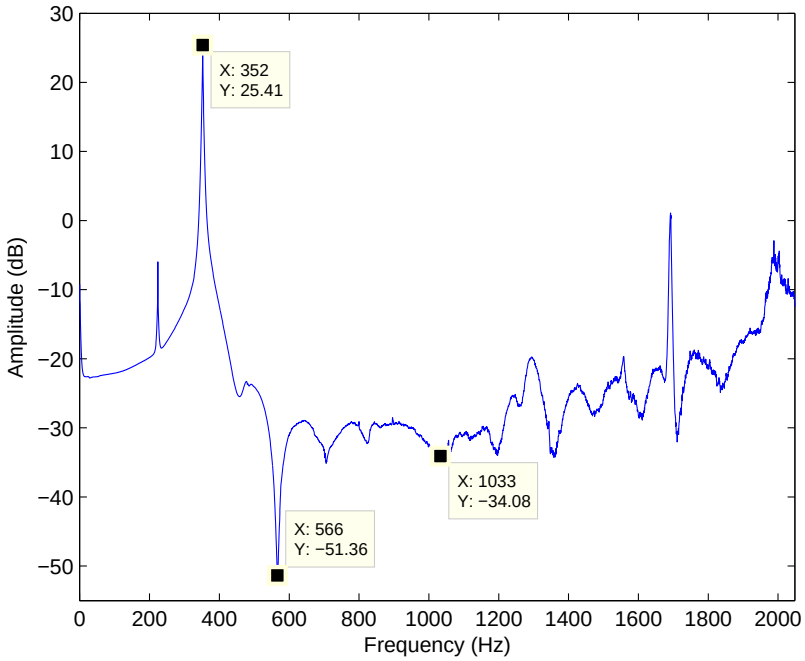



Figure 4.3. Experimental frequency response plot for isolator mass of 1.145 kg with sample frequency 4096 Hz (Figure 2.19 is restated).

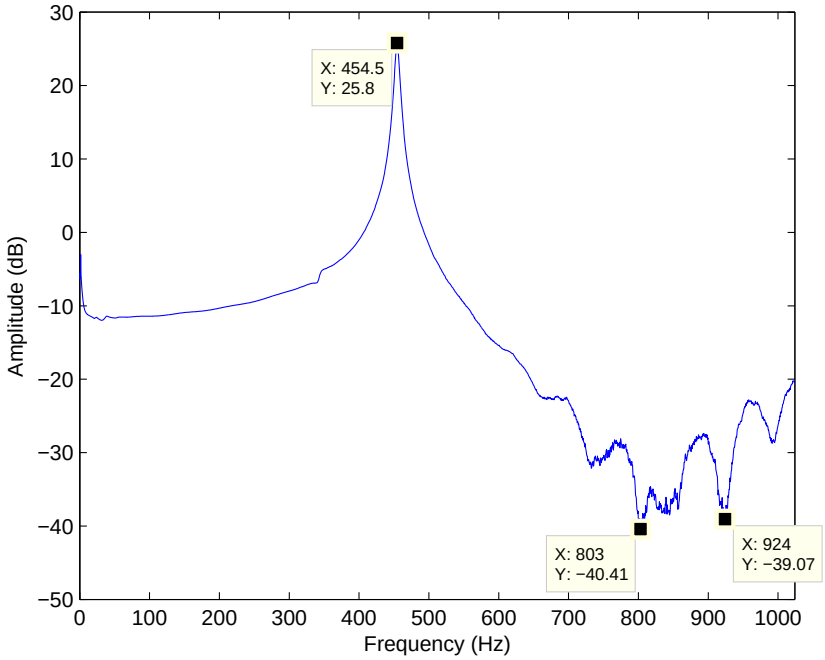



Figure 4.4. Experimental frequency response plot for isolator mass of 0.145 kg with sample frequency 2048 Hz (Figure 2.23 is restated).

Therefore, the manufactured model differentiated from the designed model. The flexure hinges have very small dimensions and these dimensions are affecting the stiffness of the system. Thus, the second reason is the impreciseness in the manufacturing process.

To overcome the errors in the first part, we proposed a vibration isolator design with multiple parts and a quasi-zero-stiffness mechanism. There are a lot of advantages of this design. By being composed of multiple parts, the parts with very small dimensions can be attached to the system and the error at low frequencies in the first section can be eliminated. Also by composed of multiple parts, the length or even the thickness of the flexure hinges can be altered, so that the stiffness of the system can be easily changed.

Achieving vibration isolation at low frequencies by passive means is a challenging problem. To achieve good isolation levels at low frequencies, the stiffness of the system should be low. The quasi-zero-stiffness mechanism provides very low stiffness values in a specific range. Therefore, the high operating frequency range of the vibration isolator in the first section is decreased. This also eliminates the disadvantage of impact hammer test which gives low coherence values at high frequencies. In addition, there is only one lever in this system since the quasi-zero-stiffness mechanism with two beams enables parallel motion.

In Section 3.1, the negative stiffness (5046 N/m) found from the analytic study (see Equation 3.19) was very similar to the FEM solution (5023 N/m). Therefore, analytic and FEM solutions agree with each other.

The resonance frequency found in the analytical study (7.2 Hz) agrees with the modal analysis (FEM) result (7.2 Hz). In the harmonic analysis, the first two resonance frequencies were found at 7.25 Hz and 249 Hz while the anti-resonance frequency was found at 11.5 Hz. Notice that, the first resonance frequency (7.25 Hz) agrees with the results found in the analytical study (7.2 Hz) and modal analysis (7.2 Hz). The anti-resonance frequency (11.5 Hz) is the same with the value found in the analytical study. Also note that corresponding experiment gives 9 Hz for the resonance frequency

and 12.5 Hz for the anti-resonance frequency. The error for the resonance and anti-resonance frequencies are 25% and 9%, respectively. However, the experiments are conducted with 0.5 Hz resolution and the error for the resonance frequency is 1.8 Hz.

The third mode in Table 3.1 corresponds to second resonance frequency in the third experiment which is at 205 Hz. Note that the error between FEM result (249 Hz) and experimental result (205 Hz) is 18%. This error arises from fastening of the positive stiffness element. The part between two flexure hinges is fastened to the part between the positive stiffness mechanism and isolator mass with two bolts. Also, the latter part deforms slightly while in operation. These factors cause the 18% error.

# 5. CONCLUSIONS

This thesis provides two new passive vibration isolator designs: first one is a lever-type vibration isolator using compliant mechanism, and second one is a lever-type vibration isolator with quasi-zero-stiffness mechanism.

It is aimed to create anti-resonance frequency by using lever-type mechanism. Anti-resonance occurs when the inertial force generated by the levered mass cancels the spring force. Since the lever-type mechanism increases the effect of the isolator mass, it is capable of isolating a relatively heavy body with little mass in itself. At first, analytic model of the lever-type vibration isolators is constructed. The systems with lumped and distributed parameters are analyzed. The model is optimized using topology optimization application. Then, finite element model of the system is provided. Static structural, modal and harmonic analysis of the system are done. Then the test results of the manufactured designs are provided. These results are compared with the results of analytic and finite element models. While the results of analytic and FEM models are compatible, the experimental results do not match with these results. There are two reasons for this: first reason is the low coherence values at high frequencies in the impact hammer test, and the second reason is the impreciseness in the manufacturing process. Therefore, a second design with multi-part and a quasi-zero-stiffness mechanism is provided.

In the second design, the equations of negative stiffness mechanism are stated. FEM and experimental results are provided. These results are compared with the analytical results. The stress requirements in the design are satisfied. Then the working principle of the adjustment mechanisms are explained. There are three different adjustment mechanisms in the system. First one is the compressive force adjustment system for the bistable mechanism that is used for adjusting the horizontal position and the compressive force or stress in the bistable mechanism. Second one is the adjustable isolator mass. Both the isolator mass and the lever ratio can be changed with this mechanism. Finally, the leveling system for the isolator is used for adjusting the ver-

tical position of the bistable mechanism and changing the length of the flexure hinges without replacing these elements. In addition to these three adjustment mechanisms, thicknesses of the positive and negative stiffness elements can be changed by replacing them with other elements which have different thicknesses.

As a result, analysis and design of a new compliant lever-type passive vibration isolator using quasi-zero-stiffness mechanism is provided. This design can be adjusted according to the frequency range of interest and good isolation levels can be acquired especially at low frequencies.

# APPENDIX A: TECHNICAL DRAWINGS

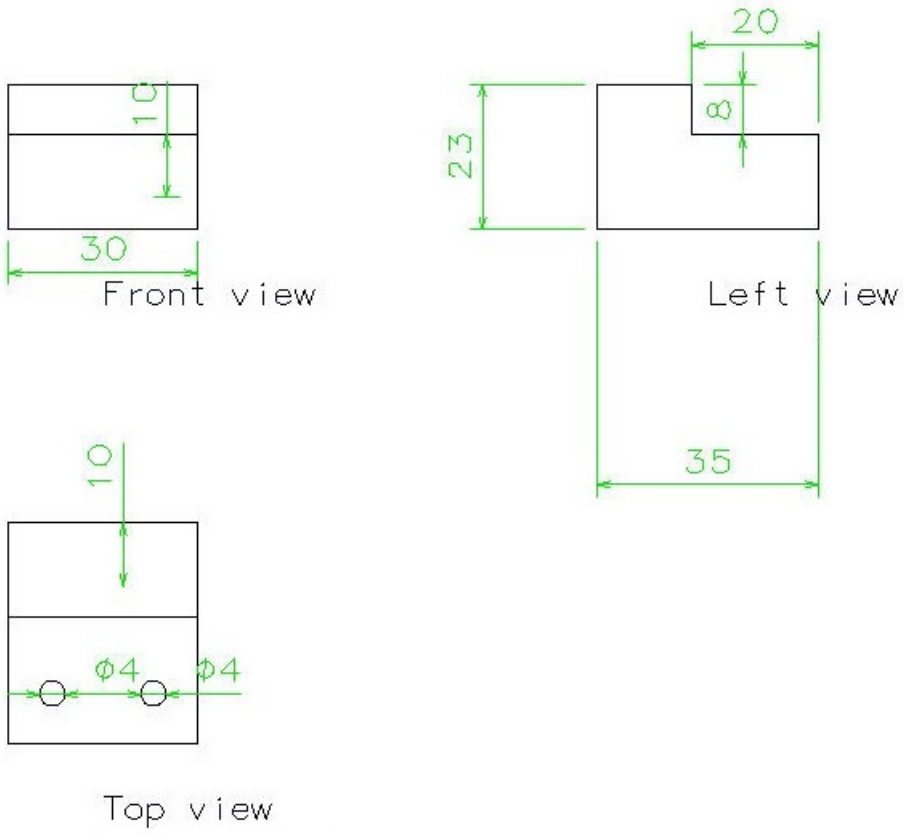
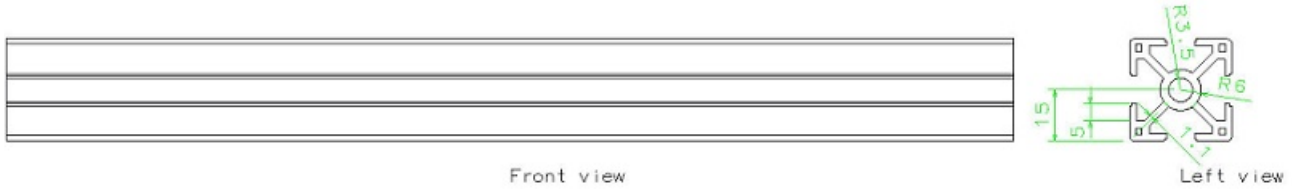



Figure A.1. Part of the leveling system for the isolator.



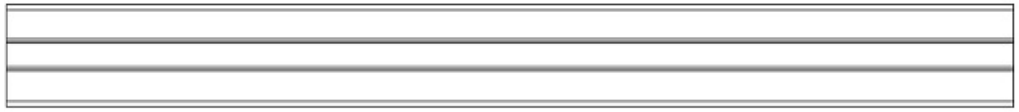




Figure A.2. Bottom part of the main structure.

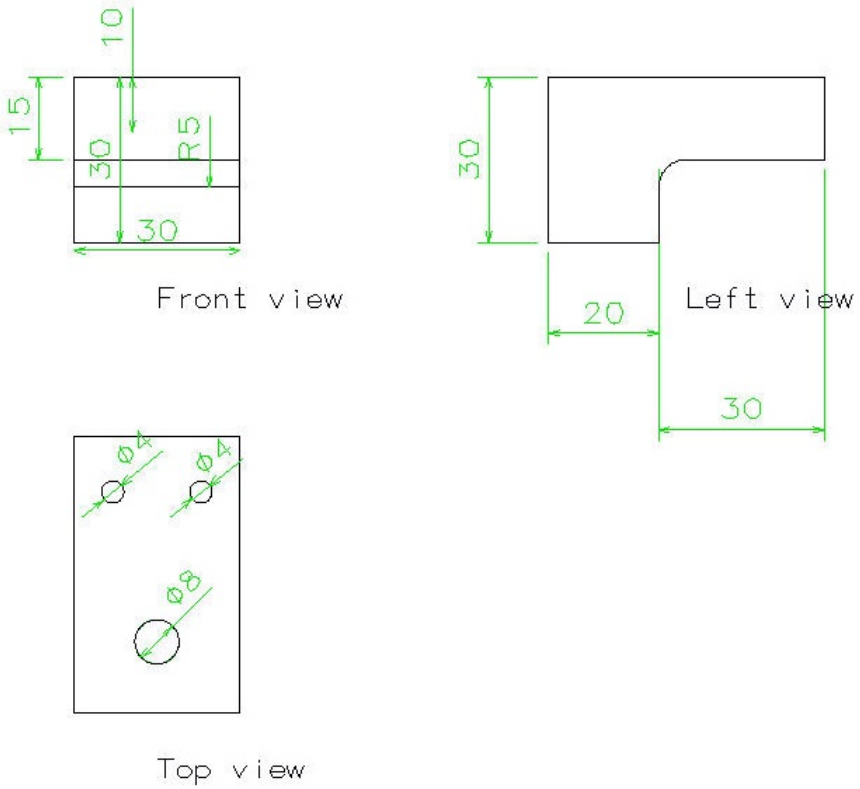



Figure A.3. Part between the positive stiffness mechanism and isolator mass.

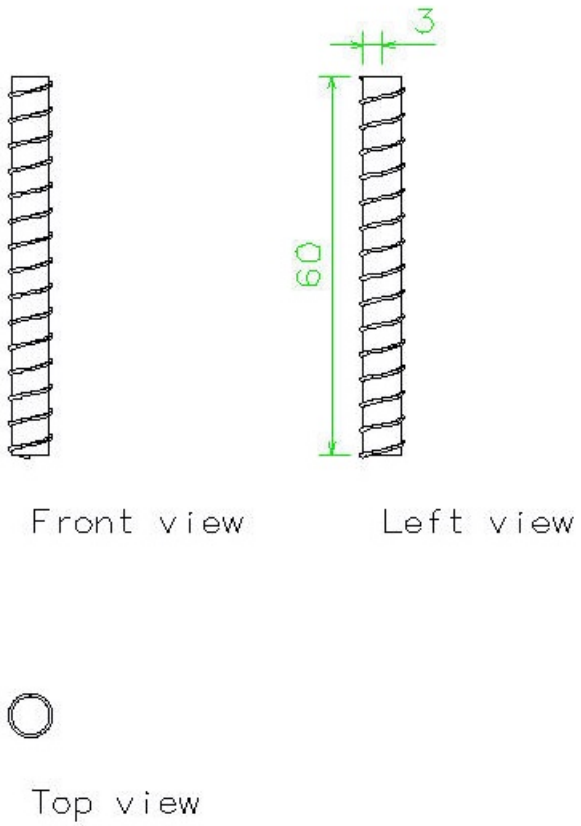



Figure A.4. M6 threaded rod at the bottom of the system.

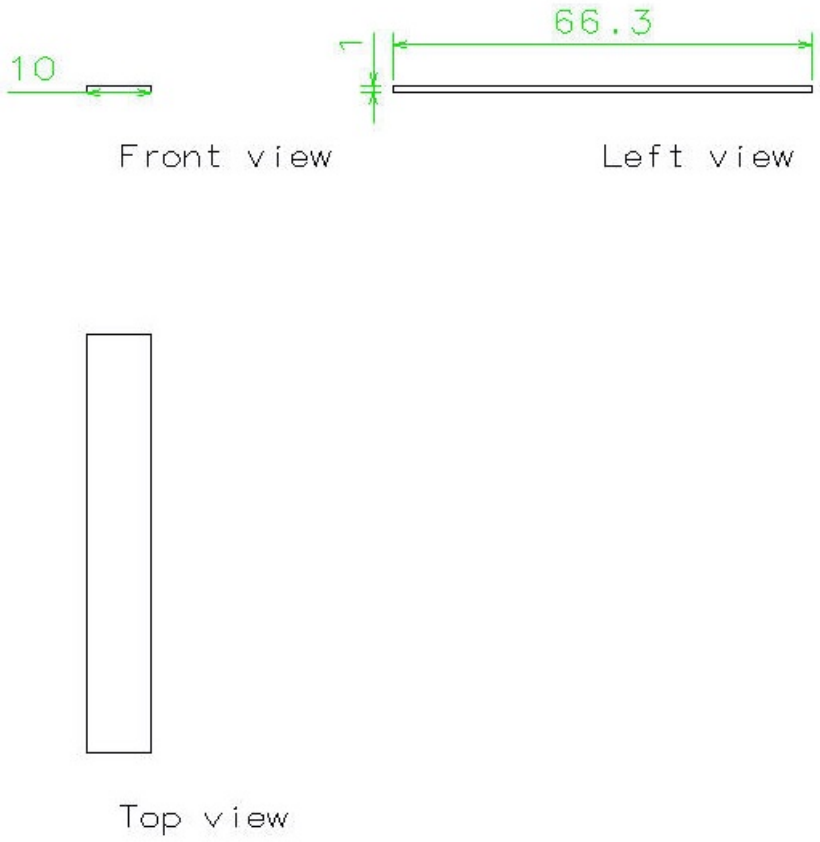



Figure A.5. Flexure hinges.

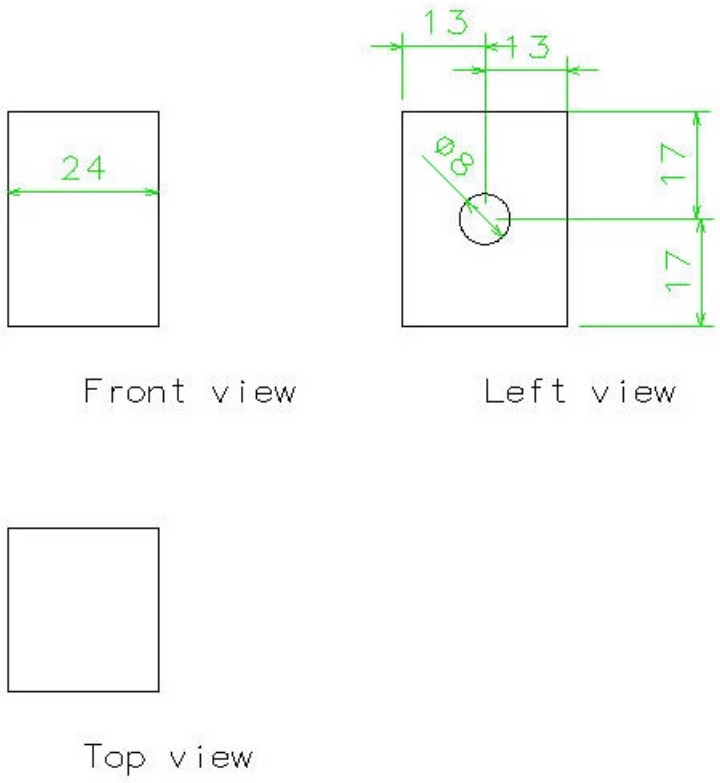



Figure A.6. Isolator mass.

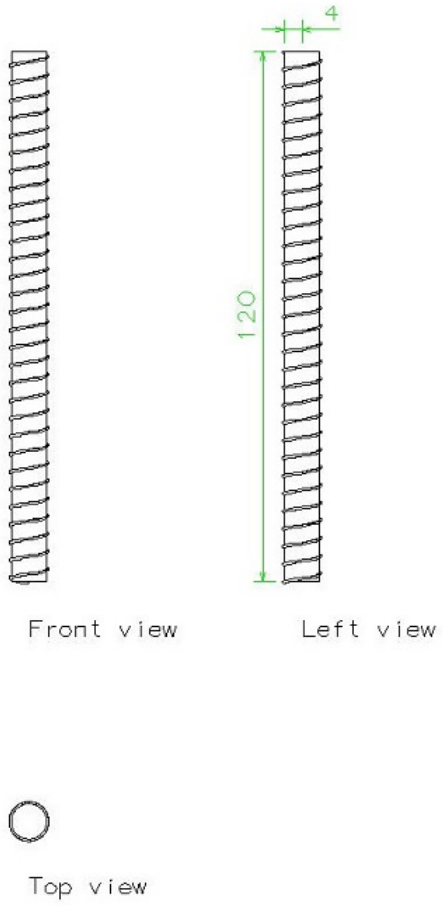



Figure A.7. M8 threaded rod that enables to change the position of the isolator mass.

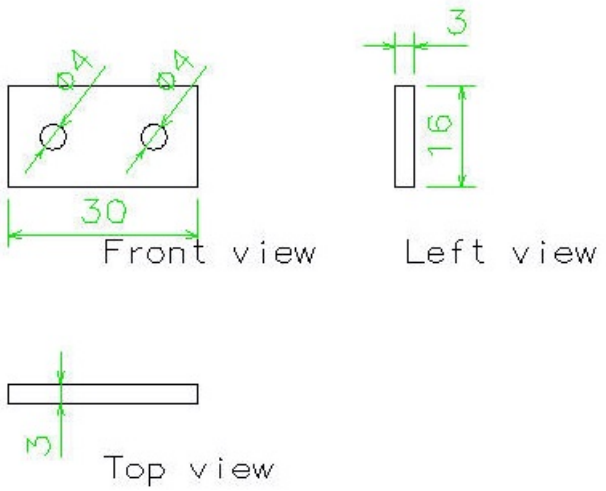



Figure A.8. Cover to satisfy clamped-clamped boundary conditions.

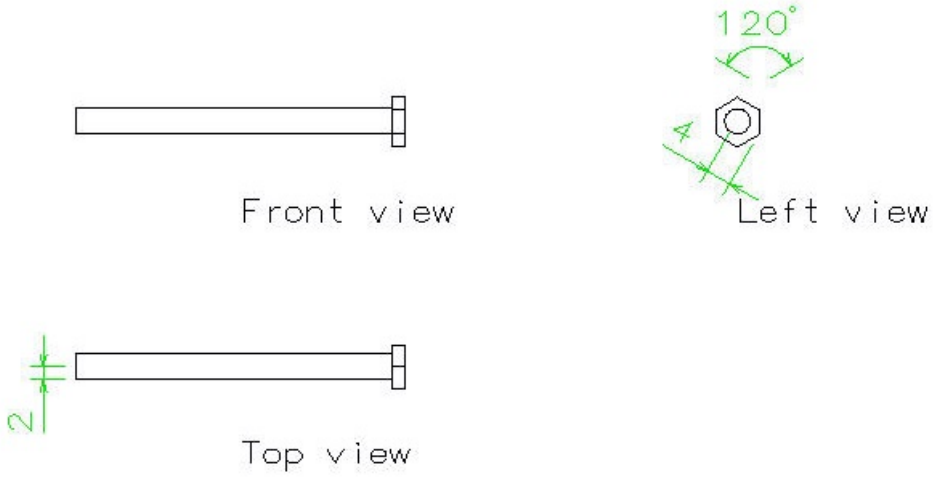



Figure A.9. M4 bolt.

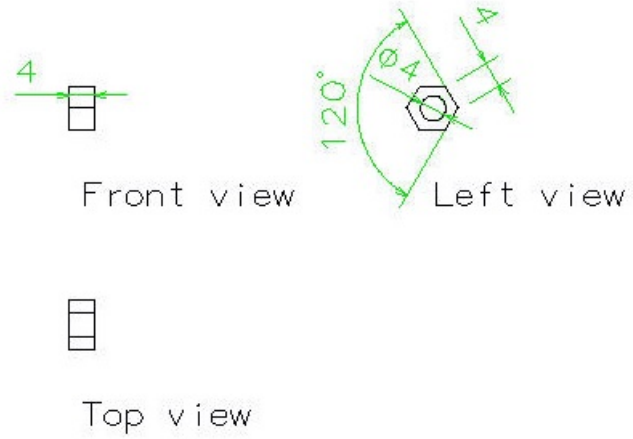



Figure A.10. Metric 4 nut.

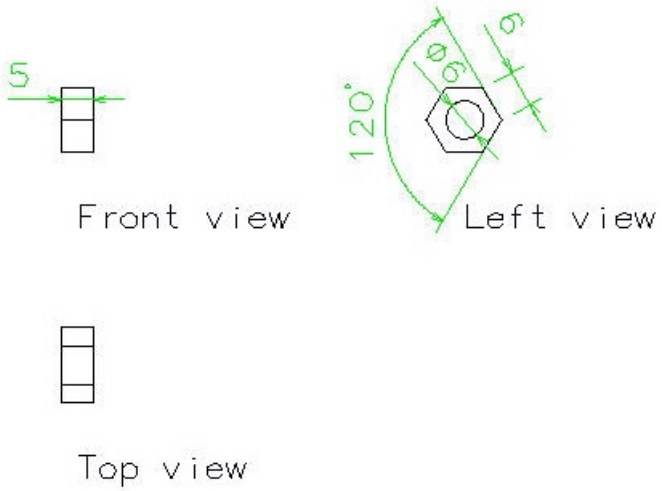



Figure A.11. Metric 6 nut.

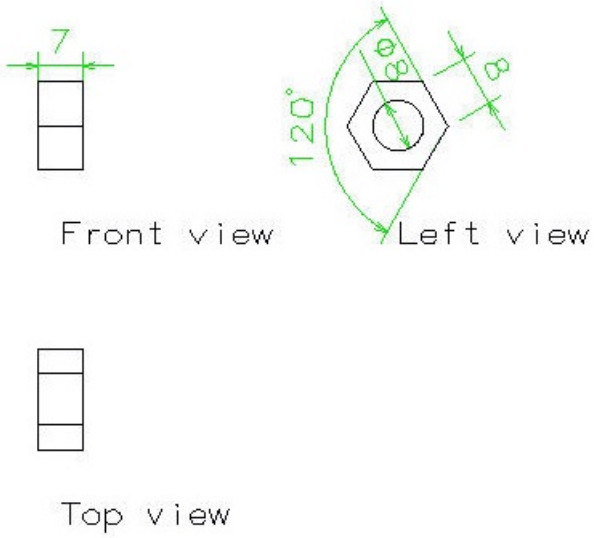



Figure A.12. Metric 8 nut.

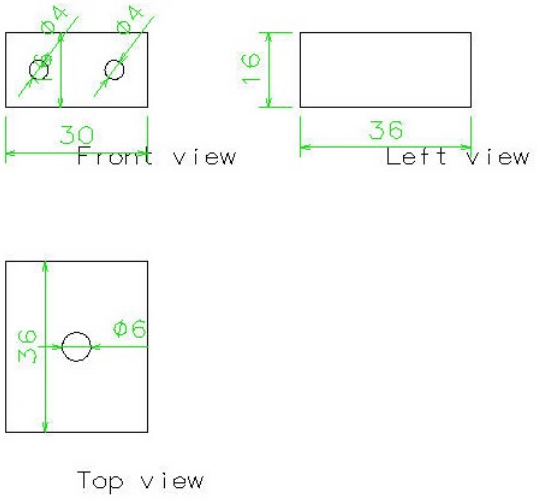



Figure A.13. Left part of the negative stiffness mechanism.

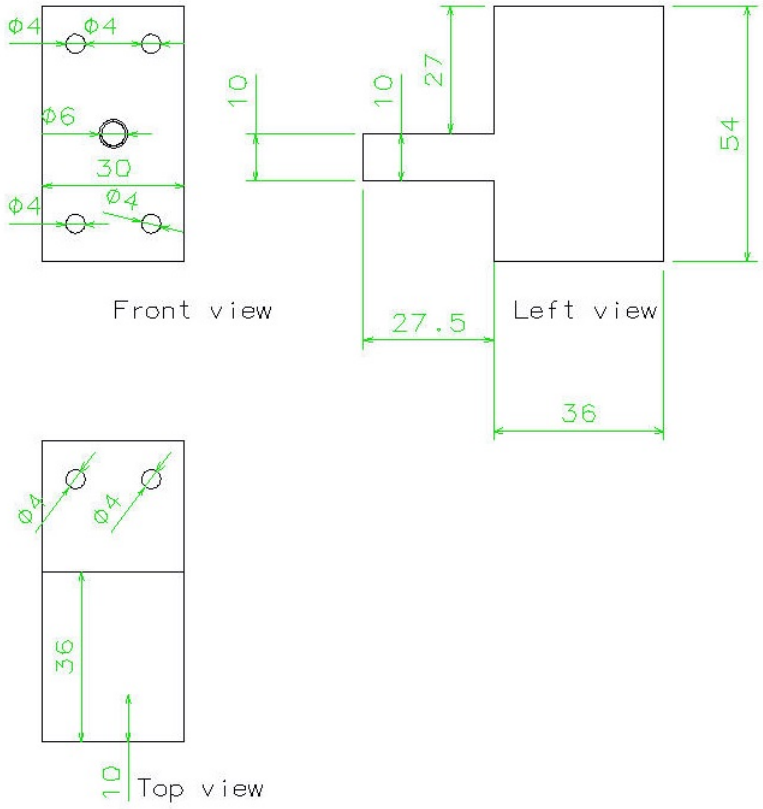



Figure A.14. Part in the middle of the negative stiffness mechanism.

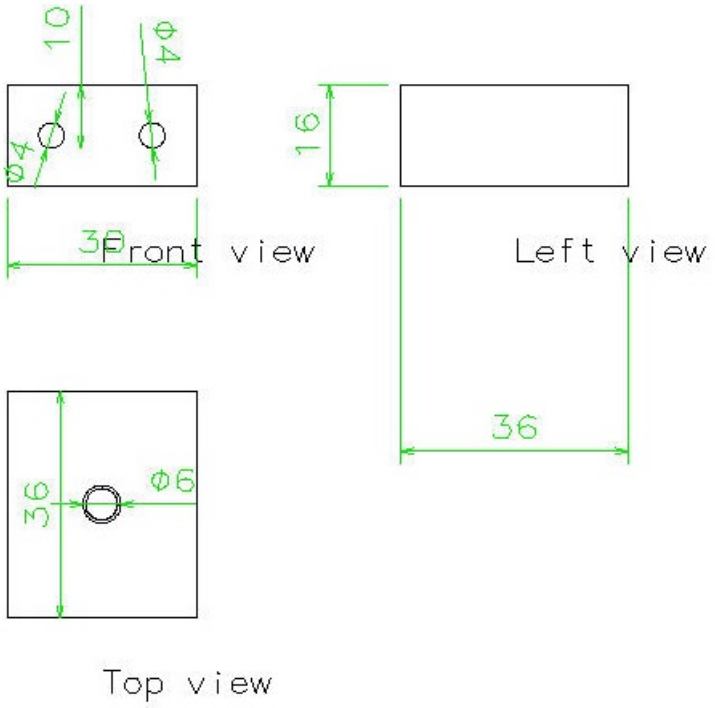



Figure A.15. Right part of the negative stiffness mechanism.

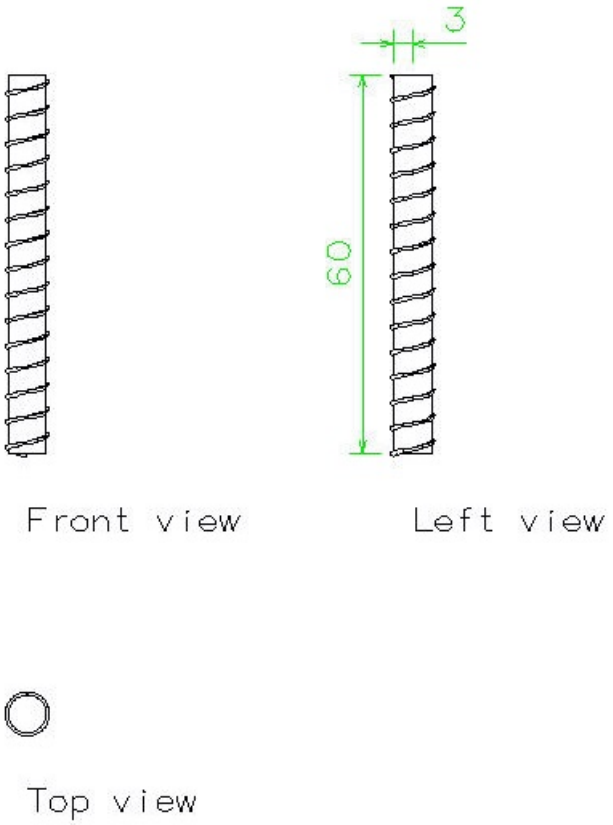



Figure A.16. M6 threaded rod at the right of the system.

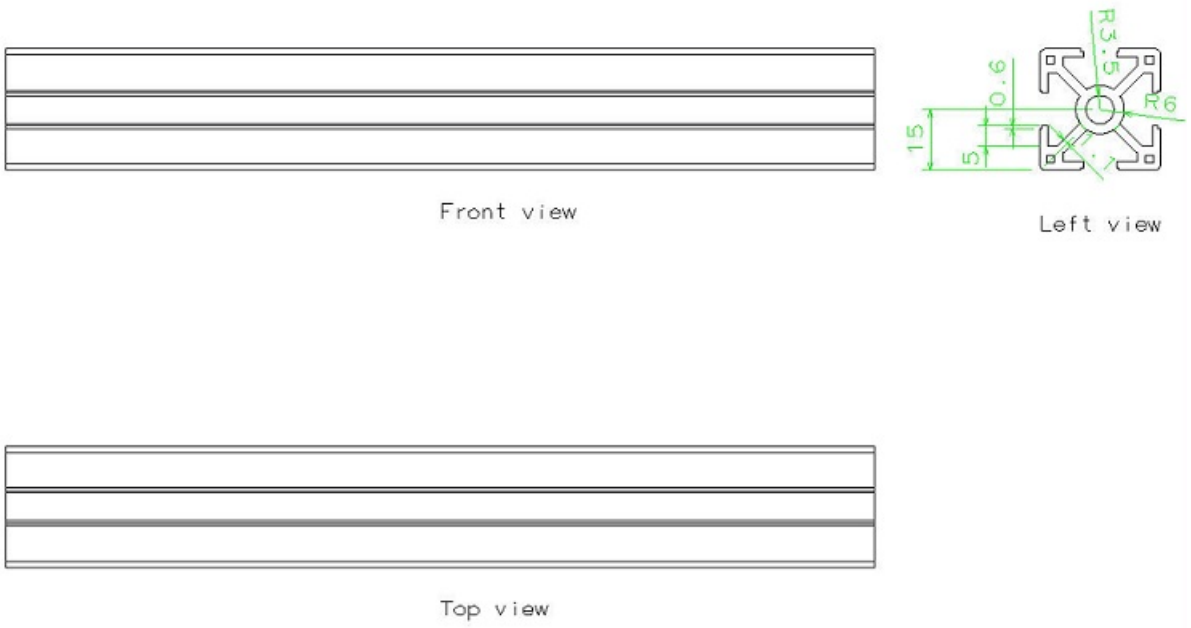



Figure A.17. Side parts of the main structure.

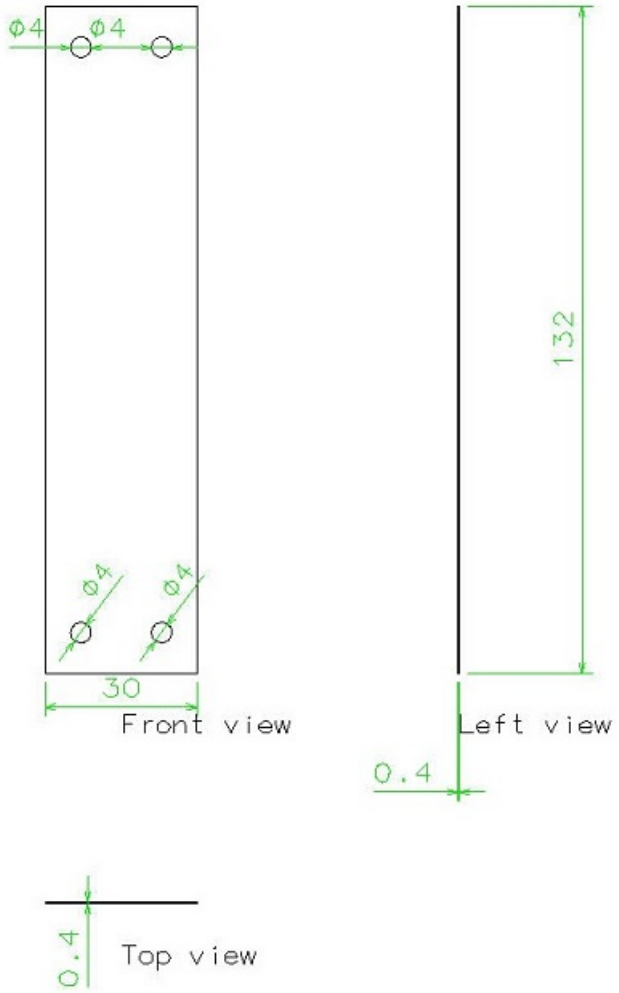



Figure A.18. Spring steels that produce negative stiffness.

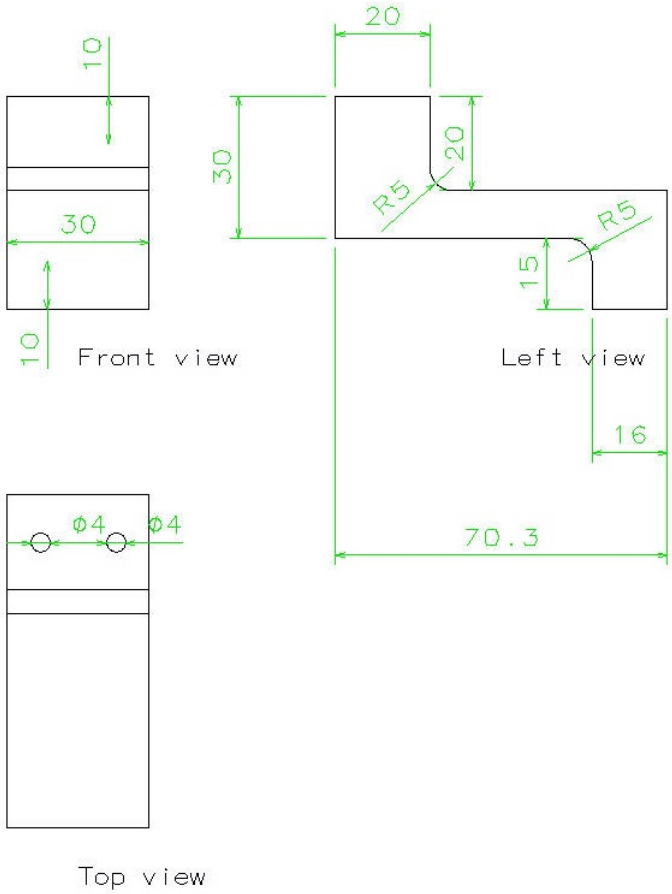



Figure A.19. Part between two flexure hinges.

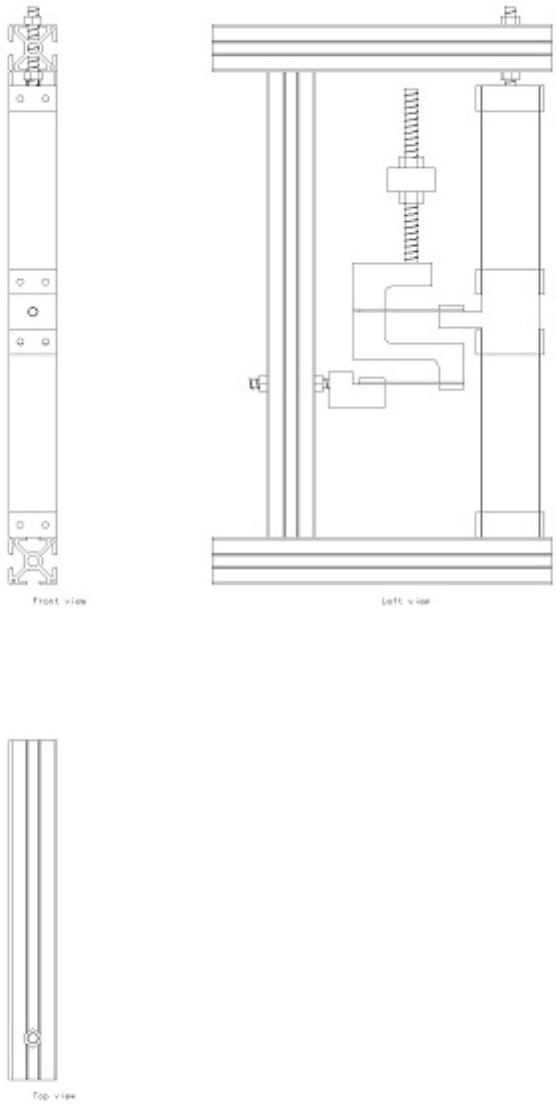



Figure A.20. Final Design.

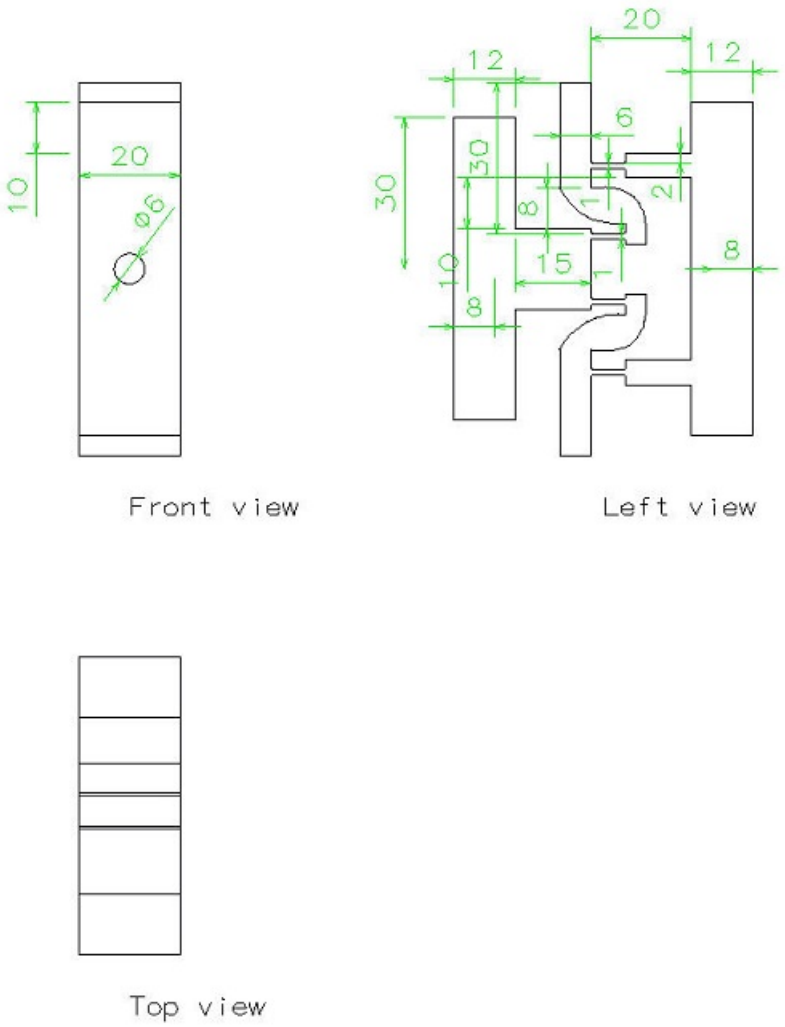



Figure A.21. Design without QZS mechanism.

# REFERENCES


1. Rao, S. S., *Mechanical Vibrations*, Pearson Prentice Hall International Edition, New Jersey, NJ, USA, 2004.

2. "NVH Analysis in Automobiles", http://www.scribd.com/doc/38931577/Noise-Vibration-Analysis-in-Automobiles, accessed at May 2011.

3. Yilmaz, C., and N. Kikuchi, "Analysis and Design of Passive Low-Pass Filter-Type Vibration Isolators Considering Stiffness and Mass Limitations", *Journal of Sound and Vibration*, Vol. 293, pp. 171-195, 2006.

4. Frahm, H., "Device for Damping Vibrations of Bodies", U.S. Patent No. 989958, 1911.

5. Harris, C. M., and C. E. Crede, *Shock and Vibration Handbook*, Vol. 1, McGraw-Hill, New York, NY, USA, 1961.

6. Flannelly, W. G., "Dynamic Antiresonant Vibration Isolator", U.S. Patent No. 3322379, 1967.

7. Goodwin, A. J. H., "Vibration Isolators", U.S. Patent No. 3202388, 1965.

8. Yilmaz, C., and N. Kikuchi, "Analysis and Design of Passive Band-Stop Filter-Type Vibration Isolators for Low-Frequency Applications", *Journal of Sound and Vibration*, Vol. 291, pp. 1004-1028, 2006.

9. Braun, D., "Vibration Isolator Particularly of the Antiresonance Force Type", U.S. Patent No. 4781363, 1988.

10. Carrella, A., M. J. Brennan, and T. P. Waters, "Optimization of a Quasi-Zero-Stiffness Isolator", *Journal of Mechanical Science and Technology*, Vol. 21, No. 6, pp. 946-949, 2006.

11. Carrella, A., M. J. Brennan, and T. P. Waters, "Static Analysis of a Passive Vibration Isolator with Quasi-Zero-Stiffness Characteristic", *Journal of Sound and Vibration*, Vol. 301, pp. 678-689, 2007.

12. Howell, L. L., *Compliant Mechanisms*, Wiley, New York, NY, USA, 2001.

13. Tian, Y., B. Shirinzadeh, D. Zhang, and Y. Zhong, "Three Flexure Hinges for Compliant Mechanism Designs Based on Dimensionless Graph Analysis", *Precision Engineering*, Vol. 34, pp. 92-100, 2010.

14. Zhang, Z., and H. Hu, "Accurate Equivalent Beam Model of a Planar Compliant Mechanism with Elliptical Flexure Hinges", *2009 International Conference on Measuring Technology and Mechatronics Automation*, Vol. 3, pp. 11-14, 2009.

15. Xu, W., and T. G. King, "Flexure Hinges for Piezo-Actuator Displacement Amplifiers: Flexibility, Accuracy and Stress Considerations", *Precision Engineering*, Vol. 19, pp. 4-10, 1996.

16. Lobontiu, N., and E. Garcia, "Circular-Hinge Line Element for Finite Element Analysis of Compliant Mechanisms", *Journal of Mechanical Design*, Vol. 127, pp. 766-773, 2005.

17. Tantanawat, T., Z. Li, and S. Kota, "Application of Compliant Mechanisms to Active Vibration Isolation Systems", *International Design Engineering Technical Conference*, Vol. 2, pp. 1165-1172, 2004.

18. Qiu, J., J. H. Lang, and A. H. Slocum, "A Curved-Beam Bistable Mechanism", *Journal of Microelectromechanical Systems*, Vol. 13, No. 2, pp. 137-146, 2004.

19. Qiu, J., J. H. Lang, and A. H. Slocum, "A Centrally-Clamped Parallel-Beam Bistable MEMS Mechanism", *Micro Electro Mechanical Systems 2001, The 14th Institute of Electrical and Electronics Engineers International Conference on Micro Electro Mechanical Systems*, pp. 353-356, 2001.

20. Vangbo, M., and Y. Backlund, "A Lateral Symmetrically Bistable Buckled Beam", *Journal of Micromechanics and Microengineering*, Vol. 8, pp. 29-32, 1998.

21. Park, S., and D. Hah, "Pre-Shaped Buckled-Beam Actuators: Theory and Experiments", *Sensors and Actuators A: Physical*, Vol. 148, pp. 186-192, 2008.

22. Sonmez, U., and C. C. Tutum, "A Compliant Bistable Mechanism Design Incorporating Elastica Buckling Beam Theory and Pseudo-Rigid-Body Model",*Journal of Mechanical Design*, Vol. 130, No. 4, pp. 1-14, 2008.

23. Kreider, W., and A. H. Nayfeh, "Experimental Investigation of SingleMode Responses in a Fixed-Fixed Buckled Beam", *Nonlinear Dynamics*, Vol. 15, pp. 155-177, 1998.

24. Masters, N. D., and L. L. Howell, "A Self-Retracting Fully Compliant Bistable Micromechanism", *Journal of Microelectromechanical Systems*, Vol. 12, No. 3, pp. 273-280, 2003.

25. Wilcox, D. L., and L. L. Howell, "Fully Compliant Tensural Bistable Micromechanisms (FTBM)", *Journal of Microelectromechanical Systems*, Vol. 14, No. 6, pp. 1223-1234, 2005.

26. Parkinson, M. B., B. D. Jensen, and G. M. Roach, "Optimization-Based Design of a Fully-Compliant Bistable Micromechanism", *American Society of Mechanical Engineers 2000, Design Engineering Technical Conferences and Computers and Information in Engineering Conference*, pp. 1-7, September 2000.

27. Jensen, B. D., M. B. Parkinson, K. Kurabayashi, L. L. Howell, and M. S. Baker, "Design Optimization of a Fully-Compliant Bistable Micro-Mechanism", *Proceedings of 2001 American Society of Mechanical Engineers International Mechanical Engineering Congress and Exposition*, pp. 357-363, November 2001.

28. Todd, B., B. D. Jensen, S. M. Schultz, and A. R. Hawkins, "Design and Testing

of a Thin-Flexure Bistable Mechanism Suitable for Stamping From Metal Sheets", *Journal of Mechanical Design*, Vol. 132, No. 7, pp. 111-117, 2010.

29. Ouyang P. R., W. J. Zhang, and M. M. Gupta, "A New Compliant Mechanical Amplifier Based on a Symmetric Five-Bar Topology", *Journal of Mechanical Design*, Vol. 130, No. 10, pp. 1-5, 2008.

30. Ouyang P. R., W. J. Zhang, and M. M. Gupta, "Design of a New Compliant Mechanical Amplifier", *American Society of Mechanical Engineers 2005, International Design Engineering Technical Conferences and Computers and Information in Engineering Conference*, Vol. 7, pp. 15-24, 2005.

31. Xu, W., and T. G. King, "Mechanical Amplifier Design for Piezo-Actuator Applications", *The Institution Electrical Engineers of Colloquium on Innovative Actuators for Mechatronic Systems*, pp. 1-5, 1995.

32. Ramrkahyani, D. S., G. A. Lesieutre, M. Frecker, and S. Bharti, "Aircraft Structural Morphing using Tendon Actuated Compliant Cellular Trusses", *Journal of Aircraft*, Vol. 42, pp. 1615-1621, 2004.

33. Cannon, J. R., *Compliant Mechanisms to Perform Bearing and Spring Functions in High Precision Applications*, M. S. Thesis, Brigham Young University, 2004.

34. Kota, S., K. J. Lu, Z. Kreiner, B. Trease, J. Arenas, and J Geiger, "Design and Application of Compliant Mechanisms for Surgical Tools", *Journal of Biomechanical Engineering*, Vol. 127, No. 6, pp. 981-989, 2005.

35. Tam, M. C. S, S. Payandeh, and A. M. Parameswaran, "Design and Development of a Multiple DOF Compliant Robot", *Institute of Electrical and Electronics Engineers*, pp. 876-881, 2005.

36. Henein, S., I. Kjelberg and S. Zelenika, "Flexible Bearings for High-Precision Mechanisms in Accelerator Facilities", *Proceedings NANOBEAM 2002. 26th Ad-*

*vanced International Committee for Future Accelerators Beam Dynamics Workshop on Nanometre Size Colliding Beams*, pp. 103-110, 2002.

37. Platus, D. L., "Negative-Stiffness-Mechanism Vibration Isolation Systems", *Society of Photographic Instrumentation Engineers Vibration Control in Microelectronics, Optics, and Metrology*, Vol. 1619, pp. 44-54, 1991.

38. Platus, D. L., "Smoothing Out Bad Vibes", *Machine Design*, pp. 123-130, 1993.

39. Platus, D. L., "Negative-Stiffness-Mechanism Vibration Isolation Systems", *Proceedings of Society of Photographic Instrumentation Engineers Reprint*, Vol. 3786, pp. 98-105, 1999.

40. Miller, S. F., C. C. Kao, A. J. Shih, and J. Qu, "Investigation of wire electrical discharge machining of thin cross-sections and compliant mechanisms", *International Journal of Machine Tools and Manufacture*, Vol. 45, pp. 1717-1725, 2005.

41. Miller, S. F., E. Shi, C. C. Kao, A. J. Shih, and J. Qu, "Investigation of wire electrical discharge machining of thin cross-sections and compliant mechanisms", *American Society of Mechanical Engineers, Manufacturing Engineering Division*, Vol. 15, pp. 165-171, 2004.

42. Rakwal, D., S. Heamawatanachai, P. Tathireddy, F. Solzbacher, and E. Bamberg, "Fabrication of compliant high aspect ratio silicon microelectrode arrays using micro-wire electrical discharge machining", *Microsystem Technologies*, Vol. 15, pp. 789-797, 2009.

43. Choi, K. B., and J. J. Lee, "Analysis and design of linear parallel compliant stage for ultra-precision motion based on 4-PP flexural joint mechanism", *International Conference on Smart Manufacturing Application 2008*, pp. 35-38, April 2008.

44. Technical University of Denmark Mechanical Engineering - Technical University of Denmark Mathematics, "Topopt Research Group World Wide Web site",

http://www.topopt.dtu.dk/?q=node/9, accessed at May 2011.

45. Bendsoe, M.P., and N. Kikuchi, "Generating Optimal Topologies in Structural Design Using a Homogenization Method", *Computer Methods in Applied Mechanics and Engineering*, Vol. 71, pp. 197-224, 1988.

46. Inman, D. J., *Engineering Vibrations*, Pearson Prentice Hall International Edition, New Jersey, NJ, USA, 2009.

47. Vangbo, M., "Analytical analysis of a compressed bistable buckled beam", *Sensors and Actuators A: Physical*, Vol. 69, No. 3, pp. 212-216, 1998.